Further developments of multi-reflection time-of-flight mass spectrometry and first application for cluster research

I n a u g u r a l d i s s e r t a t i o n

zur

Erlangung des akademischen Grades eines

Doktors der Naturwissenschaften (Dr. rer. nat.)

der

Mathematisch-Naturwissenschaftlichen Fakultät

der

Universität Greifswald

vorgelegt von

Paul Fischer

geboren am 15.10.1992

in Ribnitz-Damgarten

Greifswald, 03.03.2020

Dekan:	Prof. Dr. Werner Weitschies
1. Gutachter:	Prof. Dr. Lutz Schweikhard
2. Gutachter:	Prof. Dr. Klaus Blaum
Tag der Disputation:	28.02.2020

Contents

List of Figures

Nomenclature

Acronyms

CLS	collinear laser spectroscopy
EIBT	electrostatic ion beam trap
ELIT	electrostatic linear ion trap
FT-ICR	Fourier-transform ion-cyclotron-resonance
FWHM	full width at half maximum
MR-ToF	multi-reflection time-of-flight
MS	mass spectrometry
RF	radio frequency

Symbols

ΔE_{kin}	distribution of kinetic energies of an ion bunch
Δm	mass difference
ΔT	change in revolution period
Δt	temporal width of an ion bunch
Δ_{ref}	difference of square roots of reference masses
δ	mass divergence due to electron mass
λ	photon wavelength
Σ_{ref}	sum of square roots of reference masses
A	mass number
a	mass-spectrometer constant (scaling parameter)
C_{TOF}	experimental observable for two-reference MR-ToF mass measurements
E_{kin}	kinetic energy
f	focal length

L ..... length of (ion-)optical resonator

m ..... mass

N ..... revolution number

n ..... cluster size

q ..... ion charge

R ..... mass resolving power

T ..... revolution period

t ..... flight time

t_0 ..... mass-spectrometer constant (common offset)

v ..... velocity

1 Introduction

The origin of mass spectrometry (MS), the technique of measuring an ion's mass-to-charge ratio m/q, can be traced back to experiments in the late 19^{th} century concerning the understanding of electricity [1]. German physicist E. Goldstein discovered positive rays in gas discharges in 1886, W. Wien improved upon this in 1898 by deflecting them in strong magnetic fields according to their m/q. Continued work by J.J. Thomson and F.W. Aston on what turned out to be ionized atoms lead to the first mass spectra recorded on photographic plates and the discovery of isotopes [2]. With the advancement of MS techniques yielding higher accuracy, Aston went on to show deviations from the "whole number rule" in the form of "packing fractions", that is, he found the mass-to-charge ratios of ions not to be mere multiples of one another [3]. In fact, atomic weights were lower than that of the sum of their constituents, consistent with the idea of a mass defect representing the nuclear binding energy.

The first mass spectrometer in the modern sense of the term was developed by A.J. Dempster in 1918 [4], leading to the discovery of the fissile ^{235}U isotope and, later on, the quest for its separation within the Manhattan Project. J. Mattauch and R. Herzog later combined aspects of both Aston's and Dempster's design, resulting in the first achromatic mass spectrometer (focusing in velocity and direction) [5].

In the 1950s and 1960s, the next advancement in the field of mass spectrometry was introduced in the form of ion traps. Based on either radio-frequency (RF) fields ("Paul trap" [6]) or a superposition of static electric and magnetic fields ("Penning trap" [7]), these tools allowed the prolonged confinement of charged particles for the precise study of their properties. Modeled after large accelerator rings utilized at, e.g., CERN at the time, smaller storage rings were eventually designed in the late 1980s and early 1990s to further combine aspects of mass spectrometry and ion trapping [8–10].

The concept of time-of-flight mass spectrometry (ToF MS [11]) was first presented by W.E. Stephens in 1946, followed by its implementation by A.E. Cameron and D.F. Eggers two years later [12]. Offering pulsed operation for the fast monitoring of systems with rapidly changing compositions, the concept was later enhanced by W.C. Wiley and I.H. McLaren in 1955 [13] and then B.A. Mamyrin in 1973 [14]. Despite these advancements, the technique's principal traits would stay largely constant: While ToF devices were compact and exceptionally quick compared to setups based on other concepts, their mass resolving power $R = m/\Delta m$, i.e. their ability to separate small relative mass differences, remained on the lower end of the experimental spectrum. This only changed in the 1990s, when the concept of multi-reflection time-of-flight (MR-ToF) mass spectrometry was introduced.

An MR-ToF mass spectrometer is a device consisting of two opposing electrostatic ion mirrors enclosing a field-free drift section. Injected ions are reflected between the mirrors, allowing them to complete multiple laps and thus increasing their flight-path lengths far beyond the dimensions of the system. This concept, within the context of

ToF MS, was demonstrated by H. Wollnik in 1990 [15], a similar design was also shown by W. Tretner as early as 1960 [16]. Closely related, the principle of a trap utilizing electrostatic mirrors to contain ions for extended periods of time was introduced in 1997 by D. Zajfman [17] and W.H. Benner [18], independently. These trapping devices, also referred to as electrostatic ion beam traps (EIBTs) [19] or electrostatic linear ion traps (ELITs) [20–22], focus on the storage capabilities of the MR-principle rather than its use for mass spectrometry.

At the University of Greifswald, an MR-ToF mass spectrometer is in operation for the research of atomic clusters. It comprises a laser-ablation source for cluster production [23–26], an ion-optical guiding system including a quadrupole deflector, and a channeltron detector and fast multiscaler for single-ion counting. All electrodes and fixtures have been developed and machined in-house; voltages are provided by a series of commercial, precision high-voltage power supplies and switches. Experimental control is realized with a LabVIEW-based, self-maintained software. Details relevant for the present studies are given in Sec. 2, further information can be found in a recent publication [27].

This thesis highlights recent developments at the Greifswald setup to further the field of MR-ToF mass spectrometry involving ions with large mass differences. These techniques are then used to perform photodissociation studies on atomic clusters within the device, making it the first such application that, while utilizing the trap characteristics of the MR-ToF principle, still maintains bunched operation and the high resolving powers associated therewith. Based on this, the first instance of tandem MR-ToF MS is performed, that is, two steps of MR-ToF mass spectrometry are used for subsequent precursor selection and product analyses. This novel measurement scheme is applied to determine the photodissociation behavior of Bi-Pb compound clusters, which have not been investigated experimentally prior to this work.

2 The multi-reflection time-of-flight mass spectrometer

A multi-reflection time-of-flight mass spectrometer, as shown in Fig. 2.1, aims to repeatedly use a part of the ions' flight path by reflecting them through the same field-free drift section. The resulting elongated flight times make MR-ToF devices excellent high-resolution mass spectrometers that can reach mass resolving powers R beyond 100 000 in just a few tens of milliseconds [27–30]. For the required axial ion confinement, the maximum of the electrostatic mirror potentials must exceed the ions' total energy (Fig. 2.2). Ion injection and ejection can be performed by switching off the corresponding mirror potential for a short time and allowing ion bunches to pass. Alternatively, an "in-trap lift" can be used to lower and raise the ion energy between the mirrors, as was first introduced at the ISOLTRAP MR-ToF mass spectrometer at ISOLDE/CERN [31]. By switching a voltage applied to the device's central drift tube while ions are inside of it, their energy can be adjusted without disturbance (Faraday-cage principle). The principal gain from this type of operation lies in the fact that the ion energy during storage is decoupled from the transfer energy outside of the analyzer. This significantly reduces the experimental complexity of adjusting either one and is especially useful for tuning the MR-ToF temporal focus (see next section): the gradient of the mirror potentials that is experienced by stored ions can be changed by adjusting only a single voltage. Another advantage of the in-trap lift is an increased mirror-voltage stability. Since all of the reflecting potentials are entirely static, flight-time fluctuations arising from switching noise and ringing are eliminated.

Following the technique's implementation at ISOLTRAP, several MR-ToF experiments have since incorporated such electrodes into their setups [22,32–35], including the present one at the University of Greifswald [27]. Here, a combination of both in-trap lift and mirror operation has been introduced recently [36], which retains the lift's advantages with respect to the ion capture. Simultaneously, it ensures that a large portion of the

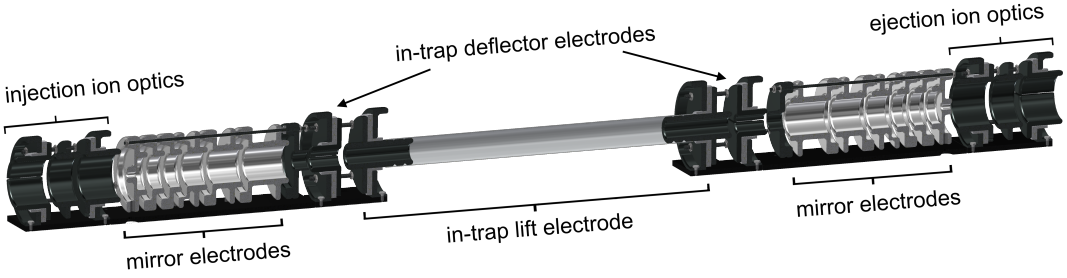

Figure 2.1: Sectional view of the MR-ToF analyzer at the Greifswald setup. Ions are injected from the left and ejected towards a channeltron detector on the right to record their flight time.

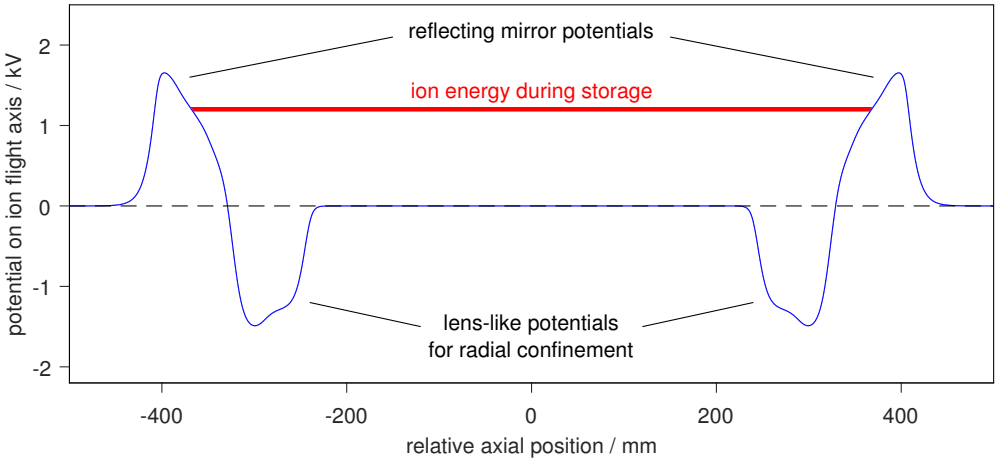

Figure 2.2: MR-ToF-analyzer potential at the Greifswald setup (blue) and typical ion storage energy of about 1200 eV (red). The ions' transfer energy outside of the analyzer is 2000 eV.

stored ions are guided towards the detector upon their release by opening the exit-side mirror. This operation has become standard practice for wide-band investigations such as those presented in Sec. 3 and 4.

Apart from the ion energy having to remain below the mirror potentials, there exists a second storage criterion in an MR-ToF analyzer related to the ions' radial confinement. Analogously to an optical resonator, reflection without some means of radial re-focusing is inherently unstable. In photon optics, the resonator criterion

$$0 \leq \left(1 - \frac{L}{2f_1}\right)\left(1 - \frac{L}{2f_2}\right) \leq 1 \tag{2.1}$$

can be found linking the length L of an optical cavity to the focal lengths f of its encasing mirrors [37]. The expression

$$\frac{L}{4} \leq f \leq \infty \tag{2.2}$$

is equivalent for symmetric cavities: The focal lengths $f = f_1 = f_2$ of the (curved) mirrors must not be shorter than a quarter of their separation.

For MR-ToF devices in the sense of an ion-optical resonator, radial focusing is realized by ion-lens-like potentials next to the reflecting potential walls (Fig. 2.2), the focal lengths of which have to satisfy the same criterion [17, 38, 39]. It can also be refined further using more sophisticated models [39]. For proper potential setups, the storage life time of an MR-ToF analyzer is largely defined by residual-gas collisions, reaching several hundreds of milliseconds for room-temperature [38] and a few hundred seconds for cryogenic setups [40].

Being an entirely electrostatic system, an MR-ToF mass spectrometer offers unique features in comparison to other MS techniques. Like for all electrostatic devices, its ion trajectories are identical for identical ratios of kinetic energy and charge E_{kin}/q regardless of mass. An ion's revolution period T, however, is proportional to the square root of its mass-to-charge ratio m/q. Consequently, MR-ToF devices show no mass-dependent

storage criterion as is the case in RF ion traps or magnetic systems. The absence of superconducting magnets leads to the additional advantage of an open geometry and easy access to the beam path between the electrostatic mirrors, which is useful for merged- or cross-beam configurations. This is further aided by the fact that the center region of the analyzer is field free, leading to straight ion trajectories that do not exist for electrostatic storage devices such as the Orbitrap [41] or its historical predecessor, the Kingdon trap [42].

Due to the energy-based storage criterion, however, the kinetic energy of confined ions is limited by the applied potentials. Most MR-ToF devices are operated at a few keV due to the increasing challenge of routing and switching high voltages to the system's electrodes, although a prospected 30 kV-setup is currently being designed for the first time [35, 43]. This is similar to the conditions for electrostatic storage rings, which can be understood as the MR-ToF mass spectrometer's larger counterpart: Fully electrostatic rings are used to store ions at some tens to a few hundreds of keV [44–47] whereas magnetic ones reach the MeV range at the tradeoff of introducing an upper mass limit [48].

Lastly, the nature of MR-ToF devices might seem at odds with "Earnshaw's theorem" [49], which forbids the stable confinement of charges by purely electrostatic means. However, this only applies to the storage of ions without kinetic energy. MR-ToF storage is possible due to the ions moving. In turn, they are strictly required to exhibit a nonzero total energy during storage, as no particles can be trapped at rest.

2.1 Modes of operation

The working principle of any time-of-flight mass spectrometer is illustrated in Fig. 2.3: Due to the velocity difference of ions with different m/q ratios at identical kinetic energies, their separation in time increases with longer total flight times. One of the limiting factors of this, however, is the fact that an ion bunch consisting of only a single species will typically exhibit some distribution of kinetic energies [11]. Its temporal width will thus increase over time, counteracting the growing ToF separation between the different species. The first remediation of this behavior (before the introduction of the MR-ToF principle) was performed by B.A. Mamyrin in 1973 by introducing a "mass-reflectron" capable of folding back ion trajectories [14]. The underlying principle is the fact that ions with higher kinetic energies will penetrate deeper into a reflecting potential barrier, leading to longer flight paths that compensate for their increased velocity in the field-free drift section(s). The time focus, i.e. the point along the trajectory where faster ions catch up with the slower ones, can be tuned to coincide with the system's detector location after the reflection. The resolving power of the respective ToF mass spectrometer rises from few hundred [13] to several thousand [14] in response.

The MR-ToF mass spectrometer—as the reflectron's intellectual descendant—has an even more powerful means of adjusting ion flight paths based on their energy: An ion's revolution period T is dependent on its kinetic energy E_{kin}, the coefficient

$$\frac{\partial T}{\partial E_{\mathrm{kin}}}$$

of which can be tuned via the shape of the analyzer's reflecting potentials [31, 50, 51]. As

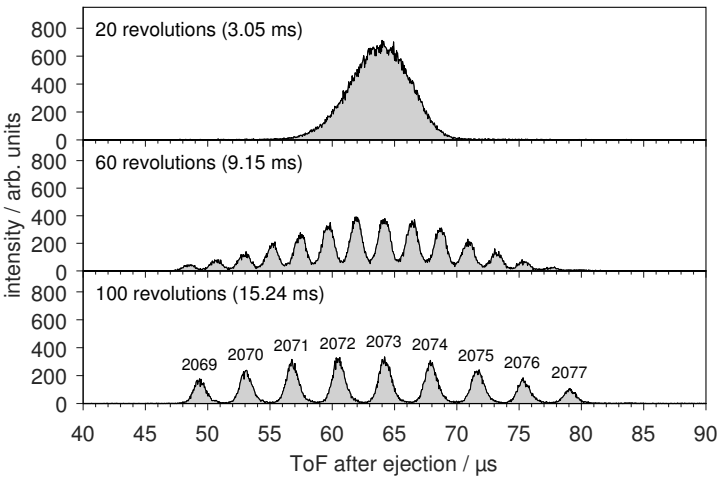

Figure 2.3: Time-of-flight spectra of Pb_{10}^- clusters for increasing revolution numbers (20, 60, and 100 from top to bottom) and thus total flight times. Different combinations of stable lead isotopes lead to ion species with different mass numbers A ("isotopologues"), as labeled in the bottom spectrum. No ions can be detected below ≈ 45 and above $\approx 80\,\mu s$ after the ejection from the analyzer due to them entering the mirror potentials and not being properly ejected.

is shown in Fig. 2.1, each electrostatic mirror is formed of several stacked ring electrodes for better control over the potential gradient. In setups incorporating an in-trap lift, the ions' storage energy can itself be easily adjusted to move an ensemble with some energy spread ΔE_{kin} along different parts of the mirror potential. This allows tuning as demonstrated in [52] and shown in Fig. 2.4 for the present setup.

Three general regions can be distinguished in Fig. 2.4, correlating to different operational parameters of the MR-ToF analyzer. The center part, where the ions' revolution period is barely dependent on the lift voltage (and thus E_{kin}) can be described by the $\partial T/\partial E_{\mathrm{kin}}$ coefficient being close to zero. This is referred to as an isochronous region [31, 53]. An ion bunch with sufficiently-small ΔE_{kin} will stay synchronized and experience no intrinsic ToF broadening with increasing flight time. As can be inferred, tuning of an MR-ToF device often aims to reach such a state. In reality, a bunch's temporal spread will still increase, however, this is the case primarily due to drifts in the applied mirror voltages (see Sec. 3.2), imperfections of the mirror electrodes, and aberration effects. The resolving power increases quickly with the revolution number for some hundreds to thousands of laps before leveling off (see, e.g., [52]).

For a positive coefficient, $\partial T/\partial E_{\mathrm{kin}} > 0$, ions with higher kinetic energy exhibit larger revolution periods. If a temporal focus exists between the source and analyzer, high-energy ions will already be at the front of the bunch upon entering the MR-ToF device. However, they will then be moved back with each revolution, resulting in a decreasing temporal width Δt. This can be used to tune a minimum Δt for a specific revolution number N, leading to resolving powers (on that N) comparable to those of isochronous settings [31]. For even higher revolution numbers, however, the resolving power quickly drops, as the bunch spreads out in the opposite direction. This is an advantage of isochonous settings, which allow measurements at different revolution numbers without the need to re-tune the analyzer/ion energy in between. The present

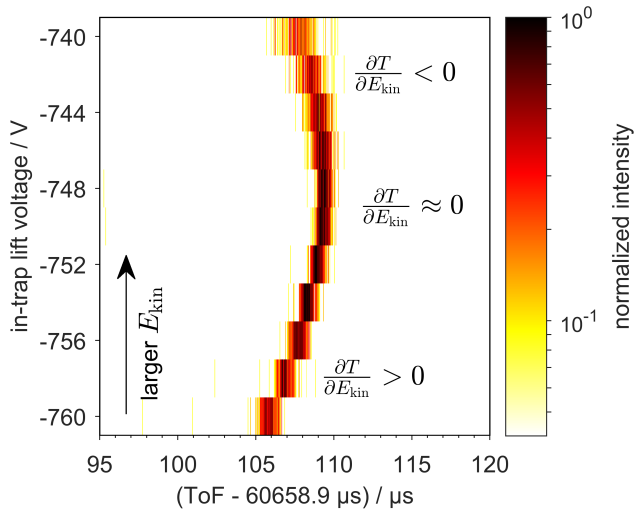

Figure 2.4: 2D color plot of ToF spectra recorded for different in-trap lift voltages and thus different storage ion energies. The ion species retained in the analyzer is $^{209}Bi_{10}^-$, the measurement is performed at 400 revolution periods.

setup is thus operated at $\partial T/\partial E_{\mathrm{kin}} \approx 0$.

There is a second phenomenon associated with $\partial T/\partial E_{\mathrm{kin}} > 0$ conditions, rising from Coulomb interactions between the ions of a large cloud: It has been observed that such bunches will stay coherent for extended periods of time [54]. This well-documented behavior is referred to as "self-synchronization" or "self-bunching" [50, 51, 54–57], and results from the fast ions being shifted towards the back of the bunch on each revolution. For sufficient particle densities, the space-charge interactions keep them from quickly moving towards the front again. While of interest for ion trapping, these effects are undesirable in precision mass spectrometry, as they can lead to the synchronization of distinct ion clouds with small mass differences [32, 56]. This is known as "peak coalescence" in Fourier-transform ion-cyclotron-resonance (FT-ICR) MS [58] and is the reason why MR-ToF MS is typically performed with small ion numbers per cycle.

The third regime, $\partial T/\partial E_{\mathrm{kin}} < 0$, generally leads to a quick increase of the width of a stored ion bunch over time [50, 51]. The fact that fast, high-energy ions are moving to the front of the bunch outside of the analyzer is aided by them exhibiting shorter revolution periods within. This "non-bunching" mode of operation is of less interest for mass spectrometry, although it has been used for molecule-interaction studies to ensure ions quickly fill the entire trap volume [59–61].

2.2 Applications

Historically, MR-ToF devices have been primarily used as ion traps for the study of molecular and cluster properties for some time. In this capacity, EIBT-setups are currently being operated at the Weizmann Institute of Science (Rehovot, Israel) [17, 62, 63], the Bhabha Atomic Research Centre (Mumbai, India) [64], LKB (Paris, France) [65], MPIK (Heidelberg, Germany) [40], the University of Lyon (Lyon, France)

[66], Queen's University Belfast (Belfast, UK) [67], the University of California (San Diego, USA) [68], Purdue University (West Lafayette, USA) [69], and Indiana University (Bloomington, USA) [70]. Typical investigations include the study of photodetachment and -fragmentation [59–61, 66, 71–73], electron-impact detachment [74], and molecular decay [75–77]. Many of these devices are operated in non-bunching mode (see previous section) or rely, for high-resolution applications, on capacitive pickup detection ("Fourier-transform MR-ToF") [21,64,66,70,78]. As is the case for most pickup-based measurement techniques, they thus require either highly-charged ions or large ion numbers.

In nuclear physics, MR-ToF mass spectrometers have become increasingly popular since their first application for mass separation [79] and determination [80] in 2013. Their ability to reach high resolving powers—higher than FT-ICR Penning traps for measurements restricted to a few tens of miliseconds of observaton time [52]—makes them excellent tools for precision mass measurements of exotic nuclei with very short half-lifes. Today, MR-ToF MS on radioactive beams is performed or under construction at ISOLTRAP at ISOLDE/CERN (Geneva, Switzerland) [52], SLOWRI at RIBF/RIKEN (Wakō, Japan) [28], RISP at RAON (Daejeon, South Korea) [81], TITAN at ISAC/TRIUMF (Vancouver, Canada) [82], the FRS Ion-Catcher at FRS/GSI (Darmstadt, Germany) [29], PILGRIM at S^3-SPIRAL2/GANIL (Caen, France) [33], CARIBU at ATLAS/ANL (Argonne, USA) [34], the Notre Dame Cyclotron Facility (Notre Dame, USA) [83], SHANS at IMP/CAS (Lanzhou, China) [84], and MARA-LEB at the University of Jyväskylä (Jyväskylä, Finland) [85]. For many of theses setups, the MR-ToF analyzer also doubles as an isobar separator in front of precision Penning traps, which are prone to systematic errors in the presence of contaminants [58, 86, 87].

An entirely new multi-reflection application utilizing short ion bunches is currently being developed at the MIRACLS project at ISOLDE/CERN [35,43]. It aims to perform in-trap collinear laser spectroscopy (CLS [88, 89]) for the investigation of nuclear ground- and isomeric-state properties. For exotic nuclei, conventional CLS is performed by overlapping the ion and laser beams in a single-pass fashion, often limiting the available observation time much more than the half-life of the radioactive isotopes. By storing an ion bunch in an MR-ToF device to repeatedly probe it, a significant improvement in experimental sensitivity is being projected.

It is apparent that MR-ToF applications in molecular and nuclear physics differ somewhat in terms of their techniques, operational parameters, and investigated mass ranges. While precision mass spectrometry is performed with small, coherent ion bunches, studies of molecular properties often rely on large ion numbers or forgo bunched operation entirely in favor of easier trapping and interaction requisites. This thesis, in contrast, introduces the use of an MR-ToF device in its function as a mass spectrometer to investigate molecular properties. To this end, a set of wide-band MS techniques, i.e. methods to separate and investigate ion species of very different m/q values simultaneously, is developed (Sec. 3) and a novel measurement scheme for in-trap photoexcitation is used to probe the fragmentation behavior of bismuth clusters (Sec. 4). All of the following considerations assume the MR-ToF device to be operated as a mass spectrometer, i.e. with distinct ion bunches small enough to not incur significant Coulomb interactions within the cloud.

3 MR-ToF developments for wide-band applications

The nature of the multi-reflection time-of-flight mass spectrometer, namely its principal feature of leading to ion species of different m/q ratios lapping one another, can make applications involving broad mass ranges challenging. Time-of-flight spectra recorded after specific storage times quickly become ambiguous if multiple species are involved [90, 91]. On the other hand, the absence of intrinsic mass limitations due to the analyzer's electrostatic nature makes it especially attractive for precisely these wide-band investigations.

MR-ToF devices operated in non-bunching mode (see Sec. 2.1) make full use of their excellent ion-storage capabilities, however, they forfeit the traits of a high-resolution mass spectrometer arising from bunched operation in turn. Applications utilizing high resolving powers, in contrast, are usually restricted to small mass ranges in exchange. Interest to bring both of these fields closer together has been growing recently, that is, increasing efforts are being made to apply high-resolution MR-ToF MS to wide-band studies [36, 90, 92, 93]. In this section, novel developments for investigations involving ions with very different masses are presented.

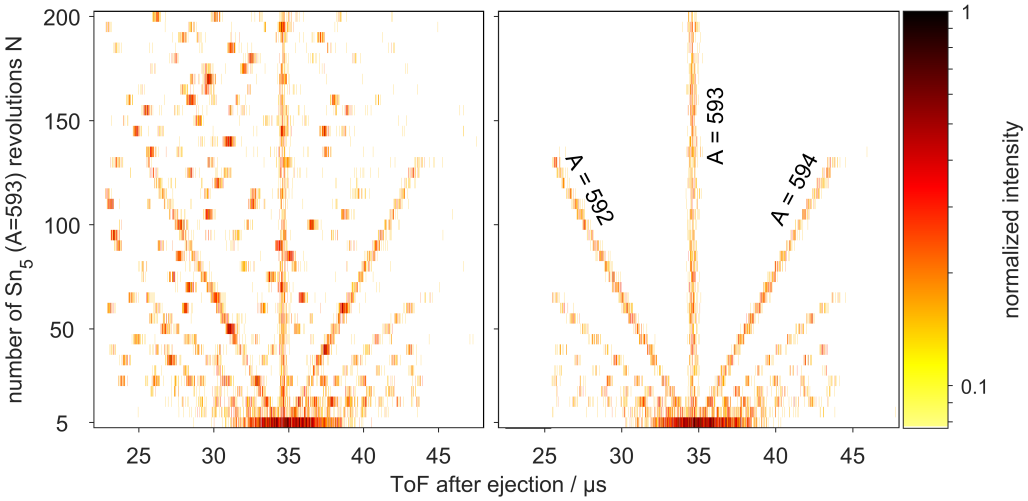

Figure 3.1: N-versus-ToF plots after the capture of several Sn_n^- cluster sizes, each incorporating a number of isotopologues. The left plot is recorded without any means of in-trap selection, the right with transversal ejection synchronized to retain only the $A = 593$ species. Picture modified from [94].

3.1 Selection of ion species with disparate m/q values

A means of selectively retaining specific ion species in an MR-ToF analyzer after a wide-band capture is crucial, as can be inferred from Fig. 3.1. Both plots show time-of-flight spectra of anionic tin clusters in an "N-versus-ToF" fashion [90], meaning that ion flight times are subsequently recorded after increasing storage times similar to Fig. 2.3 and visualized as a two-dimensional map. The left measurement has been performed without any ion selection, the right one with the technique of transversal ejection [94] employed to retain only the Sn_5^- clusters with an isotopic composition yielding mass number $A = 593$. To this end, a sliced, off-center ring electrode located between the lift and mirror electrodes (see Fig. 2.1) is utilized to form a radially-deflecting electric field. Opposing halves of the ring are switched between ground potential and $\pm 10\,\mathrm{V}$, the phase and frequency of which is synchronized to the ion species to be retained.

Even without the selection, some ion species with masses close to that of the $A = 593$ target can be identified in the left plot by matching signals from one horizontal spectrum to the next. However, species with larger mass differences—those that move through the spectra at apparently random intervals—are harder to connect. In addition, signals of different ions can coincide at identical post-ejection flight times, complicating the task of finding a revolution number where a species of interest can be observed unobstructed. Unless extensive knowledge of all ions revolving between the mirrors has been obtained beforehand, matching individual signals to their species and predicting signal distributions in a standalone ToF spectrum becomes virtually impossible.

In-trap ion selection is thus a typical prerequisite for MR-ToF investigations. Next to techniques involving the synchronized switching of in-trap deflector electrodes [94, 95],

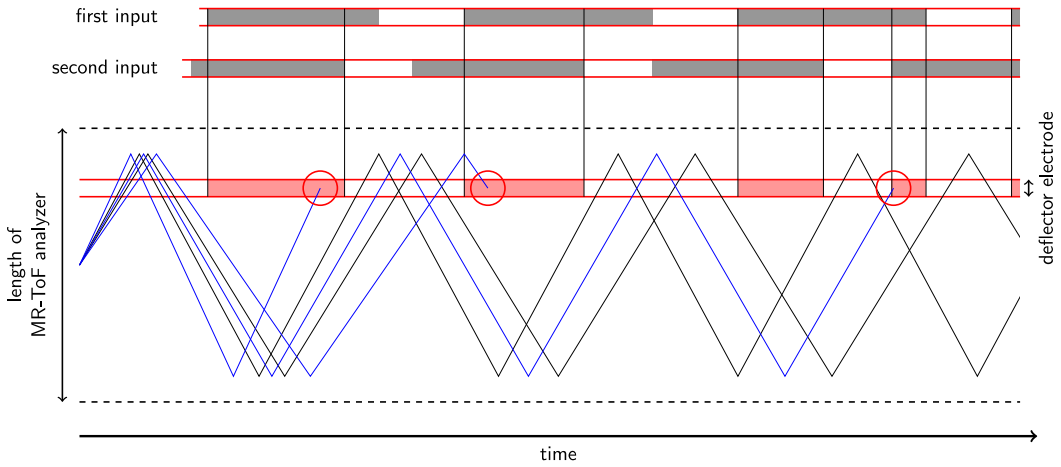

Figure 3.2: Axial ion positions as a function of time in an MR-ToF analyzer for species with different m/q values. A deflecting potential is only applied to the ring electrode (red bars) when both input signals (gray bars) permit it simultaneously. Two ion species with disparate m/q are retained (black lines) while lighter, heavier, and intermediate species (blue lines) eventually sample a deflecting field, as indicated by red circles. Picture modified from [94].

similar effects have been achieved by switching some of the trap's mirror potentials [96,97]. Note that all methods of an in-trap nature fundamentally differ from those aiming to perform post-trap selection by means of, e.g., a fast Bradbury-Nielsen gate [98]. These latter schemes [29, 99] are subject to the actual ToF difference between ion species oscillating due to their lapping behavior. Even if the resolving power would be high enough to separate species in time by a large margin, the actual resolution in the spectrum may not be sufficient to select them. These issues do not arise for in-trap applications, as the selection mechanism is typically applied over a large portion of the storage duration. Additionally, purification from contaminant species is critical for interaction-based studies performed within the trap itself (see Sec. 4). This is, by definition, not possible with post-trap equipment.

It is readily apparent that in-trap ion selection reduces an MR-ToF device's capabilities for wide-band applications by design. For all techniques mentioned above, the operating principle restricts the retained mass range around a single target m/q value. In this thesis, a scheme allowing the selective retention of multiple, disparate mass ranges is demonstrated for the first time ([100], cumulative thesis article, Sec. 7.2). Together with the implementation of multiple subsequent capture pulses to load more species into the analyzer than would be possible with a single one, the technique of transversal ejection is adapted to select several ion species from the stored ensemble simultaneously (Fig. 3.2).

Since every ion bunch's position in the analyzer over time is governed by its revolution period, a deflector function of the same period is needed for each species of interest in the multiple-selection scheme (gray bars in Fig. 3.2). These functions are logical representations of whether a deflecting field will disturb the corresponding ions at specific points in time. Thus, the output of an AND gate taking all individual functions as

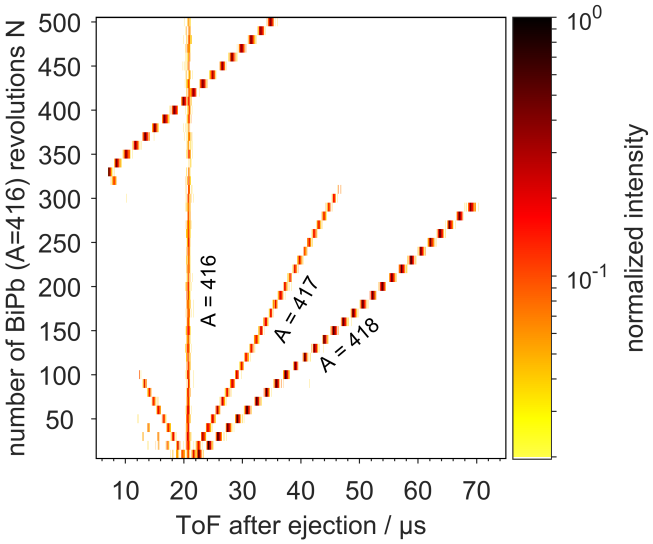

Figure 3.3: N-versus-ToF plot showing $BiPb^+$ compound-cluster isotopologues with ion selection of both the $A = 416$ and 418 species.

inputs will only allow the deflector to be engaged as long as all species of interest are sufficiently far away from it simultaneously.

Multiple ion selection is demonstrated in Fig. 3.3 for isotopologues produced by laser irradiation of a Bi-Pb alloy target. All species shown consist of two atoms; ions with mass number $A = 416$ (^{207}Pb^{209}Bi$^+$ or ^{208}Pb$_2^+$, not resolved in the present spectra) and 418 (^{209}Bi$_2^+$) are retained. The improvement over single-range selection is apparent, as such a configuration of mass numbers could not be reached without the logical addition. The selection resolving power, i.e. the level of control over the trapped species that can be exerted in a specific mass range, is no longer coupled to the overall width of said range. This allows more freedom for, e.g., multiplexed MS/MS studies or correction setups such as those introduced in the next section. Note that since the publication of these developments [100], a second group has also demonstrated simultaneous ion selection with disparate m/q ranges [93].

3.2 Time-of-flight correction with non-isobaric reference species

For precision MR-ToF measurements aiming for state-of-the-art resolving powers beyond 100 000 [27–30], the devices' long-term stability is of significant importance. Since the principal observable, an ion's revolution period T, is dependent on its kinetic energy as well as the trap's reflecting mirror potentials, changes in either of them directly lead to different periods and thus overall flight times. Proportionality factors describing relative ToF changes for relative changes in the mirror voltages can be measured, typical values of which are on the order of $5 \cdot 10^{-1}$ for the most significant mirror electrode [27, 99]. Due to drifts in the high voltages forming the mirrors, additional sources of fluctuation are introduced to the measurement, which can significantly worsen the resulting mass resolving power.

This is illustrated in Fig. 3.4, where the flight time of Cr_2^+ cluster ions is monitored for 25 minutes. Even though the experimental cycle is not changed between the individual measurements forming the horizontal slices of the plots, the ions' ToF is clearly subject to long-term drifts. For slow changes in the analyzer's potential configuration with respect to the measurement time, the resulting flight-time changes increase with increasing revolution numbers: The right plot in Fig. 3.4 shows larger ToF fluctuations than the left. The full width at half maximum (FWHM) of the summed signal (top of Fig. 3.4) is a convolution of the intrinsic bunch width Δt in an individual measurement and the magnitude of the drifts. While the former does not significantly increase from 400 to 1600 revolutions in the present case due to the isochronous mirror tune (see Sec. 2.1), the latter does, leading to the FWHM of the summed signal roughly doubling from 200(2) to 382(4) ns. This becomes the primary limiting factor for the device's mass resolving power in longer measurements.

It is possible, however, to correct this type of drift using an additional ion species measured simultaneously to the species of interest [52]. Since both of them experience identical conditions for each measurement, the flight time of the correction ion can be retroactively used to rectify that of the ion of interest. Doing so has become standard practice for precision MR-ToF mass measurements in nuclear physics (see,

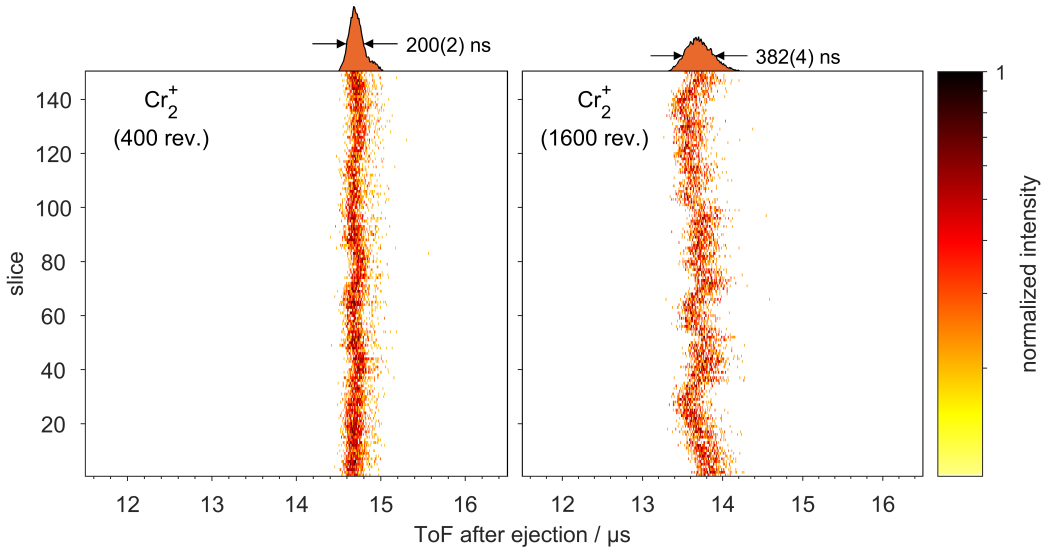

Figure 3.4: ToF spectra from 150 individual 10 s measurements of Cr_2^+ at 400 (left) and 1600 revolutions (right) with the same experimental cycle each.

e.g., [101, 102]) and is typically performed with isobaric correction species that are present as contaminants in radioactive beams. Thus, both species complete the same number of revolutions—and follow identical flight paths—for a given storage time

This thesis demonstrates the use of a correction ion with a significant mass difference to the ion of interest ([103], cumulative thesis article, Sec. 7.3). Consequently, identical storage times lead to different revolution numbers and thus different flight-path lengths. Nevertheless, the ToF drifts of the two species are identical, meaning they are solely dependent on the total flight time. This results from the fact that, for any species with a given revolution period T, changes in the analyzer's potential configuration incur a corresponding period change ΔT. The total ToF shift against some reference after N revolutions consequently amounts to $N\,\Delta T$. Since ΔT scales with the square root of an ion's m/q ratio and the number of completed revolutions for a fixed storage time inversely scales with the same value, the overall ToF shift is itself independent of m/q.

As is shown in [103], this allows virtually any ion that is stored simultaneously to the species of interest to be employed for correction. In cases where no high-abundance isobaric species are present, this can lead to significantly simpler measurements. For the present case of Cr_2^+ isotopologues, only two isobars are observed at the $A = 106$ mass number, namely $^{52}Cr^{54}Cr^+$ and $^{53}Cr_2^+$, which exhibit a relative mass difference of $1.8 \cdot 10^{-5}$. A requirement for retroactive ToF correction is the accumulation of sufficient statistics of the reference in each individual measurement to accurately determine its flight time. Since all $A = 106$ isobars are present in very low abundance, the correction can only be performed using a non-isobaric species. To this end, $^{52}Cr_2^+$ ($A = 104$) and $^{52}Cr^{16}O^+$ ($A = 68$) are employed in two individual runs, both of which yield comparable results. This obviates the need to measure an additional cycle with an "external reference" in an interweaved fashion, which would not be simultaneously and, thus, directly correlate to a loss of statistics per unit of measurement time.

Note that a new development concerning the long-term stability of MR-ToF mirror potentials has been reported recently [104], employing a software-implemented PID controller to actively measure and correct the applied voltages. An extended version of this stabilization has since been incorporated at the Greifswald setup (as briefly reported in [105], cumulative thesis article, Sec. 7.4), the full characterization of which is ongoing.

3.3 Multiple-ejection scheme for single-reference mass determinations

As described above, ion species with large differences in their m/q values will quickly lap one another for increasing MR-ToF storage times. This is especially restrictive for the principal purpose of MR-ToF mass spectrometry: precision mass measurements. For any time-of-flight application, the relation between an ion's mass-to-charge ratio and its flight time t is governed by

$$t = a\sqrt{\frac{m}{q}} + t_0\,, \tag{3.1}$$

where a and t_0 are device-specific parameters. The common offset time t_0 is, for a given mass spectrometer, independent of the ions' flight path. It incorporates any delay between their actual start time and the start of the data acquisition due to, e.g., cable lengths. The a parameter, however, is flight-path dependent and thus, in an MR-ToF device, a function of the revolution number.

To determine both parameters, two independent reference measurements are required, using either two known reference species or the same species at two different revolution numbers [52]. If two species with well-known masses $m_{\mathrm{ref},1}$, $m_{\mathrm{ref},2}$ and flight times $t_{\mathrm{ref},1}$, $t_{\mathrm{ref},2}$ are measured, an unknown mass can be determined as

$$\sqrt{m} = C_{\mathrm{TOF}}\Delta_{\mathrm{ref}} + \frac{\Sigma_{\mathrm{ref}}}{2}\,, \tag{3.2}$$

where

$$\Delta_{\mathrm{ref}} = \sqrt{m_{\mathrm{ref},1}} - \sqrt{m_{\mathrm{ref},2}} \quad \text{and} \tag{3.3}$$

$$\Sigma_{\mathrm{ref}} = \sqrt{m_{\mathrm{ref},1}} + \sqrt{m_{\mathrm{ref},2}} \tag{3.4}$$

are the difference and sum of the square roots of the reference masses and

$$C_{\mathrm{TOF}} = \frac{2t - t_{\mathrm{ref},1} - t_{\mathrm{ref},2}}{2(t_{\mathrm{ref},1} - t_{\mathrm{ref},2})} \tag{3.5}$$

is the experimental observable [80].

However, changes in the offset parameter t_0 are generally expected to be insignificant unless modifications are performed on the setup's signal or trigger lines. Flight-time drifts such as those observed in Fig. 3.4 result from changes in a rather than t_0 (due to changing analyzer potentials). It is thus possible to determine the offset individually—either by manually measuring cable and trigger delays or by employing a single reference measurement with known ions such as performed in, e.g., [101, 102]—and move to a single-reference scheme for mass determinations. As implied by its name, this has the

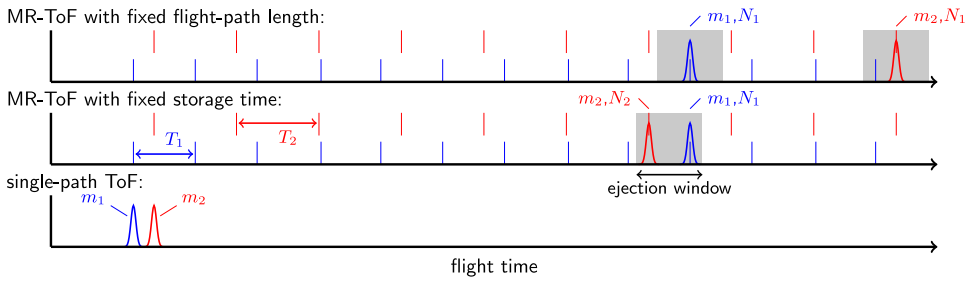

Figure 3.5: Ion flight times for different (MR-)ToF measurement schemes. The colored vertical lines indicate the revolution periods T_1 and T_2 of two ion species with $m_1 < m_2$. The gray boxes indicate the flight-time window that species of different masses can be observed in when ejected after the same storage time [36]. For more information, see text.

benefit of reducing the number of required reference species to one. The mass of an ion of interest is given by

$$m = m_{\mathrm{ref}} \left(\frac{t - t_0}{t_{\mathrm{ref}} - t_0} \right)^2 . \tag{3.6}$$

This is useful in cases where a second species of well-known mass is not available and two experimental cycles at different revolution periods are suboptimal due to the decrease in statistics per unit of measurement time. Ideally, a single-reference setup incorporates only a single experimental cycle, however, it strictly requires both the reference and ion of interest to have completed the same number of laps.

This thesis demonstrates such single-reference mass determinations at identical flight-path lengths in an MR-ToF device. For the first time, the measurements are performed with an ion pair exhibiting a significant mass difference, namely $^{208}\mathrm{Pb}_3^+$ and $^{208}\mathrm{Pb}_4^+$ ([105], cumulative thesis article, Sec. 7.4). In a single-path ToF application, i.e. one without the use of multi-reflection, a mass determination using (3.6) poses no additional challenge if t_0 is known (bottom part of Fig. 3.5). The resolving power and accuracy reached in simple time-of-flight mass spectrometers is, however, insufficient for precision measurements [13, 14]. For typical MR-ToF operation with a fixed storage time (middle part of Fig. 3.5), both species cannot be measured at identical revolution numbers at the same time due to their lapping behavior.

Thus, two separate ejections are performed in [105] to subsequently release the ion species from the MR-ToF analyzer after different storage times (top part of Fig. 3.5). Their flight times after traversing identical flight paths are recorded in a single ToF spectrum with a single experimental cycle, even though the $^{208}\mathrm{Pb}_3^+$ ion bunch initially laps the $^{208}\mathrm{Pb}_4^+$ one over a hundred times. For the present case, the ions' total flight times for the chosen flight-path length of 959 laps roughly amount to 80.32 and 92.75 ms at revolution periods of 83.68 and 96.62 µs, respectively. Since both clusters are formed solely from ^{208}Pb atoms, their mass ratio is very close to 4/3. In fact, the expected ratio, excluding molecular binding energies on the order of 10^{-12}, is $(1-\delta)4/3$, where $\delta = 2.2 \cdot 10^{-7}$ is the mass divergence due to the electron mass. For the present study, the single-reference determination yields $\delta = 0.6(3.0) \cdot 10^{-7}$ for a measurement of about ten minutes and $\delta = 2.3(6) \cdot 10^{-7}$ for a two-hour measurement, matching the expected value.

4 Bismuth-cluster investigations via in-trap photodissociation

Atomic clusters—systems comprised of some number n of atoms of the same or different elements [106, 107]—have been a focus of molecular physics and chemistry ever since the 1980s. Most prominently, R.E. Smalley et al. discovered the very stable C_{60} fullerene associated with a special geometry [108], W.D. Knight et al. found "magic numbers" in sodium clusters associated with electronic shell closures [109], and O. Echt et al. found them in xenon clusters arising from closed geometric shells [110]. All three findings highlight the two main ingredients to a cluster's overall stability: its geometric and electronic configuration.

Present-day cluster research has since advanced to more and more complex systems, especially in the field of doped and compound clusters, i.e. clusters containing more than one element [111–113]. This results from the fact that the number of a cluster's valence electrons is—apart from different charge states—tightly linked to its size n for monoatomic species. A second element can act as a tuning parameter and help disentangle the overall molecule's geometry from its electronic structure.

To measure molecular properties such as fragmentation thresholds or decay constants, two subsequent steps of mass spectrometry are typically applied in what is known as tandem MS, MS/MS or MS^2 [114]. The general principle of such a measurement is outlined in Fig. 4.1: Since the species of interest is often produced together with other, unwanted ions ("contaminants"), a first selective mass-spectrometry stage is needed as a means of preparation. The property of the molecule is probed by some interaction afterwards, e.g. with photons, electrons or other molecules, the reaction products of which are resolved and analyzed using the second MS stage. It follows that the requirements for the specific MS technique in terms of mass resolving power, sensitivity, and permissible mass range are governed by the investigated system.

MR-ToF devices make excellent tools for the study of cluster properties, specifically for the determination of their dissociation pathways as response to photoexcitation (see Sec. 2.2). Product clusters resulting from fragmentation can span large mass ranges,

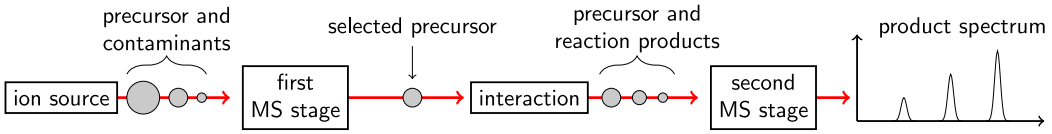

Figure 4.1: Schematic principle of interaction-based MS/MS studies. The first MS stage selects an ion species of interest prior to the interaction, the second one analyzes the reaction products afterwards to yield a spectrum.

making an electrostatic trap a convenient choice. However, the resolving power needed to distinguish between individual products quickly rises beyond several thousands with growing n, especially for doped and compound clusters. So far, electrostatic ion beam traps in cluster research have been mostly operated as such, i.e. without the use of their features as precision mass spectrometers, leaving the increasingly challenging product analysis to be performed externally. High-resolution Fourier transform MR-ToF MS is only suitable for large ion numbers, whereas in practice, cluster production and interaction rates can be very low. In terms of sensitivity and long-term stability, however, conventional MR-ToF MS has already proven itself well adapted for the study of low-abundance, exotic nuclei in radioactive beams. The following sections thus demonstrate the use of an MR-ToF mass spectrometer for high-resolution MS/MS studies in cluster research for the first time.

4.1 Photodissociation of pure bismuth clusters

Photoexcitation has proved itself to be an invaluable tool for the study of cluster properties since the early days of the field. Time-resolved investigations of photodetachment and -dissociation after excitation with defined amounts of energy have been successfully applied to monitor the delayed emission of electrons and atoms from clusters. With that, their internal energy and cooling behavior can be probed [59, 61, 73, 115–117].

Where single atoms can be resonantly excited at discrete energies, clusters are capable of absorbing photons by collective responses of the electronic system referred to as (Mie) plasmons [118, 119]. For large nanoparticles, these allow quasi-continuous excitation, but even small clusters are known to exhibit broad collective resonances [120–122]. Due to the coupling of electronic and ro-vibrational degrees of freedom, the absorbed photon energy thermalizes to the atomic system, where it is available for dissociation processes [59].

Simple metal clusters—those with a strongly metallic character like the ones formed from noble and alkali metals—are known to favor the sequential loss of neutral atoms or dimers as a dissociative cooling channel [123–125], whereas nonmetals and metalloids show further pathways. Carbon clusters, for example, mostly decay by loss of neutral C_3 [126], cationic silicon clusters prefer the formation of Si_6^+ or Si_{12}^+ [127]. The post-transition metals, such as tin, lead, and bismuth (Fig. 4.2), are especially interesting within these considerations: The evolution of their metallic features with their cluster size can be inferred from their dissociation behavior. Due to their closeness to the metal-nonmetal border, these elements tend to change their behavior as they grow: lead clusters show the loss of neutral Pb_7 [128] and tin clusters that of neutral Sn_7 and Sn_{10} [129] above certain threshold sizes. For large clusters, however, monomer evaporation takes over in both cases, exemplifying the materials' evolution towards their metallic bulk character.

As the heaviest naturally-occurring post-transition metal save for the trace radioisotope ^{210}Po, bismuth shows the same metal-to-nonmetal alteration as its lighter neighbors, found, e.g., as a phase transition in thin films [131]. Prior to this thesis, however, experimental data on Bi-cluster dissociation has been sparse, amounting to the size range $n = 2$ through 14 for the cationic species [132–135] and none for the anionic one.

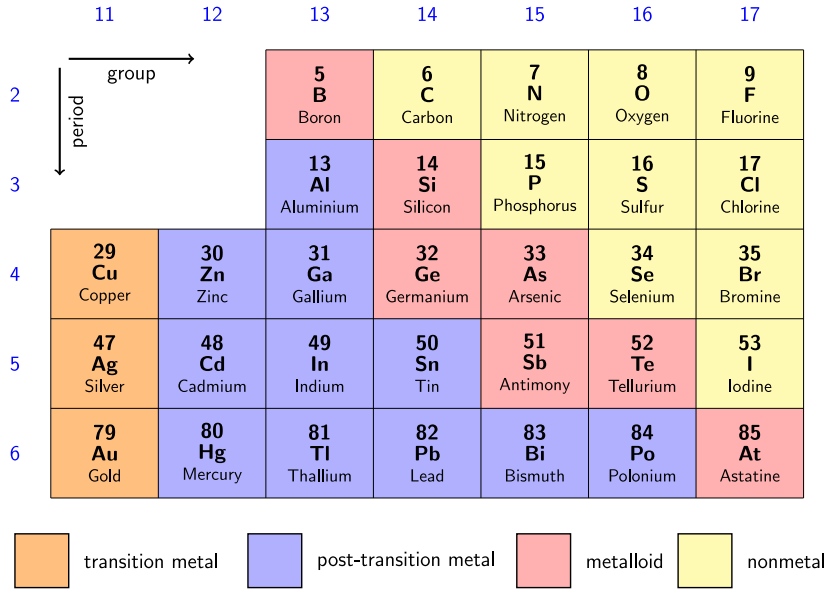

Figure 4.2: Post-transition metals as classified by J.E. Huheey [130] and their surrounding elements in the periodic table.

The $n = 8$ cluster size has been found as a crucial threshold at which a dominant cooling channel via the loss of neutral tetramers Bi_4 opens up. In this thesis, the probed range is extended substantially, as the sizes $n = 2$–19 are investigated for both ion polarities ([136], cumulative thesis article, Sec. 7.5).

To this end, a novel type of photoexcitation scheme has been developed, making use of the MR-ToF analyzer for both the selection and product-analysis step of the tandem MS investigation and slotting an in-trap excitation in between. The selected precursor is stored for some hundreds of revolutions, which allows its separation from all species with $\Delta m \geq 1\,\mathrm{u}$. This amounts to a selection resolving power of 4000 for the case of the heaviest ion of interest, Pb_{19}, and is necessary to prevent contamination from low-abundant Bi-Pb compound species. Photoexcitation is subsequently performed without ejecting the precursor, using the second harmonic of a Nd:YAG laser ($\lambda = 532\,\mathrm{nm}$, 6 ns pulse duration) guided through the analyzer coaxially. Care is taken to time the laser pulse with respect to the precursor's revolution period, according to the following considerations:

The kinetic energies of a pair of fragment and precursor ions with identical charge states are given by

$$E_{\mathrm{kin,f}} = \frac{m_\mathrm{f}}{2} v_\mathrm{f}^2 \quad \text{and} \tag{4.1}$$

$$E_{\mathrm{kin,p}} = \frac{m_\mathrm{p}}{2} v_\mathrm{p}^2\,, \tag{4.2}$$

respectively, where v_f and v_p are their particular velocities. In-flight dissociation will lead to all fragments retaining the precursor's velocity. It follows that their kinetic

energy reduces according to the mass ratio of both species, i.e.

$$E_{\mathrm{kin,f}} = \frac{m_{\mathrm{f}}}{m_{\mathrm{p}}} E_{\mathrm{kin,p}} \,. \tag{4.3}$$

Since electrostatic systems are energy-selective by nature, different fragment species will thus exhibit different trajectories and might not be properly focused towards the detector. For any post-excitation MR-ToF storage (see next section), a change in kinetic energy almost guarantees the loss of coherent bunches, as can be inferred from Fig. 2.4.

The nature of the MR-principle, however, can also be used to circumvent this problem: The photoexcitation is timed to the precursor's turn-around point in one of the mirror potentials, where its kinetic energy is sufficiently close to zero for a short time. All (prompt) fragment ions are produced with a kinetic energy of (close to) zero, leading to total energies identical to that of the precursor regardless of mass. For the measurements performed in [136], the exit-side mirror potential is opened simultaneously to the ions' photoexciation in the entrance-side mirror, allowing all fragment species to be recorded within a single spectrum. The overall experimental cycle can be described as MR-ToF/ToF MS.

The results obtained in the present study show the prominent Bi_4 loss channel for both ion polarities. This matches up with the narrative that the pathway results in large parts from the exceptional stability of the neutral tetramer itself [137–139]. However, discrepancies between the fragment spectra of same-size cat- and anion precursors suggest the configuration of the charged fragment as a second defining factor. For larger clusters, strong evidence for the breakoff of even bigger neutral fragments—namely the neutral bismuth octamer Bi_8—is found. Although this cannot be conclusively disentangled from a possible sequential tetramer loss within the present data set, multiple large neutrals acting as competing dissociation channels is not atypical for post-transition-metal clusters such as tin, as stated above.

4.2 Change in dissociation pathways from lead doping

The complexity of bimetallic systems increases the challenge for gaining experimental access, both to their production and their separation. Sophisticated dual-target sources for gas-phase compound clusters have been employed in the past, allowing control over individual production rates and mixing ratios [140–143]. However, metal-alloy targets provide a simple alternative [144–146], which is made use of in this thesis to produce lead-doped bismuth clusters ([147], cumulative thesis article, Sec. 7.6). The dissociation behavior of these systems has not yet been studied experimentally, as the mass difference of only one atomic mass unit between the elements' stable isotopes demands high resolving powers for both precursor separation and fragment analysis.

Yet, Bi-Pb compound species offer auspicious insights into the behavior of doped systems, as lead and bismuth are direct neighbors in the periodic table. Both elements are classified as post-transition metals with similar bulk properties. However, while bismuth possesses five valence electrons (s^2p^3 configuration), lead only has four (s^2p^2 configuration). This makes their compounds prime candidates for the study of changing molecular properties resulting from slight differences in overall composition.

As a first case of interest, the cationic bismuth octamer $^{209}Bi_8^+$ is compared to its doped equivalent, $^{209}Bi_7{}^{208}Pb^+$. For the pure species, $n = 8$ marks the first cluster size at which neutral tetramer breakoff constitutes the most abundant dissociation pathway [136]. This changes for the doped system. Here, the $n = 6$ fragment, which is least abundant in the Bi_8^+ spectrum, becomes most abundant. To fully investigate the effects of the lead atom, however, the resolving power of the fragment spectrum has to be increased to separate the pure and doped species for each fragment size. Consequently, the MR-ToF analyzer is employed for the second MS stage as well, resulting in a seamless ion confinement from the capture of the precursor over the photoexcitation up to the fragment ejection after some additional post-excitation storage time. This MR-ToF/MR-ToF MS cycle allows the determination of the Bi_7Pb^+ ion's full dissociation behavior.

The $n = 6$ fragment size is revealed to consist of 95% Bi_5Pb^+ and only 5% Bi_6^+. In fact, the overall abundance of Bi_6^+ (respective to all detected fragment ions) is only 2% and thus roughly comparable to the 6% it represents in the pure precursor's fragment spectrum. However, the additional degree of freedom provided by the lead atom opens strongly preferential dissociation pathways: due to the valence-electron difference of lead and bismuth, both the neutral and charged fragment can simultaneously exhibit even electron numbers, something that is not possible for dissociation from Bi_8^+. This effect is so pervasive that it outstrips the neutral tetramer breakoff dominating the pure species.

Since only the case of Bi_7Pb^+ is investigated in [147], it is not yet possible to assess the effect of lead doping for the overall dissociation behavior of bismuth clusters. More precursor sizes together with other doping ratios and species will have to be probed for a comprehensive picture, something for which high-resolution MR-ToF/MR-ToF MS and the Greifswald setup in particular is especially suited for.

5 Conclusion and outlook

This thesis presents advancements in multi-reflection time-of-flight mass spectrometry for the study of ions with large masses and mass differences. Several novel techniques for wide-band applications are introduced and the molecular properties of atomic clusters are probed with a new photoexcitation measurement scheme. This marks the first use of MR-ToF MS for cluster research and the first photodissociation study of anionic bismuth clusters. Additionally, the lead-doped Bi_7Pb^+ cluster is probed, representing a challenging compound-cluster species due to the small mass difference between the involved elements. High-resolution tandem MR-ToF mass spectrometry is demonstrated to be a powerful new addition to the ever-growing toolbox of multi-reflection devices.

In the future, the experimental portfolio at the Greifswald MR-ToF setup is planned to be further expanded to new cluster species. The regime of doped clusters is of particular interest, especially for compounds that may be difficult to access with other techniques. Photodissociation studies are also expected to incorporate photon-energy variation with a tuneable laser to better disentangle competing pathways. This is crucial for the determination of fragmentation and detachment threshold energies.

Closely related, the investigation of delayed cooling channels is known to be an exceptional gateway to monitor a cluster's internal distribution of energies. Such channels have in fact been observed during the present measurements, as briefly noted in [136]. The periodic nature of the MR-ToF analyzer offers unique possibilities for

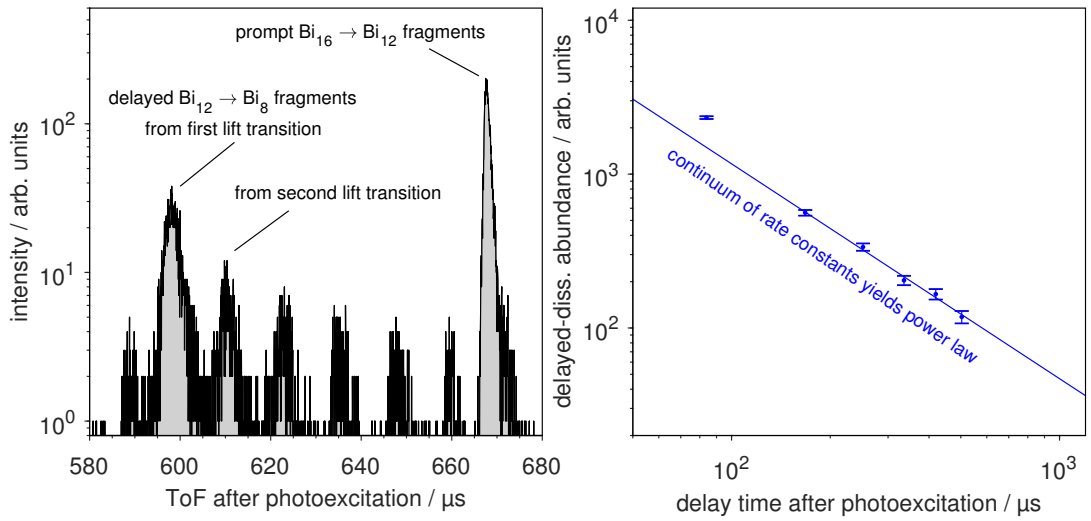

Figure 5.1: Delayed $Bi_{12}^- \rightarrow Bi_8^-$ after prompt $Bi_{16}^- \rightarrow Bi_{12}^-$ fragmentation as response to photoexcitation at 532 nm. A single ToF spectrum after several post-excitation Bi_{12}^- revolutions shows multiple delayed Bi_8^- signals (left), the abundances of which can be approximated by a power law (right). Investigation of this behavior is ongoing.

the study of these pathways, which is illustrated by preliminary results in Fig. 5.1: A revolving ion bunch with a dissociation time constant far larger than its revolution period will lead to multiple fragment signals. These can be matched to the precursor's transitions through the in-trap lift, as fragment ions produced within will retain their velocity rather than energy. The respective signals of the delayed fragments will thus accumulate flight-time shifts with each subsequent revolution, leading to a comb-like structure after some number of laps. The intensity ratio between the individual signals allows conclusions about the clusters' internal energy. For example, the presence of multiple rate constants results in a power-law behavior [61, 115], as is observed in the present case. Future studies of these effects also require adjustable photon energies for a better control over the probed energy ranges.

6 Bibliography

[1] J. J. Thomson. Bakerian Lecture: Rays of positive electricity. *Proc. R. Soc. Lond. Ser. A*, 89(607):1–20, 1913. doi:10.1098/rspa.1913.0057.

[2] J. J. Thomson. *Recollections and Reflections*. G. Bell and Sons Ltd., 1936.

[3] F. W. Aston. Atoms and their Packing Fractions. *Nature*, 120:956–959, 1927. doi:10.1038/120956a0.

[4] A. J. Dempster. A new Method of Positive Ray Analysis. *Phys. Rev.*, 11:316–325, 1918. doi:10.1103/PhysRev.11.316.

[5] J. Mattauch and R. Herzog. Über einen neuen Massenspektrographen. *Z. Phys.*, 89(11):786–795, 1934. doi:10.1007/BF01341392.

[6] W. Paul and H. Steinwedel. Ein neues Massenspektrometer ohne Magnetfeld. *Z. Naturforsch. A*, 8:448–450, 1953. doi:10.1515/zna-1953-0710.

[7] L. S. Brown and G. Gabrielse. Geonium theory: Physics of a single electron or ion in a Penning trap. *Rev. Mod. Phys.*, 58:233–311, 1986. doi:10.1103/RevModPhys.58.233.

[8] R. Stensgaard. ASTRID - The Aarhus Storage Ring. *Phys. Scripta*, T22:315–317, 1988. doi:10.1088/0031-8949/1988/t22/051.

[9] D. Habs, W. Baumann, J. Berger, P. Blatt, A. Faulstich, P. Krause, G. Kilgus, R. Neumann, W. Petrich, R. Stokstad, D. Schwalm, E. Szmola, K. Welti, A. Wolf, S. Zwickler, E. Jaeschke, D. Krämer, G. Bisoffi, M. Blum, A. Friedrich, C. Geyer, M. Grieser, H. W. Heyng, B. Holzer, R. Ihde, M. Jung, K. Matl, W. Ott, B. Povh, R. Repnow, M. Steck, E. Steffens, D. Dutta, T. Kühl, D. Marx, S. Schröder, M. Gerhard, R. Grieser, G. Huber, R. Klein, M. Krieg, N. Schmidt, R. Schuch, J. F. Babb, L. Spruch, W. Arnold, and A. Noda. First experiments with the heidelberg test storage ring TSR. *Nucl. Instrum. Meth. B*, 43(3):390–410, 1989. doi:10.1016/0168-583X(89)90383-2.

[10] K. Abrahamsson, G. Andler, L. Bagge, E. Beebe, P. Carlé, H. Danared, S. Egnell, K. Ehrnstén, M. Engström, C. J. Herrlander, J. Hilke, J. Jeansson, A. Källberg, S. Leontein, L. Liljeby, A. Nilsson, A. Paal, K.-G. Rensfelt, U. Rosengård, A. Simonsson, A. Soltan, J. Starker, M. af Ugglas, and A. Filevich. CRYRING — a synchrotron, cooler and storage ring. *Nucl. Instrum. Meth. B*, 79(1):269–272, 1993. doi:10.1016/0168-583X(93)95341-2.

[11] R. J. Cotter. *Time-of-flight Mass Spectrometry: Instrumentation and Applications in Biological Research.* American Chemical Society, 1997.

[12] A. E. Cameron and D. F. Eggers. An Ion "Velocitron". *Rev. Sci. Instrum.*, 19(9):605–607, 1948. doi:10.1063/1.1741336.

[13] W. C. Wiley and I. H. McLaren. Time-of-Flight Mass Spectrometer with Improved Resolution. *Rev. Sci. Instrum.*, 26(12):1150–1157, 1955. doi:10.1063/1.1715212.

[14] B. A. Mamyrin, V. I. Karataev, D. V. Shmikk, and V. A. Zagulin. The mass-reflectron, a new nonmagnetic time-of-flight mass spectrometer with high resolution. *Zh. Eksp. Teor. Fiz.*, 64:82, 1973.

[15] H. Wollnik and M. Przewloka. Time-of-flight mass spectrometers with multiply reflected ion trajectories. *Int. J. Mass Spectrom.*, 96(3):267–274, 1990. doi:10.1016/0168-1176(90)85127-N.

[16] W. Tretner. An electrostatic mass spectroscope. *Vacuum*, 10(1):31–34, 1960. doi:10.1016/0042-207X(60)90104-4.

[17] D. Zajfman, O. Heber, L. Vejby-Christensen, I. Ben-Itzhak, M. Rappaport, R. Fishman, and M. Dahan. Electrostatic bottle for long-time storage of fast ion beams. *Phys. Rev. A*, 55:R1577–R1580, 1997. doi:10.1103/PhysRevA.55.R1577.

[18] W. H. Benner. A Gated Electrostatic Ion Trap To Repetitiously Measure the Charge and m/z of Large Electrospray Ions. *Anal. Chem.*, 69(20):4162–4168, 1997. doi:10.1021/ac970163e.

[19] D. Zajfman, Y. Rudich, I. Sagi, D. Strasser, D. W. Savin, S. Goldberg, M. Rappaport, and O. Heber. High resolution mass spectrometry using a linear electrostatic ion beam trap. *Int. J. Mass Spectrom.*, 229(1):55–60, 2003. doi:10.1016/S1387-3806(03)00255-0.

[20] T. Suzuki and Y. Yamauchi. Electrostatic linear ion trap for low-energy ion beam storage. *Nucl. Instrum. Meth. A*, 562(1):53–56, 2006. doi:10.1016/j.nima.2006.02.196.

[21] R. T. Hilger, P. J. Wyss, R. E. Santini, and S. A. McLuckey. Absorption Mode Fourier Transform Electrostatic Linear Ion Trap Mass Spectrometry. *Anal. Chem.*, 85(17):8075–8079, 2013. doi:10.1021/ac401935e.

[22] E. T. Dziekonski, R. E. Santini, and S. A. McLuckey. A dual detector Fourier transform electrostatic linear ion trap utilizing in-trap potential lift. *Int. J. Mass Spectrom.*, 405:1–8, 2016. doi:10.1016/j.ijms.2016.05.010.

[23] R. L. Hettich. Structural investigations of aluminum cluster ions, Al_n^- (n=3-50). *J. Am. Chem. Soc.*, 111(23):8582–8588, 1989. doi:10.1021/ja00205a004.

[24] A. Drescher, J. Kitching, J. E. Crawford, J. K. P. Lee, and G. Thekkadath. Studies of Sb and Bi cluster produced by laser desorption. *Z. Phys. D*, 19(4):203–206, 1991. doi:10.1007/BF01448292.

[25] H. S. Kim, T. D. Wood, A. G. Marshall, and J. Lee. Production of gold cluster ions by laser desorption/ionization Fourier-transform ion cyclotron resonance mass spectrometry. *Chem. Phys. Lett.*, 224(5):589–594, 1994. doi:10.1016/0009-2614(94)00584-2.

[26] C. Stoermer, J. Friedrich, and M. M. Kappes. Observation of multiply charged cluster anions upon pulsed UV laser ablation of metal surfaces under high vacuum. *Int. J. Mass Spectrom.*, 206(1):63–78, 2001. doi:10.1016/S1387-3806(00)00390-0.

[27] S. Knauer, P. Fischer, G. Marx, M. Müller, M. Rosenbusch, B. Schabinger, L. Schweikhard, and R. N. Wolf. A multi-reflection time-of-flight setup for the improvement and development of new methods and the study of atomic clusters. *Int. J. Mass Spectrom.*, 446:116189, 2019. doi:10.1016/j.ijms.2019.116189.

[28] P. Schury, M. Wada, Y. Ito, F. Arai, S. Naimi, T. Sonoda, H. Wollnik, V. A. Shchepunov, C. Smorra, and C. Yuan. A high-resolution multi-reflection time-of-flight mass spectrograph for precision mass measurements at RIKEN/SLOWRI. *Nucl. Instrum. Meth. B*, 335:39–53, 2014. doi:10.1016/j.nimb.2014.05.016.

[29] T. Dickel, W. R. Plaß, A. Becker, U. Czok, H. Geissel, E. Haettner, C. Jesch, W. Kinsel, M. Petrick, C. Scheidenberger, A. Simon, and M. I. Yavor. A high-performance multiple-reflection time-of-flight mass spectrometer and isobar separator for the research with exotic nuclei. *Nucl. Instrum. Meth. A*, 777:172–188, 2015. doi:10.1016/j.nima.2014.12.094.

[30] F. Wienholtz, D. Atanasov, S. Kreim, V. Manea, M. Rosenbusch, L. Schweikhard, A. Welker, and R. N. Wolf. Towards ultrahigh-resolution multi-reflection time-of-flight mass spectrometry at ISOLTRAP. *Phys. Scripta*, T166:014068, 2015. doi:10.1088/0031-8949/2015/t166/014068.

[31] R. N. Wolf, G. Marx, M. Rosenbusch, and L. Schweikhard. Static-mirror ion capture and time focusing for electrostatic ion-beam traps and multi-reflection time-of-flight mass analyzers by use of an in-trap potential lift. *Int. J. Mass Spectrom.*, 313:8–14, 2012. doi:10.1016/j.ijms.2011.12.006.

[32] M. Rosenbusch, S. Kemnitz, R. Schneider, L. Schweikhard, R. Tschiersch, and R. N. Wolf. Towards systematic investigations of space-charge phenomena in multi-reflection ion traps. *AIP Conf. Proc.*, 1521(1):53–62, 2013. doi:10.1063/1.4796061.

[33] P. Chauveau, P. Delahaye, G. De France, S. El Abir, J. Lory, Y. Merrer, M. Rosenbusch, L. Schweikhard, and R. N. Wolf. PILGRIM, a Multi-Reflection Time-of-Flight Mass Spectrometer for Spiral2-S^3 at GANIL. *Nucl. Instrum. Meth. B*, 376:211–215, 2016. doi:10.1016/j.nimb.2016.01.025.

[34] T. Y. Hirsh, N. Paul, M. Burkey, A. Aprahamian, F. Buchinger, S. Caldwell, J. A. Clark, A. F. Levand, L. L. Ying, S. T. Marley, G. E. Morgan, A. Nystrom, R. Orford, A. P. Galván, J. Rohrer, G. Savard, K. S. Sharma, and K. Siegl. First operation and mass separation with the CARIBU MR-TOF. *Nucl. Instrum. Meth. B*, 376:229–232, 2016. doi:10.1016/j.nimb.2015.12.037.

[35] S. Sels, P. Fischer, H. Heylen, V. Lagaki, S. Lechner, F. M. Maier, P. Plattner, M. Rosenbusch, F. Wienholtz, R. N. Wolf, W. Nörtershäuser, L. Schweikhard, and S. Malbrunot-Ettenauer. First steps in the development of the Multi Ion Reflection Apparatus for Collinear Laser Spectroscopy (in press). *Nucl. Instrum. Meth. B*, 2019. doi:10.1016/j.nimb.2019.04.076.

[36] S. Knauer, P. Fischer, G. Marx, B. Schabinger, L. Schweikhard, and R. N. Wolf. Multi-reflection time-of-flight mass spectrometry with combined in-trap lift capture and mirror-switch ejection. *Int. J. Mass Spectrom.*, 423:46–53, 2017. doi:10.1016/j.ijms.2017.10.007.

[37] A. Yariv. *Quantum electronics*, page 142. Wiley, 1989.

[38] M. Dahan, R. Fishman, O. Heber, M. Rappaport, N. Altstein, D. Zajfman, and W. J. van der Zande. A new type of electrostatic ion trap for storage of fast ion beams. *Rev. Sci. Instrum.*, 69(1):76–83, 1998. doi:10.1063/1.1148481.

[39] H. B. Pedersen, D. Strasser, O. Heber, M. L. Rappaport, and D. Zajfman. Stability and loss in an ion-trap resonator. *Phys. Rev. A*, 65:042703, 2002. doi:10.1103/PhysRevA.65.042703.

[40] M. Lange, M. Froese, S. Menk, J. Varju, R. Bastert, K. Blaum, J. R. Crespo López-Urrutia, F. Fellenberger, M. Grieser, R. von Hahn, O. Heber, K.-U. Kühnel, F. Laux, D. A. Orlov, M. L. Rappaport, R. Repnow, C. D. Schröter, D. Schwalm, A. Shornikov, T. Sieber, Y. Toker, J. Ullrich, A. Wolf, and D. Zajfman. A cryogenic electrostatic trap for long-time storage of keV ion beams. *Rev. Sci. Instrum.*, 81(5):055105, 2010. doi:10.1063/1.3372557.

[41] A. Makarov. Electrostatic Axially Harmonic Orbital Trapping: A High-Performance Technique of Mass Analysis. *Anal. Chem.*, 72(6):1156–1162, 2000. doi:10.1021/ac991131p.

[42] K. H. Kingdon. A Method for the Neutralization of Electron Space Charge by Positive Ionization at Very Low Gas Pressures. *Phys. Rev.*, 21:408–418, 1923. doi:10.1103/PhysRev.21.408.

[43] F. M. Maier, P. Fischer, H. Heylen, V. Lagaki, S. Lechner, P. Plattner, S. Sels, F. Wienholtz, W. Nörtershäuser, L. Schweikhard, and S. Malbrunot-Ettenauer. Simulations of a proof-of-principle experiment for collinear laser spectroscopy within a multi-reflection time-of-flight device. *Hyperfine Interact.*, 240(1):54, 2019. doi:10.1007/s10751-019-1575-x.

[44] S. P. Møller. ELISA, an electrostatic storage ring for atomic physics. *Nucl. Instrum. Meth. A*, 394(3):281–286, 1997. doi:10.1016/S0168-9002(97)00673-6.

[45] R. D. Thomas, H. T. Schmidt, G. Andler, M. Björkhage, M. Blom, L. Brännholm, E. Bäckström, H. Danared, S. Das, N. Haag, P. Halldén, F. Hellberg, A. I. S. Holm, H. A. B. Johansson, A. Källberg, G. Källersjö, M. Larsson, S. Leontein, L. Liljeby, P. Löfgren, B. Malm, S. Mannervik, M. Masuda, D. Misra, A. Orbán,

A. Paál, P. Reinhed, K.-G. Rensfelt, S. Rosén, K. Schmidt, F. Seitz, A. Simonsson, J. Weimer, H. Zettergren, and H. Cederquist. The double electrostatic ion ring experiment: A unique cryogenic electrostatic storage ring for merged ion-beams studies. *Rev. Sci. Instrum.*, 82(6):065112, 2011. doi:10.1063/1.3602928.

[46] Y. Nakano, W. Morimoto, T. Majima, J. Matsumoto, H. Tanuma, H. Shiromaru, and T. Azuma. A cryogenic electrostatic storage ring project at RIKEN. *J. Phys. Conf. Ser.*, 388(14):142027, 2012. doi:10.1088/1742-6596/388/14/142027.

[47] R. von Hahn, A. Becker, F. Berg, K. Blaum, C. Breitenfeldt, H. Fadil, F. Fellenberger, M. Froese, S. George, J. Göck, M. Grieser, F. Grussie, E. A. Guerin, O. Heber, P. Herwig, J. Karthein, C. Krantz, H. Kreckel, M. Lange, F. Laux, S. Lohmann, S. Menk, C. Meyer, P. M. Mishra, O. Novotný, A. P. O'Connor, D. A. Orlov, M. L. Rappaport, R. Repnow, S. Saurabh, S. Schippers, C. D. Schröter, D. Schwalm, L. Schweikhard, T. Sieber, A. Shornikov, K. Spruck, S. Sunil Kumar, J. Ullrich, X. Urbain, S. Vogel, P. Wilhelm, A. Wolf, and D. Zajfman. The cryogenic storage ring CSR. *Rev. Sci. Instrum.*, 87(6):063115, 2016. doi:10.1063/1.4953888.

[48] A. Wolf. *Heavy-Ion Storage Rings*, pages 3–29. Springer Berlin Heidelberg, 1999. doi:10.1007/978-3-642-58580-7_1.

[49] S. Earnshaw. On the Nature of the Molecular Forces which Regulate the Constitution of the Luminiferous Ether. *Trans. Camb. Phil. Soc.*, 7:97–112, 1842.

[50] H. B. Pedersen, D. Strasser, B. Amarant, O. Heber, M. L. Rappaport, and D. Zajfman. Diffusion and synchronization in an ion-trap resonator. *Phys. Rev. A*, 65:042704, 2002. doi:10.1103/PhysRevA.65.042704.

[51] D. Zajfman, D. Strasser, O. Heber, S. Goldberg, A. Diner, and M. L. Rappaport. Dynamics of stored ions in an electrostatic ion beam trap. *Nucl. Instrum. Meth. A*, 532(1):196–202, 2004. doi:10.1016/j.nima.2004.06.045.

[52] R. N. Wolf, F. Wienholtz, D. Atanasov, D. Beck, K. Blaum, Ch. Borgmann, F. Herfurth, M. Kowalska, S. Kreim, Yu. A. Litvinov, D. Lunney, V. Manea, D. Neidherr, M. Rosenbusch, L. Schweikhard, J. Stanja, and K. Zuber. ISOLTRAP's multi-reflection time-of-flight mass separator/spectrometer. *Int. J. Mass Spectrom.*, 349-350:123–133, 2013. doi:10.1016/j.ijms.2013.03.020.

[53] H. Wollnik and A. Casares. An energy-isochronous multi-pass time-of-flight mass spectrometer consisting of two coaxial electrostatic mirrors. *Int. J. Mass Spectrom.*, 227(2):217–222, 2003. doi:10.1016/S1387-3806(03)00127-1.

[54] H. B. Pedersen, D. Strasser, S. Ring, O. Heber, M. L. Rappaport, Y. Rudich, I. Sagi, and D. Zajfman. Ion Motion Synchronization in an Ion-Trap Resonator. *Phys. Rev. Lett.*, 87:055001, 2001. doi:10.1103/PhysRevLett.87.055001.

[55] D. Strasser, T. Geyer, H. B. Pedersen, O. Heber, S. Goldberg, B. Amarant, A. Diner, Y. Rudich, I. Sagi, M. Rappaport, D. J. Tannor, and D. Zajfman. Negative Mass

Instability for Interacting Particles in a 1D Box: Theory and Application. *Phys. Rev. Lett.*, 89:283204, 2002. doi:10.1103/PhysRevLett.89.283204.

[56] P. A. Bolotskikh, D. E. Grinfeld, A. A. Makarov, and M. A. Monastyrskiy. Coulomb dynamics of ion bunches in multi-reflection electrostatic traps. *Nucl. Instrum. Meth. A*, 645(1):146–152, 2011. doi:10.1016/j.nima.2010.12.170.

[57] C. Breitenfeldt, M. W. Froese, K. Blaum, S. George, M. Grieser, M. Lange, S. Menk, R. Repnow, D. Schwalm, L. Schweikhard, R. von Hahn, and A. Wolf. Spreading times of ion-bunches in the Cryogenic Trap for Fast ion beams. *Int. J. Mass Spectrom.*, 396:1–4, 2016. doi:10.1016/j.ijms.2015.11.011.

[58] A. G. Marshall, C. L. Hendrickson, and G. S. Jackson. Fourier transform ion cyclotron resonance mass spectrometry: A primer. *Mass Spectrom. Rev.*, 17(1):1–35, 1998. doi:10.1002/(SICI)1098-2787(1998)17:1<1::AID-MAS1>3.0.CO;2-K.

[59] O. Aviv, Y. Toker, D. Strasser, M. L. Rappaport, O. Heber, D. Schwalm, and D. Zajfman. Competition between delayed ionization and fragmentation of laser-excited Al_4^-. *Phys. Rev. A*, 83:023201, 2011. doi:10.1103/PhysRevA.83.023201.

[60] O. Aviv, B. Kafle, V. Chandrasekaran, O. Heber, M. L. Rappaport, H. Rubinstein, D. Schwalm, D. Strasser, Y. Toker, and D. Zajfman. Absolute photo-destruction and photo-fragmentation cross section measurements using an electrostatic ion beam trap. *Rev. Sci. Instrum.*, 84(5):053106, 2013. doi:10.1063/1.4804646.

[61] C. Breitenfeldt, K. Blaum, S. George, J. Göck, G. Guzmán-Ramírez, J. Karthein, T. Kolling, M. Lange, S. Menk, C. Meyer, J. Mohrbach, G. Niedner-Schatteburg, D. Schwalm, L. Schweikhard, and A. Wolf. Long-Term Monitoring of the Internal Energy Distribution of Isolated Cluster Systems. *Phys. Rev. Lett.*, 120:253001, 2018. doi:10.1103/PhysRevLett.120.253001.

[62] O. Heber, P. D. Witte, A. Diner, K. G. Bhushan, D. Strasser, Y. Toker, M. L. Rappaport, I. Ben-Itzhak, N. Altstein, D. Schwalm, A. Wolf, and D. Zajfman. Electrostatic ion beam trap for electron collision studies. *Rev. Sci. Instrum.*, 76(1):013104, 2005. doi:10.1063/1.1832192.

[63] O. Aviv, Y. Toker, M. Errit, K. G. Bhushan, H. B. Pedersen, M. L. Rappaport, O. Heber, D. Schwalm, and D. Zajfman. A bent electrostatic ion beam trap for simultaneous measurements of fragmentation and ionization of cluster ions. *Rev. Sci. Instrum.*, 79(8):083110, 2008. doi:10.1063/1.2972151.

[64] K. G. Bhushan, S. C. Gadkari, J. V. Yakhmi, and V. C. Sahni. Electrostatic ion trap and fourier transform measurements for high-resolution mass spectrometry. *Rev. Sci. Instrum.*, 78(8):083302, 2007. doi:10.1063/1.2777195.

[65] A. Gumberidze, D. Attia, C. I. Szabo, P. Indelicato, A. Vallette, and S. Carmo. Trapping of highly charged ions with an electrostatic ion trap. *J. Phys. Conf. Ser.*, 163:012110, 2009. doi:10.1088/1742-6596/163/1/012110.

[66] T. Doussineau, C. Yu Bao, C. Clavier, X. Dagany, M. Kerleroux, R. Antoine, and P. Dugourd. Infrared multiphoton dissociation tandem charge detection-mass spectrometry of single megadalton electrosprayed ions. *Rev. Sci. Instrum.*, 82(8):084104, 2011. doi:10.1063/1.3628667.

[67] J. B. Greenwood, O. Kelly, C. R. Calvert, M. J. Duffy, R. B. King, L. Belshaw, L. Graham, J. D. Alexander, I. D. Williams, W. A. Bryan, I. C. E. Turcu, C. M. Cacho, and E. Springate. A comb-sampling method for enhanced mass analysis in linear electrostatic ion traps. *Rev. Sci. Instrum.*, 82(4):043103, 2011. doi:10.1063/1.3572331.

[68] C. J. Johnson, B. B. Shen, B. L. J. Poad, and R. E. Continetti. Photoelectron-photofragment coincidence spectroscopy in a cryogenically cooled linear electrostatic ion beam trap. *Rev. Sci. Instrum.*, 82(10):105105, 2011. doi:10.1063/1.3641875.

[69] R. T. Hilger, R. E. Santini, and S. A. McLuckey. Nondestructive Tandem Mass Spectrometry Using a Linear Quadrupole Ion Trap Coupled to a Linear Electrostatic Ion Trap. *Anal. Chem.*, 85(10):5226–5232, 2013. doi:10.1021/ac4007182.

[70] J. A. Hogan and M. F. Jarrold. Optimized Electrostatic Linear Ion Trap for Charge Detection Mass Spectrometry. *J. Am. Soc. Mass Spectrom.*, 29(10):2086–2095, 2018. doi:10.1007/s13361-018-2007-x.

[71] C. J. Johnson and R. E. Continetti. Dissociative Photodetachment Studies of Cooled $HOCO^-$ Anions Revealing Dissociation Below the Barrier to H + CO_2. *J. Phys. Chem. Lett.*, 1(12):1895–1899, 2010. doi:10.1021/jz100621k.

[72] B. B. Shen, B. L. J. Poad, and R. E. Continetti. Photoelectron-Photofragment Coincidence studies of the tert-Butoxide Anion $(CH_3)_3CO^-$, the Carbanion Isomer $(CH_3)_2CH_2COH^-$, and Corresponding Radicals. *J. Phys. Chem. A*, 118(44):10223–10232, 2014. doi:10.1021/jp5090235.

[73] B. Kafle, O. Aviv, V. Chandrasekaran, O. Heber, M. L. Rappaport, H. Rubinstein, D. Schwalm, D. Strasser, and D. Zajfman. Electron detachment and fragmentation of laser-excited rotationally hot Al_4^-. *Phys. Rev. A*, 92:052503, 2015. doi:10.1103/PhysRevA.92.052503.

[74] M. Eritt, A. Diner, Y. Toker, O. Aviv, O. Heber, M. L. Rappaport, and D. Zajfman. Size effects in the interaction between ionic clusters and low-energy electrons. *Phys. Scripta*, 73(1):C32–C35, 2005. doi:10.1088/0031-8949/73/1/n06.

[75] O. Heber, R. Golser, H. Gnaser, D. Berkovits, Y. Toker, M. Eritt, M. L. Rappaport, and D. Zajfman. Lifetimes of the negative molecular hydrogen ions: H_2^-, D_2^-, and HD^-. *Phys. Rev. A*, 73:060501, 2006. doi:10.1103/PhysRevA.73.060501.

[76] Y. Toker, I. Rahinov, D. Schwalm, U. Even, O. Heber, M. L. Rappaport, D. Strasser, and D. Zajfman. Blackbody-induced radiative dissociation of cationic SF_6 clusters. *Phys. Rev. A*, 86:023202, 2012. doi:10.1103/PhysRevA.86.023202.

[77] S. Menk, S. Das, K. Blaum, M. W. Froese, M. Lange, M. Mukherjee, R. Repnow, D. Schwalm, R. von Hahn, and A. Wolf. Vibrational autodetachment of sulfur hexafluoride anions at its long-lifetime limit. *Phys. Rev. A*, 89:022502, 2014. doi:10.1103/PhysRevA.89.022502.

[78] S. Ring, H. B. Pedersen, O. Heber, M. L. Rappaport, P. D. Witte, K. G. Bhushan, N. Altstein, Y. Rudich, I. Sagi, and D. Zajfman. Fourier transform time-of-flight mass spectrometry in an electrostatic ion beam trap. *Analytical Chemistry*, 72(17):4041–4046, 2000. doi:10.1021/ac000317h.

[79] R. N. Wolf, D. Beck, K. Blaum, Ch. Böhm, Ch. Borgmann, M. Breitenfeldt, N. Chamel, S. Goriely, F. Herfurth, M. Kowalska, S. Kreim, D. Lunney, V. Manea, E. Minaya Ramirez, S. Naimi, D. Neidherr, M. Rosenbusch, L. Schweikhard, J. Stanja, F. Wienholtz, and K. Zuber. Plumbing Neutron Stars to New Depths with the Binding Energy of the Exotic Nuclide ^{82}Zn. *Phys. Rev. Lett.*, 110:041101, 2013. doi:10.1103/PhysRevLett.110.041101.

[80] F. Wienholtz, D. Beck, K. Blaum, Ch Borgmann, M. Breitenfeldt, R. B. Cakirli, S. George, F. Herfurth, J. D. Holt, M. Kowalska, S. Kreim, D. Lunney, V. Manea, J. Menendez, D. Neidherr, M. Rosenbusch, L. Schweikhard, A. Schwenk, J. Simonis, J. Stanja, R. N. Wolf, and K. Zuber. Masses of exotic calcium isotopes pin down nuclear forces. *Nature*, 498(7454):346–349, 2013. doi:10.1038/nature12226.

[81] J. W. Yoon, Y.-H. Park, S. J. Park, G. D. Kim, and Y. K. Kim. Design of the multi-reflection time-of-flight mass spectrometer for the RAON facility. *EPJ Web Conf.*, 66:11042, 2014. doi:10.1051/epjconf/20146611042.

[82] C. Jesch, T. Dickel, W. R. Plaß, D. Short, S. Ayet San Andres, J. Dilling, H. Geissel, F. Greiner, J. Lang, K. G. Leach, W. Lippert, C. Scheidenberger, and M. I. Yavor. The MR-TOF-MS isobar separator for the TITAN facility at TRIUMF. *Hyperfine Interact.*, 235(1):97–106, 2015. doi:10.1007/s10751-015-1184-2.

[83] B. E. Schultz, J. M. Kelly, C. Nicoloff, J. Long, S. Ryan, and M. Brodeur. Construction and simulation of a multi-reflection time-of-flight mass spectrometer at the University of Notre Dame. *Nucl. Instrum. Meth. B*, 376:251–255, 2016. doi:10.1016/j.nimb.2016.02.043.

[84] J.-Y. Wang, Y.-L. Tian, Y.-S. Wang, Z.-G. Gan, X.-H. Zhou, H.-S. Xu, and W.-X. Huang. A multi-reflection time-of-flight mass analyzer at IMP/CAS (in press). *Nucl. Instrum. Meth. B*, 2019. doi:10.1016/j.nimb.2019.05.067.

[85] J. Uusitalo, J. Sarén, J. Partanen, and J. Hilton. Mass Analyzing Recoil Apparatus, MARA. *Acta Phys. Pol. B*, 50(3):319–327, 2019. doi:10.5506/APhysPolB.50.319.

[86] G. Bollen, H. Hartmann, H.-J. Kluge, M. König, T. Otto, G. Savard, H. Stolzenberg, and The ISOLDE Collaboration. Towards a "perfect" Penning trap mass spectrometer for unstable isotopes. *Phys. Scripta*, 46(6):581–586, 1992. doi:10.1088/0031-8949/46/6/016.

[87] D. Beck, F. Ames, M. Beck, G. Bollen, B. Delauré, P. Schuurmans, S. Schwarz, P. Schmidt, N. Severijns, and O. Forstner. Space Charge Effects in a Gas Filled Penning Trap. *Hyperfine Interact.*, 132(1):469–474, 2001. URL: 10.1023/A:1011974828147, doi:10.1023/A:1011974828147.

[88] K. Blaum, J. Dilling, and W. Nörtershäuser. Precision atomic physics techniques for nuclear physics with radioactive beams. *Phys. Scripta*, T152:014017, 2013. doi:10.1088/0031-8949/2013/t152/014017.

[89] P. Campbell, I. D. Moore, and M. R. Pearson. Laser spectroscopy for nuclear structure physics. *Prog. Part. Nucl. Phys.*, 86:127–180, 2016. doi:10.1016/j.ppnp.2015.09.003.

[90] P. Schury, Y. Ito, M. Wada, and H. Wollnik. Wide-band mass measurements with a multi-reflection time-of-flight mass spectrograph. *Int. J. Mass Spectrom.*, 359:19–25, 2014. doi:10.1016/j.ijms.2013.11.005.

[91] M. I. Yavor, W. R. Plaß, T. Dickel, H. Geissel, and C. Scheidenberger. Ion-optical design of a high-performance multiple-reflection time-of-flight mass spectrometer and isobar separator. *Int. J. Mass Spectrom.*, 381-382:1–9, 2015. doi:10.1016/j.ijms.2015.01.002.

[92] P. Schury, Y. Ito, M. Rosenbusch, H. Miyatake, M. Wada, and H. Wollnik. Improving wide-band mass measurements in a multi-reflection time-of-flight mass spectrograph by usage of a concomitant measurement scheme. *Int. J. Mass Spectrom.*, 433:40–46, 2018. doi:10.1016/j.ijms.2018.08.007.

[93] J. T. Johnson, I. J. Carrick, G. S. Eakins, and S. A. McLuckey. Simultaneous Isolation of Nonadjacent m/z Ions Using Mirror Switching in an Electrostatic Linear Ion Trap. *Anal. Chem.*, 91(19):12574–12580, 2019. doi:10.1021/acs.analchem.9b03560.

[94] P. Fischer, S. Knauer, G. Marx, and L. Schweikhard. In-depth study of in-trap high-resolution mass separation by transversal ion ejection from a multi-reflection time-of-flight device. *Rev. Sci. Instrum.*, 89(1):015114, 2018. doi:10.1063/1.5009167.

[95] Y. Toker, N. Altstein, O. Aviv, M. L. Rappaport, O. Heber, D. Schwalm, D. Strasser, and D. Zajfman. The kick-out mass selection technique for ions stored in an Electrostatic Ion Beam Trap. *J. Instrum.*, 4(09):P09001, 2009. doi:10.1088/1748-0221/4/09/P09001.

[96] R. T. Hilger, R. Santini, and S. A. Mcluckey. Square Wave Modulation of a Mirror Lens for Ion Isolation in a Fourier Transform Electrostatic Linear Ion Trap Mass Spectrometer. *Int. J. Mass Spectrom.*, 362:1–8, 2014. doi:10.1016/j.ijms.2014.02.003.

[97] J. T. Johnson, I. J. Carrick, G. S. Eakins, and S. A. McLuckey. Mirror Switching for High-Resolution Ion Isolation in an Electrostatic Linear Ion Trap. *Anal. Chem.*, 91(14):8789–8794, 2019. doi:10.1021/acs.analchem.9b00874.

[98] N. E. Bradbury and R. A. Nielsen. Absolute Values of the Electron Mobility in Hydrogen. *Phys. Rev.*, 49:388–393, 1936. doi:10.1103/PhysRev.49.388.

[99] R. N. Wolf, D. Beck, K. Blaum, Ch. Böhm, Ch. Borgmann, M. Breitenfeldt, F. Herfurth, A. Herlert, M. Kowalska, S. Kreim, D. Lunney, S. Naimi, D. Neidherr, M. Rosenbusch, L. Schweikhard, J. Stanja, F. Wienholtz, and K. Zuber. On-line separation of short-lived nuclei by a multi-reflection time-of-flight device. *Nucl. Instrum. Meth. A*, 686:82–90, 2012. doi:10.1016/j.nima.2012.05.067.

[100] P. Fischer, G. Marx, and L. Schweikhard. Multiple ion capture and separation in an electrostatic storage device. *Int. J. Mass Spectrom.*, 435:305–314, 2019. doi:10.1016/j.ijms.2018.11.010.

[101] E. Leistenschneider, M. P. Reiter, S. Ayet San Andrés, B. Kootte, J. D. Holt, P. Navrátil, C. Babcock, C. Barbieri, B. R. Barquest, J. Bergmann, J. Bollig, T. Brunner, E. Dunling, A. Finlay, H. Geissel, L. Graham, F. Greiner, H. Hergert, C. Hornung, C. Jesch, R. Klawitter, Y. Lan, D. Lascar, K. G. Leach, W. Lippert, J. E. McKay, S. F. Paul, A. Schwenk, D. Short, J. Simonis, V. Somà, R. Steinbrügge, S. R. Stroberg, R. Thompson, M. E. Wieser, C. Will, M. Yavor, C. Andreoiu, T. Dickel, I. Dillmann, G. Gwinner, W. R. Plaß, C. Scheidenberger, A. A. Kwiatkowski, and J. Dilling. Dawning of the N=32 Shell Closure Seen through Precision Mass Measurements of Neutron-Rich Titanium Isotopes. *Phys. Rev. Lett.*, 120:062503, 2018. doi:10.1103/PhysRevLett.120.062503.

[102] M. Rosenbusch, Y. Ito, P. Schury, M. Wada, D. Kaji, K. Morimoto, H. Haba, S. Kimura, H. Koura, M. MacCormick, H. Miyatake, J. Y. Moon, K. Morita, I. Murray, T. Niwase, A. Ozawa, M. Reponen, A. Takamine, T. Tanaka, and H. Wollnik. New mass anchor points for neutron-deficient heavy nuclei from direct mass measurements of radium and actinium isotopes. *Phys. Rev. C*, 97:064306, 2018. doi:10.1103/PhysRevC.97.064306.

[103] P. Fischer, S. Knauer, G. Marx, and L. Schweikhard. Non-isobaric time-of-flight correction for isobar resolving in MR-ToF mass spectrometry. *Int. J. Mass Spectrom.*, 432:44–51, 2018. doi:10.1016/j.ijms.2018.07.004.

[104] F. Wienholtz, K. Blaum, J. Karthein, D. Lunney, S. Malbrunot-Ettenauer, V. Manea, M. Mougeot, L. Schweikhard, T. Steinsberger, and R. N. Wolf. Improved stability of multi-reflection time-of-flight mass spectrometers through passive and active voltage stabilization (in press). *Nucl. Instrum. Meth. B*, 2019. doi:10.1016/j.nimb.2019.04.061.

[105] P. Fischer and L. Schweikhard. Multiple-ion-ejection multi-reflection time-of-flight mass spectrometry for single-reference wide-band mass measurements (submitted).

[106] R. L. Johnston. *Atomic and Molecular Clusters*. Taylor & Francis, 2002.

[107] J. A. Alonso. *Structure and Properties of Atomic Nanoclusters*. Imperial College Press, 2nd edition, 2011.

[108] H. W. Kroto, J. R. Heath, S. C. O'Brien, R. F. Curl, and R. E. Smalley. C60: Buckminsterfullerene. *Nature*, 318:162–163, 1985. doi:10.1038/318162a0.

[109] W. D. Knight, K. Clemenger, W. A. de Heer, W. A. Saunders, M. Y. Chou, and M. L. Cohen. Electronic Shell Structure and Abundances of Sodium Clusters. *Phys. Rev. Lett.*, 52:2141–2143, 1984. doi:10.1103/PhysRevLett.52.2141.

[110] O. Echt, K. Sattler, and E. Recknagel. Magic Numbers for Sphere Packings: Experimental Verification in Free Xenon Clusters. *Phys. Rev. Lett.*, 47:1121–1124, 1981. doi:10.1103/PhysRevLett.47.1121.

[111] R. Ferrando, J. Jellinek, and R. L. Johnston. Nanoalloys: From Theory to Applications of Alloy Clusters and Nanoparticles. *Chem. Rev.*, 108(3):845–910, 2008. doi:10.1021/cr040090g.

[112] R. L. Johnston. *Metal Nanoparticles and Nanoalloys, Volume 3*. Elsevier, 2012.

[113] F. Calvo. *Nanoalloys: From Fundamentals to Emergent Applications*. Elsevier, 2013.

[114] K. L. Busch, G. L. Glish, and S. A. Mcluckey. *Mass spectrometry/mass spectrometry: Techniques and applications of tandem mass spectrometry*. Wiley-VCH, 1st edition, 1988.

[115] K. Hansen and O. Echt. Thermionic Emission and Fragmentation of C_{60}. *Phys. Rev. Lett.*, 78:2337–2340, 1997. doi:10.1103/PhysRevLett.78.2337.

[116] Y. Shi, V. A. Spasov, and K. M. Ervin. Competitive fragmentation and electron loss kinetics of photoactivated silver cluster anions: Dissociation energies of Ag_n^- (n=7-11). *J. Chem. Phys.*, 111(3):938–949, 1999. doi:10.1063/1.479186.

[117] C. Walther, G. Dietrich, W. Dostal, K. Hansen, S. Krückeberg, K. Lützenkirchen, and L. Schweikhard. Radiative Cooling of a Small Metal Cluster: The Case of V_{13}^+. *Phys. Rev. Lett.*, 83:3816–3819, 1999. doi:10.1103/PhysRevLett.83.3816.

[118] H. Haberland, B. von Issendorff, J. Yufeng, T. Kolar, and G. Thanner. Ground state and response properties of mercury clusters. *Z. Phys. D*, 26(1):8–12, 1993. doi:10.1007/BF01429096.

[119] C. Sönnichsen, T. Franzl, T. Wilk, G. von Plessen, and J. Feldmann. Plasmon resonances in large noble-metal clusters. *New J. Phys.*, 4:93–93, 2002. doi:10.1088/1367-2630/4/1/393.

[120] C. Bréchignac, Ph. Cahuzac, F. Carlier, and J. Leygnier. Collective excitation in closed-shell potassium cluster ions. *Chem. Phys. Lett.*, 164(4):433–437, 1989. doi:10.1016/0009-2614(89)85233-9.

[121] C. Bréchignac, Ph. Cahuzac, F. Carlier, M. de Frutos, and J. Leygnier. Optical excitation in small ionized sodium clusters: closed-shell and open-shell systems. *Chem. Phys. Lett.*, 189(1):28–34, 1992. doi:10.1016/0009-2614(92)85148-4.

[122] I. Vasiliev, S. Öğüt, and J. R. Chelikowsky. Ab Initio Excitation Spectra and Collective Electronic Response in Atoms and Clusters. *Phys. Rev. Lett.*, 82:1919–1922, 1999. doi:10.1103/PhysRevLett.82.1919.

[123] C. Bréchignac, Ph. Cahuzac, F. Carlier, M. de Frutos, and J. Leygnier. Alkali-metal clusters as prototypes of metal clusters. *J. Chem. Soc., Faraday Trans.*, 86:2525–2531, 1990. doi:10.1039/FT9908602525.

[124] O. Ingólfsson, U. Busolt, and K. Sugawara. Energy-resolved collision-induced dissociation of Cu_n^+ (n=2-9): Stability and fragmentation pathways. *J. Chem. Phys.*, 112(10):4613–4620, 2000. doi:10.1063/1.481017.

[125] M. Vogel, A. Herlert, and L. Schweikhard. Photodissociation of small group-11 metal cluster ions: Fragmentation pathways and photoabsorption cross sections. *J. Am. Soc. Mass Spectrom.*, 14(6):614–621, 2003. doi:10.1016/S1044-0305(03)00203-4.

[126] M. E. Geusic, M. F. Jarrold, T. J. McIlrath, R. R. Freeman, and W. L. Brown. Photodissociation of carbon cluster cations. *J. Chem. Phys.*, 86(7):3862–3869, 1987. doi:10.1063/1.451946.

[127] L. A. Bloomfield, R. R. Freeman, and W. L. Brown. Photofragmentation of Mass-Resolved $Si_{2\text{-}12}^+$ Clusters. *Phys. Rev. Lett.*, 54:2246–2249, 1985. doi:10.1103/PhysRevLett.54.2246.

[128] S. König, F. Martinez, L. Schweikhard, and M. Wolfram. Photodecay Pathways of Stored, Size-Selected Lead Clusters Pb_n^+, n = 6-41 and Pb_n^-, n = 9-56. *J. Phys. Chem. C*, 121(20):10858–10864, 2017. doi:10.1021/acs.jpcc.6b12074.

[129] S. König, M. Wolfram, S. Bandelow, G. Marx, and L. Schweikhard. Interaction of anionic tin clusters Sn_n^-, n=7-75 with electrons – polyanion production and cluster decay. *Eur. Phys. J. D*, 72(9):153, 2018. doi:10.1140/epjd/e2018-90158-y.

[130] J. E. Huheey. *Inorganic Chemistry: Principles of Structure and Reactivity*. Addison-Wesley, 4th edition, 1993.

[131] M. G. Mitch, S. J. Chase, J. Fortner, R. Q. Yu, and J. S. Lannin. Phase transition in ultrathin Bi films. *Phys. Rev. Lett.*, 67:875–878, 1991. doi:10.1103/PhysRevLett.67.875.

[132] M. E. Geusic, R. R. Freeman, and M. A. Duncan. Photofragmentation of antimony and bismuth cluster cations at 248 nm. *J. Chem. Phys.*, 88(1):163–166, 1988. doi:10.1063/1.454631.

[133] M. M. Ross and S. W. McElvany. Production and fragmentation of antimony and bismuth cluster ions. *J. Chem. Phys.*, 89(8):4821–4828, 1988. doi:10.1063/1.455676.

[134] T. M. Bernhardt, B. Kaiser, and K. Rademann. Fragmentation of clusters induced by collision with a solid surface: comparison of antimony and bismuth cluster ions. *Z. Phys. D*, 40(1):327–330, 1997. doi:10.1007/s004600050219.

[135] R. Kelting, A. Baldes, U. Schwarz, T. Rapps, D. Schooss, P. Weis, C. Neiss, F. Weigend, and M. M. Kappes. Structures of small bismuth cluster cations. *J. Chem. Phys.*, 136(15):154309, 2012. doi:10.1063/1.3703014.

[136] P. Fischer and L. Schweikhard. Photofragmentation of $Bi_n^{+/-}$ clusters (n = 2-19) in an electrostatic ion beam trap. *Eur. Phys. J. D*, 73(5):105, 2019. doi:10.1140/epjd/e2019-100027-0.

[137] L. Gao, P. Li, H. Lu, S. F. Li, and Z. X. Guo. Size- and charge-dependent geometric and electronic structures of Bi_n (Bi_n^-) clusters (n=2-13) by first-principles simulations. *J. Chem. Phys.*, 128(19):194304, 2008. doi:10.1063/1.2920484.

[138] J. M. Jia, G. B. Chen, D. N. Shi, and B. L. Wang. Structural and electronic properties of Bi_n (n = 2-14) clusters from density-functional calculations. *Eur. Phys. J. D*, 47(3):359–365, 2008. doi:10.1140/epjd/e2008-00029-y.

[139] H. K. Yuan, H. Chen, A. L. Kuang, Y. Miao, and Z. H. Xiong. Density-functional study of small neutral and cationic bismuth clusters Bi_n and Bi_n^+ (n=2-24). *J. Chem. Phys.*, 128(9):094305, 2008. doi:10.1063/1.2837460.

[140] S. Nonose, Y. Sone, and K. Kaya. Reactivity and stability of bimetallic clusters. *Z. Phys. D*, 19(4):357–359, 1991. doi:10.1007/BF01448328.

[141] U. Heiz, A. Vayloyan, E. Schumacher, C. Yeretzian, M. Stener, P. Gisdakis, and N. Rösch. Na_xAu and Cs_xAu bimetal clusters: Finite size analogs of sodium–gold and cesium–gold compounds. *J. Chem. Phys.*, 105(13):5574–5585, 1996. doi:10.1063/1.472397.

[142] R. L. Wagner, W. D. Vann, and A. W. Castleman. A technique for efficiently generating bimetallic clusters. *Rev. Sci. Instrum.*, 68(8):3010–3013, 1997. doi:10.1063/1.1148058.

[143] W. Bouwen, P. Thoen, F. Vanhoutte, S. Bouckaert, F. Despa, H. Weidele, R. E. Silverans, and P. Lievens. Production of bimetallic clusters by a dual-target dual-laser vaporization source. *Rev. Sci. Instrum.*, 71(1):54–58, 2000. doi:10.1063/1.1150159.

[144] M. M. Kappes, P. Radi, M. Schär, and E. Schumacher. Probes for electronic and geometrical shell structure effects in alkali-metal clusters. Photoionization measurements on K_xLi, K_xMg and K_xZn ($x < 25$). *Chem. Phys. Lett.*, 119(1):11–16, 1985. doi:10.1016/0009-2614(85)85411-7.

[145] J. L. Rousset, A. M. Cadrot, F. J. Cadete Santos Aires, A. Renouprez, P. Mélinon, A. Perez, M. Pellarin, J. L. Vialle, and M. Broyer. Study of bimetallic Pd-Pt clusters in both free and supported phases. *J. Chem. Phys.*, 102(21):8574–8585, 1995. doi:10.1063/1.468847.

[146] C. Yeretzian. Electronic structure effects in bimetallic M_xN clusters (M = alkali, N = divalent metal). *J. Phys. Chem.*, 99(1):123–130, 1995. doi:10.1021/j100001a022.

[147] P. Fischer and L. Schweikhard. Isotope-resolved photodissociation pathways of lead-doped bismuth clusters from tandem multi-reflection time-of-flight mass spectrometry. *Phys. Rev. Research*, 1:033050, 2019. doi:10.1103/PhysRevResearch.1.033050.

7 Cumulative thesis articles

7.1 Author contributions

Article I: Multiple ion capture and separation in an electrostatic storage device
P. Fischer, G. Marx, and L. Schweikhard, *Int. J. Mass Spectrom.* 435, 305-314 (2019)
P.F. performed the experiment and data analysis. P.F. and L.S. prepared the manuscript, which was edited by all co-authors.

Article II: Non-isobaric time-of-flight correction for isobar resolving in MR-ToF mass spectrometry
P. Fischer, S. Knauer, G. Marx, and L. Schweikhard, *Int. J. Mass Spectrom.* 432, 44-51 (2018)
P.F. performed the experiment and data analysis. P.F. and L.S. prepared the manuscript, which was edited by all co-authors.

Article III: Multiple-ion-ejection multi-reflection time-of-flight mass spectrometry for single-reference wide-band mass measurements (submitted)
P. Fischer and L. Schweikhard
P.F. performed the experiment and data analysis. P.F. and L.S. prepared and edited the manuscript.

Article IV: Photofragmentation of $Bi_n^{+/-}$ clusters (n = 2–19) in an electrostatic ion beam trap
P. Fischer and L. Schweikhard, *Eur. Phys. J. D* 73, 105 (2019)
P.F. performed the experiment and data analysis. P.F. and L.S. prepared and edited the manuscript.

Article V: Isotope-resolved photodissociation pathways of lead-doped bismuth clusters from tandem multi-reflection time-of-flight mass spectrometry
P. Fischer and L. Schweikhard, *Phys. Rev. Research* 1, 116189 (2019)
P.F. performed the experiment and data analysis. P.F. and L.S. prepared and edited the manuscript.

Confirmed:

Greifswald, den Paul Fischer Lutz Schweikhard

7.2 Multiple ion capture and separation in an electrostatic storage device

International Journal of Mass Spectrometry 435 (2019) 305–314

Contents lists available at ScienceDirect

International Journal of Mass Spectrometry

journal homepage: www.elsevier.com/locate/ijms

Multiple ion capture and separation in an electrostatic storage device

Paul Fischer*, Gerrit Marx, Lutz Schweikhard

Institut für Physik, Universität Greifswald, 17487 Greifswald, Germany

ARTICLE INFO

Article history:
Received 15 August 2018
Received in revised form 12 October 2018
Accepted 3 November 2018
Available online 7 November 2018

Keywords:
Multi-reflection time-of-flight (MR-ToF) mass spectrometry
Electrostatic ion beam trap (EIBT)
Transversal ion ejection
In-trap lift

ABSTRACT

The present study introduces new approaches for the capture/injection and selection of ions with large mass-to-charge (m/q) differences in an electrostatic ion beam trap (EIBT) or multi-reflection time-of-flight (MR-ToF) device. While no m/q-dependent storage criterion exists for devices of this nature, the process of injecting ions into the trap relies on a timed potential switching and is therefore mass-selective to some extent. To partially circumvent this restriction, the approach of sequential capture is presented, where additional ion species are captured while already-stored ones are unaffected by the switching pulses. Specifically, it is possible to perform a full in-trap lift capture pulse while a given, already-stored ion species is reflected in a mirror potential or passes through the lift electrode itself. Additionally, the technique of ion selection by means of transversal ejection from the trap is extended to allow ion species with large m/q differences to be retained. To this end, deflector functions with different frequencies are added with an AND logic and supplied to an in-trap deflector electrode. The combination of both techniques allows the simultaneous storage of size-selected ion species with an m/q ratio surpassing 4 : 1 at the present setup, where the single-pulse lift capture is restricted to a ratio of only 1.9.

1. Introduction and motivation

Electrostatic ion beam traps (EIBTs) [1–3] have two main applications in modern physics: precision mass spectrometry via multi-reflection time-of-flight (MR-ToF) studies [4–11] and utilization as ion traps for the study of cluster and molecule properties [12–16]. Due to the possibility to reach high resolving powers ($R \geq 10^5$) in just tens of milliseconds, they are commonly used for ion separation in preparation of other precision experiments [6,8–10,17–20].

For precision mass-spectrometry applications, the mass ranges of investigated ions are typically small, often restricted to the retention of only isobaric ion species or species with a mass difference of a few atomic mass units. However, "wide-band" investigations [21–23] for cluster or molecular applications have also been reported. In ion-trap applications, mass differences tend to be larger, e.g. involving several cluster sizes [14,24–26] or different molecules [27,28]. Next to the conventional time-of-flight investigation, non-destructive detection methods via capacitive pickup electrodes ("Fourier transform MR-ToF") have also been employed in these studies [13,16,27–33]. Lastly, marking the complete severance from the ToF application, operation where ions do not revolve as individual bunches but fill the entirety of the trap's volume (sometimes referred to as "non-bunching mode") has been reported [15,26].

Regardless of the specific application, experiments on trapped charged particles are defined by the ion species investigated, and, more generally, by the range of mass-to-charge ratios m/q that can be retained within the trap. Because of the EIBT's electrostatic nature, no direct m/q-dependent storage criterion exists. However, restrictions can emerge with respect to the capture/injection of ions, where the switching of one or several trap potential has to be employed. Typical solutions rely on the switching of the mirror potentials [24,28,34,35] or an in-trap lift electrode for adjusting the ions' energy between the mirrors [22,36–40]. Either technique relies on ion capture from an (already preselected) ion bunch of known energy traversing the trap.

It follows that such an injection is inherently limited in the mass-to-charge ratio that can be simultaneously captured, as significantly faster ions will leave the trap before the slower ones have entered. This device-specific limit depends on parameters such as the dimensions of the trap itself, its potential configuration, and the distance between the ion source (or buncher trap after a continuous source) and the EIBT, i.e. the separation of the ion bunch into its m/q components at the time of capture. Thus, it is not easily changed between individual measurements. For a given setup, optimizing the conditions of the ion injection [28,34] is a typical step to maximize an experiment's overall efficiency and feasibility.

* Corresponding author.
E-mail address: paul.fischer@uni-greifswald.de (P. Fischer).

https://doi.org/10.1016/j.ijms.2018.11.010
1387-3806/

In the present study, an in-trap lift electrode is utilized to capture ions created in a UHV laser ablation source (similar to the one reported in [41]). Next to the typical capture operation, measurements with an additional capture pulse are presented, where ions of interest from the initial capture are retained. Specifically, the potential switches are timed such that ions from the first capture are not affected by the second one due to staying either in a mirror potential or the in-trap lift electrode. This allows the sequential capture of ion species with mass-to-charge ratios beyond the limit of a single capture pulse.

In addition, the previously-reported technique of transversal ion ejection by synchronized deflection pulses after the ions' capture [23,35,42] is expanded upon. With the simultaneous storage of ions of largely different m/q values, the need of a means for simultaneous, in-trap selection becomes more pronounced. The retention of a single range of m/q-ratios is insufficient for complete control over the selection of, e.g., individual molecules, leading to the approach of adding multiple deflection functions with individually-tuned parameters. As such, it becomes possible to select several ion species from a range of m/q values while selectively ejecting species with larger, smaller or intermediate values.

2. Experimental setup

The present setup (Fig. 1) combines a UHV laser ablation source [41] (Continuum: MiniLite laser, $\leq$15 mJ pulse energy at $\lambda = 532$ nm, 6 ns pulse length, 10 Hz repetition rate) with an MR-ToF analyzer. Metal targets are irradiated, resulting in ions of both polarities as well as neutral particles being produced. The charged atoms and clusters are guided towards the analyzer and detector via several ion-optical elements and a quadrupole deflector for a 90° turn.

The potential configuration of the acceleration section and MR-ToF analyzer is identical to that given in [23] and [43], the in-trap lift electrode [36,39,40] is switched between −745 V and ground potential (for the trapping of anions). Ions are accelerated to a total energy of 2.010 keV from the target plate and are able to traverse the analyzer for "single-path" operation. However, if the in-trap lift potential is lowered while ions are within the lift tube, their total energy is reduced to 1.265 keV, resulting in their storage between the electrostatic mirrors. Ion ejection is analogously performed by reapplying the lift potential after a predetermined storage time. Both the shape of the mirror potentials and the value of the in-trap lift voltage are tuned to yield mass resolving powers exceeding 10^5 [43].

The lift potential is provided by a high-current power supply (FuG Elektronik GmbH, MCP 140-1250) and switched using a fast transistor switch (CGC Instruments, AMX1500-3F). The input voltage is additionally buffered using a 40 μF, 10 kΩ low-pass to dampen overshoot and ringing. The potentials forming the MR-ToF mirrors are provided by several precision power supplies (Stahl Electronics, HV 400) which are floated to reach the relevant voltage ranges (iseg Spezialelektronik GmbH, EHS 8240). The floating voltages themselves are again buffered by individual 40 μF, 1 MΩ low-pass filters connected to ground potential. This setup provides low-noise voltages that can still be tuned to optimize the storage conditions.

Segmented deflector ring electrodes located between the lift electrode and the stacks of mirror electrodes allows the application of pulsed, transversally-deflecting electric fields for the selective ejection of ion species from the trap [23,35,42]. To this end, the frequency and phase of the deflector function is matched to the revolution period of an ion species (more precisely, a mass-over-charge range) of interest such that the deflecting field is off whenever said species passes the ring. An in-depth characterization of this technique for the present setup has been performed in [23].

For both single-path and MR-ToF operation, ion detection is performed with a channeltron detector including a 5 kV conversion dynode. The detector signals are amplified (ORTEC, VT120a, 46 dB) and digitalized with a computer-mounted multiscaler card (Becker & Hickl GmbH, MSA-300). The control of the experimental timing pattern is performed with a LabVIEW-based control software [44] and a Field-Programmable-Gate-Array (FPGA) card (National Instruments, PCI-7811R).

The experiment cycle is synchronized to the laser pulse and, thus, the ions' production in the source region. From this starting point, the typical cycle utilizing a single-pulse in-trap lift capture consists of:

1 The capture time t_{cap}, during which ions travel from the source to the MR-ToF analyzer.
2 The storage time t_s, during which the stored ions revolve between the MR-ToF mirrors. More accurately, t_s describes the time between the (first) switching down of the in-trap lift potential for ion capture and its re-application for ejection.
3 The measured time of flight τ after the ion ejection.

The start of the multiscaler card for the time-of-flight measurement is synchronized to the source laser pulse for single-path operation and to the ion ejection for MR-ToF operation. The total flight time for a given ion consequently amounts to $t_{cap} + t_s + \tau$. Individual ion species exhibit different revolution periods T in the MR-ToF analyzer, according to their mass-to-charge ratios. For observation of an ion species after N revolution periods, the storage

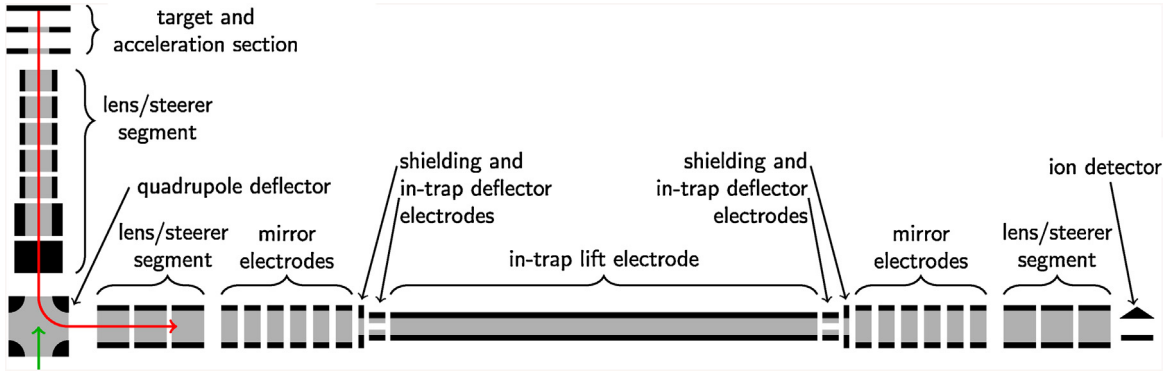

Fig. 1. Schematic of the experimental setup. From top left to bottom right: target plate and dual-stage acceleration section, ion-optical lenses and steerers, quadrupole deflector, entry-side lens/steerer, MR-ToF analyzer with in-trap lift electrode, transversal deflector electrodes, and stacks of six mirror electrodes each, exit-side lens/steerer, channeltron ion detector with conversion dynode. Ion path and ablation laser beam are indicated as red and green arrows, respectively.

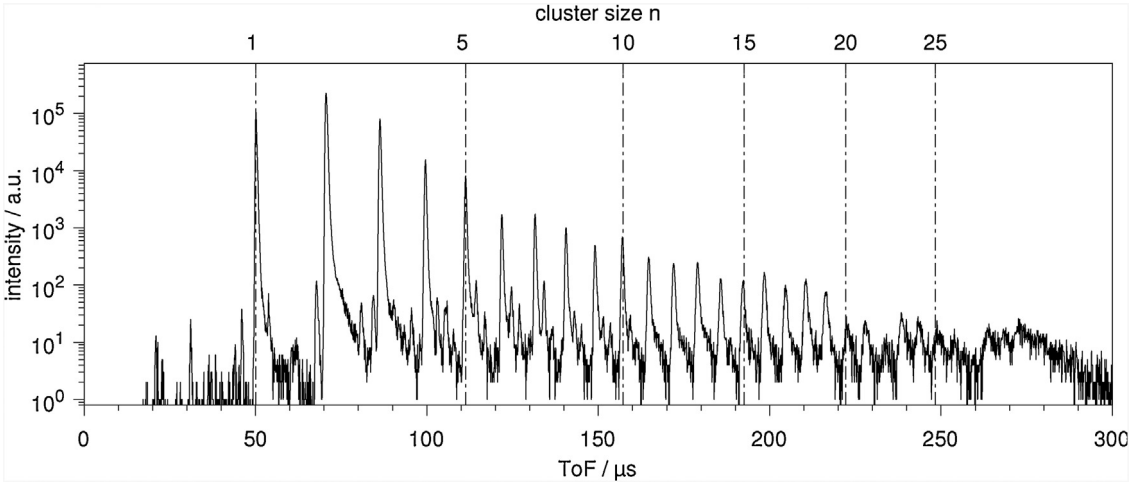

Fig. 2. Single-path spectrum of Bi_n^-. Selected signals are marked by their cluster size n.

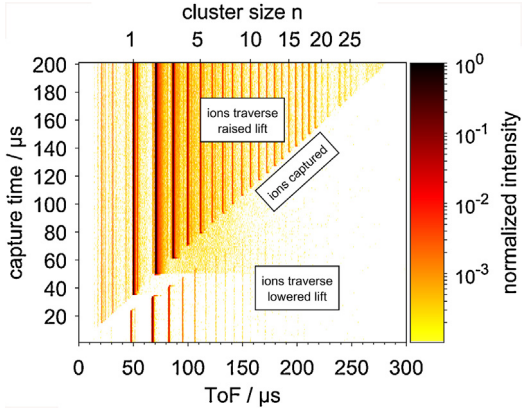

Fig. 3. 2D color-intensity plot of Bi_n^- single path spectra. The vertical axis describes the capture time, i.e. the time of the downward switch of the in-trap lift after the laser ablation/ionization. The signals in the upper left and lower right are due to ions that passed the MR-ToF analyzer during high and low lift potential, respectively. Ions "missing" from the spectra were captured. The signals on the center diagonal at capture times from 50 to 100 µs are artifacts due to the high-intensity Bi_2^- to Bi_5^- ions affected by the switching pulse.

time has to match—to some degree—the product $N \cdot T$. A detailed discussion of the range of viable ejection times is given in [22].

3. Single-pulse in-trap lift capture

The operation scheme of the present setup is primarily defined by the switching of the in-trap lift electrode. If no switching is employed at all (single-path operation), all ions are guided towards the detector and reach it at increasing times according to their m/q value. Fig. 2 shows signals of singly-charged bismuth clusters Bi_n^- with sizes resolved up to $n = 25$.

If the lift potential is switched to capture some of these ions, the single-path spectrum is split into three parts (also see Fig. 4 in [22]):

- Ions that have already fully passed the in-trap lift at the time of switching are not affected (upper left quadrant in Fig. 3).
- Ions that are in or sufficiently near the lift electrode are not visible in the single-path spectrum since they are either captured between the electrostatic mirrors or disturbed by sampling some changing electric field of the switching pulse (center diagonal in Fig. 3).
- Ions that traverse the in-trap lift after the switching are visible in the spectrum, although at reduced intensity (due to the change in ion-optical focusing) and at earlier flight times (due to the higher kinetic energy in the lift tube) (lower right quadrant in Fig. 3).

If t_{cap} is scanned (Fig. 3), its viable values for the capture of individual ion species can be roughly discerned. It also becomes apparent that the mass range of simultaneously-captured ion species from a single bunch is limited. If the difference in m/q values between two species becomes too large, they will not be in the drift tube simultaneously at any given time. For the present setup, the maximum mass ratio that can be simultaneously captured amounts to roughly 1.9 (see section 4.3). Note that, as stated in the introduction, no m/q-dependent storage criterion exists for the electrostatic trap itself, considering ions of identical energy per charge unit. Consequently, the limiting factor for wide-band investigations primarily results from the system's ability to capture/inject ions of different m/q.

4. Repeated in-trap lift capture

4.1. Principle of operation

The limitations of the in-trap lift for simultaneous capture of ion species with large m/q differences can be somewhat circumvented if a second switching pulse is utilized. To this end, a second capture is performed while an already-captured species is retained either in an ion mirror or the in-trap lift itself (left and right column of Fig. 4, respectively): An initial ion species A (blue in Fig. 4) traverses the entry-side mirror (a) and is captured in the MR-ToF analyzer at the capture time t_{cap1} (b). During a delay Δt_{down}, A moves through the lowered lift electrode and into the exit-side mirror potential. The lift potential is raised again if A is either sufficiently far away from the lift electrode (c, left column) or back in the lift tube after its reflection (c, right column). In either case, another ion species B (red in Fig. 4) is allowed to enter the raised lift electrode (d). The in-trap lift is now switched down a second time after a "lift-high" duration Δt_{up}, either before A comes close enough again to be disturbed by the switching pulse (e, left column) or before A leaves the in-trap lift (e, right column). After the completion of the sequence of switching pulses, both ion bunches A and B will have experienced a shift in their total energy, i.e. both species will be captured (f). The second capture is de facto performed at $t_{cap2} = t_{cap1} + \Delta t_{down} + \Delta t_{up}$.

It is readily apparent that this technique of "repeated capture" largely depends on the timing of the switching pulses. While Fig.

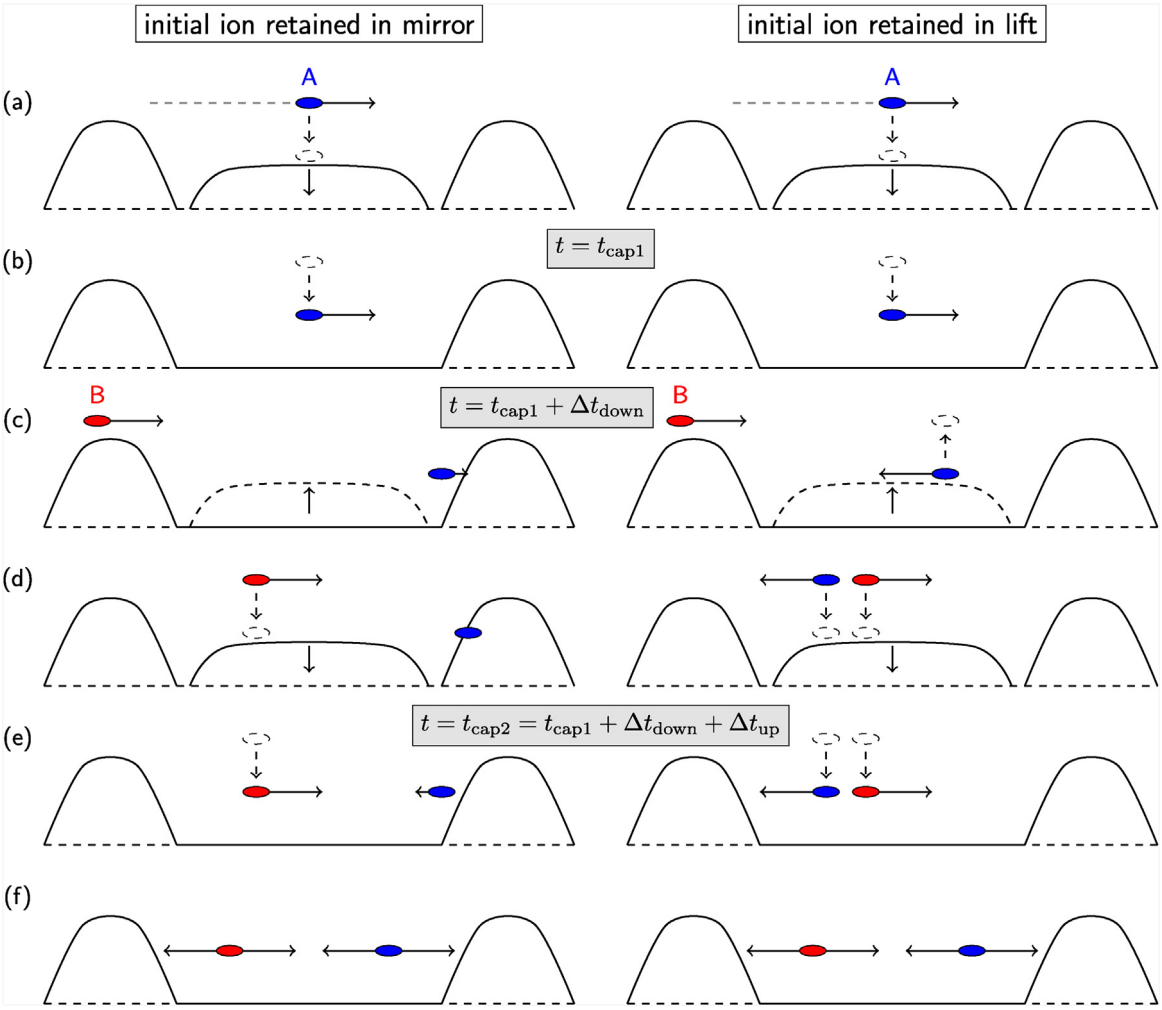

Fig. 4. Schematic illustration of the repeated-capture technique: Two ion species of different m/q-ratios (blue and red) are sequentially captured. For more information, see text.

4 demonstrates the initial ion's retention in the exit-side mirror potential, the technique can also be performed with it being located in the entry-side mirror (or the lift electrode while passing through in the opposite direction). As long as the switching is fully concluded before the ions reach the gap between a mirror and the in-trap lift, where the electric field is affected by the switching process, the method is applicable. The *A* and *B* ion species do not have to originate from a single starting pulse and can even come from different ion sources. Generally speaking, ions that could not be investigated simultaneously due to not "fitting" within a single capture pulse can be captured sequentially if multiple capture pulses are employed. However, limitations still exist due to the *A* ion species' finite turn-around/passing time in the mirrors/lift (see below).

The technique is possible because ions spend a large portion of their revolution period either fully within the mirror potentials during their reflection or in the in-trap lift tube. For the present setup, the remaining times, i.e. when the ions pass the fringe fields between mirrors and in-trap lift in which they are affected by changing electric fields from switching processes, are comparatively small (see Fig. 5). For setups where these times are larger or smaller (due to the way the voltages are applied or the geometric layout), the timing requirements are expected to be more or less demanding. Consequently, the range of ion species that can be sequentially captured is more or less restricted, respectively.

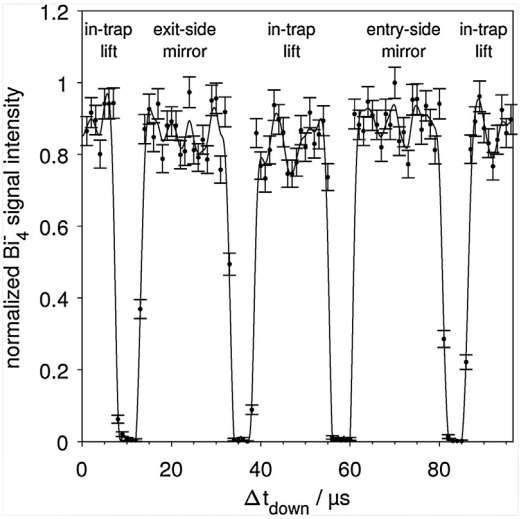

Fig. 5. Detected signal intensity of Bi_4^- ions ($T = 95.6$ µs) after 10 revolution periods. For a fixed value of $\Delta t_{up} = 4$ µs), the Δt_{down} delay of the second capture is varied. The ranges where signal is detected mark the ions' position in the individual parts of the MR-ToF analyzer as labeled in the figure.

4.2. Timing requirement for retention of the initial ions

For the present setup (ions originate from a single source-laser pulse), a scan has been performed on stored Bi_4^- clusters to deter-

mine the portion of the captured ions' revolution period affected by the second switching (Fig. 5). For a fixed value of $\Delta t_{up} = 4\,\mu s$, Δt_{down} is varied and the intensity of the Bi_4^- signal is evaluated. The total storage time is fixed at 956 µs, which amounts to 10 Bi_4^- revolution periods. Thus, the signal is always evaluated after 10 revolutions while the second-capture parameter is varied.

The signal intensity shows ranges of delay times Δt_{down} where the count rate is unaffected by the switching pulses. The scan covers one full revolution period ($T = 95.6\,\mu s$) and, thus, shows the portions of it where the ions are located in the in-trap lift itself, with a direction of motion towards either side, or in either of the mirror potentials. At the edges of these ranges, the ions sample some changing electric fields during switching, which leads to reduced intensities and deviations in the signal shapes.

The near 50/50 distribution of the revolution period between the lift and mirror potentials for the present setup is visible, with the times where the ions are unaffected due to being in the mirror potentials being slightly larger than the ones marking passage through the lift tube. The time during which ions are affected by the fringe field between two regimes amounts to ca. 5% of the revolution period. Since these regions are passed four times per period, the total portion of T viable for a subsequent capture pulse is about 80%.

It can be readily understood that the ranges of viable Δt_{down} delay times decrease for increasing Δt_{up} values, that is, if the overall duration of the second capture becomes longer, the timing conditions for successful retention of the initial ion species become more demanding. The results of the scan are qualitatively the same if the signal intensity is evaluated for a different ion species. The values of the beginning and end of the individual ranges are constant if normalized to the ion's revolution period T: 22% of an ion's revolution period are spent in either mirror and 18% in the in-trap lift for one pass.

4.3. Determination of m/q-range restrictions for single-pulse capture

With the knowledge of the individual cluster sizes' capture time ranges (i.e. Fig. 3) and the relative portions of their revolution periods viable for second capture (i.e. Fig. 5), a quantitative evaluation can be performed to assess the possibility of simultaneous storage for a given mass ratio for the present system (Fig. 6).

The minimum and maximum possible capture times have been identified for the cluster sizes $n = 1$, 2, 4, 8, and 16 by determining for which t_{cap} values a given size is no longer present in the trap (red and blue circles in Fig. 6). The data points have been fitted with square root functions

$$t_i(n) = \sqrt{\frac{n}{z}} \cdot \theta_i\,, \tag{1}$$

where z describes the clusters' charge number, yielding the red and blue lines. The parameters of the curves (for the present system, given by its potential and geometric configuration) can be specified as $\theta_{cap,min} = 24.77(7)\,\mu s$ and $\theta_{cap,max} = 34.51(6)\,\mu s$. Note that the cluster size n is in this case representative for Bi_n clusters, however, the expressions can also be phrased to directly reflect m/q values.

Evaluating Fig. 6, one can now easily discern whether the *simultaneous capture* (using a single in-trap lift switching pulse) of a given pair of ion species is possible: If a capture time t_{cap} exists where the corresponding horizontal line intersects with the blue line below the lighter ion's $t_{cap,max}$ value and with the red line above the heavier ion's $t_{cap,min}$ value, both ions can be captured with that capture pulse. Similarly, the maximum mass ratio for a pair of ion species that can be simultaneously captured is given by the ratio of the cluster sizes at the intersections of a horizontal line with the red and blue lines. This ratio is independent of the actual capture time t_{cap}, as the two lines have the same form (1). Thus, the cluster-size (or m/q) ratio is

$$\frac{n_{max}}{n_{min}} = \frac{(m/q)_{max}}{(m/q)_{min}} = 1.94(1)\,. \tag{2}$$

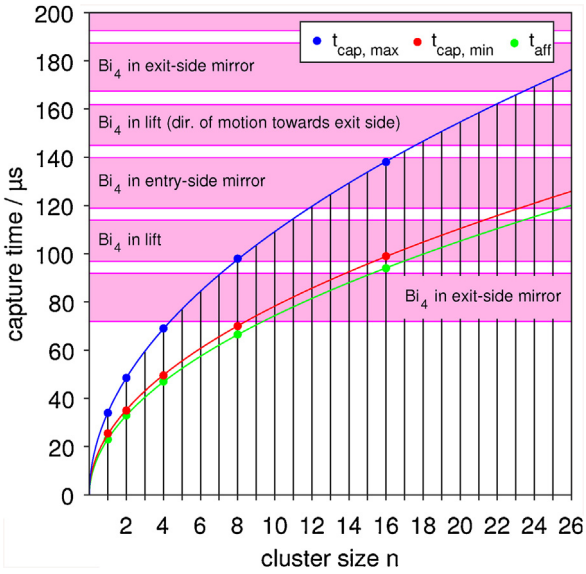

Fig. 6. (color online) Graphical representation of viable capture times for ion species and possible repeated in-trap lift captures for the case of first capturing Bi_4^-. The red and blue lines represent the minimum and maximum possible capture times for a given cluster size respectively, and the green line shows the time at which ions are first affected by the switching of the in-trap lift electrode. The magenta-shaded areas show the ranges of times where Bi_4^- is unaffected by in-trap lift switching as shown in Fig. 5. For more details, see text.

4.4. Determination of m/q-range restrictions for repeated capture

For the application of a second capture pulse, an additional criterion has to be introduced: After the switching down of the lift potential for the initial capture, it has to be raised again before the ions to be captured in the second pulse have moved into the lift tube. Specifically, the potential has to be fully raised by the time the ions have moved too close to the lift so that they would be disturbed by the switching.

The green line in Fig. 6 shows this time, t_{aff}, at which an incoming ion species is first affected by the in-trap lift switching. It has again been determined for the cluster sizes $n = 1$, 2, 4, 8, and 16 (green circles in Fig. 6), this time by varying the time at which the lift potential is raised (via varying Δt_{down}) and evaluating whether the cluster size in question can still be successfully captured. Fitting (1) yields $\theta_{aff} = 23.48(5)\,\mu s$.

The graphical criterion for the sequential capture amounts to the following: Both the $t_{cap,min}$ (red) and t_{aff} (green) values of the heavier ion species have to lie within the same timeframe where the lighter ion species is unaffected by the switching pulses (magenta-shaded area). This means that the lift potential can be raised soon enough not to disturb the heavier ion species and be lowered for a successful sequential capture while the initial ion species is still undisturbed by the potential switches.

As an example, for Bi_4^- as the lighter ion, it is possible to capture Bi_{10}^- or Bi_{11}^- (lift potential can be fully raised and switched back down again while Bi_4^- is in the exit-side mirror). It is, however, not possible to sequentially capture Bi_9^-, as the lift cannot be raised early enough (t_{aff} value for Bi_9^- lies outside the magenta area). Note that these statements are correct for cluster sizes of any cluster species.

An additional restriction can be found for the repeated capture from a single ion pulse (meaning that lighter ions will reach the trap first), namely, an upper limit for the possible mass difference of the ion species from the first and second capture pulse. Increasingly heavy ions will need longer and longer to move into the in-trap lift. It follows that the time between them first sampling the switching pulses (t_{aff}) and them having moved far enough into the lift tube so it can be switched down again ($t_{\mathrm{cap,min}}$) continues to increase. In terms of Fig. 6: The red and green lines will at some point diverge farther than the width of a magenta strip. It will consequently not be possible to both raise the lift potential soon enough and keep it raised long enough to capture the heavy ions without disturbing the lighter, previously-captured ones.

To calculate this limit for the present system, the relation

$$t_{\mathrm{cap,min}}(n_{\mathrm{max}}) - t_{\mathrm{aff}}(n_{\mathrm{max}}) < 0.22 \cdot T(n_{\mathrm{min}}) \tag{3}$$

is utilized, i.e. the difference between the blue and green line for the larger cluster size has to remain less than 22% of the smaller size's revolution period (the width of a magenta strip). The ions' revolution periods

$$T(n) = \sqrt{\frac{n}{n_{\mathrm{ref}}}} \cdot T(n_{\mathrm{ref}}) \tag{4}$$

follow a square root function, allowing their calculation with a single reference period, in this case that of Bi_4^-. For the present system, $T(4) = 95.6\,\mu s$ has been determined. Note that the uncertainty of $T(4)$ is negligible for these considerations. Using (1) and (4), (3) yields

$$\frac{n_{\mathrm{max}}}{n_{\mathrm{min}}} = \frac{(m/q)_{\mathrm{max}}}{(m/q)_{\mathrm{min}}} \lesssim 66 \tag{5}$$

for the present system.

To increase the mass range of the technique beyond this limit, multiple ion pulses have to be produced for injection into the trap. If the heavier ion species is captured first, a significantly-lighter species can always be captured later on from a different ion pulse.

Since all considered timeframes stay constant for all revolution periods, the second capture could also be performed at a much later time to—for example—introduce specific reference ions at a fixed revolution number.

We note that it would also be possible to perform multiple sequential captures, where each additional ion species is captured while all previously-stored ones are retained in the drift tube or mirror potentials. However, the timing conditions become increasingly demanding for such a scheme, making it somewhat difficult to find suitable time windows to perform the injections.

4.5. Sequential capture of Bi_4^- and Bi_{11}^-

To visualize the number of stored ion species for a specific secondary-capture scheme with $t_{\mathrm{cap1}} = 58\,\mu s$, $\Delta t_{\mathrm{down}} = 19\,\mu s$, and $\Delta t_{\mathrm{up}} = 7\,\mu s$, Fig. 7 shows two *N*-versus-ToF plots [21]. ToF spectra recorded after incremental storage times are arranged as rows of a color-intensity plot to show the movement of individual ion species over the course of several tens of revolution periods. The initial capture pulse—as can be inferred from Fig. 6—is viable to store the cluster sizes $n = 3$ to 5. Consequently, the bottom part of Fig. 7, which shows the operation without the secondary capture pulse enabled, exhibits three distinct ion species revolving in the MR-ToF analyzer. Since the incremental time between the spectra closely matches the Bi_{11}^- revolution period of 158.6 µs, all three cluster sizes change their position in the analyzer between the individual measurements, leading to the detected signals' τ-value changing. The signals can be identified in a given spectrum by their intensities

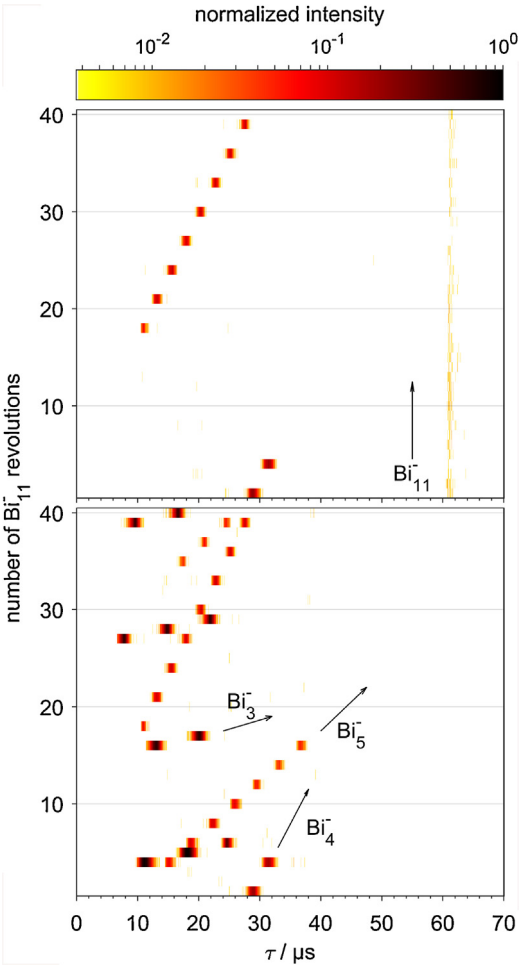

Fig. 7. (color online) *N*-versus-ToF plots [21] after repeated capture with $t_{\mathrm{cap1}} = 58\,\mu s$, $\Delta t_{\mathrm{down}} = 19\,\mu s$, and $\Delta t_{\mathrm{up}} = 7\,\mu s$. Bottom: second capture disabled. Top: second capture enabled. For more information, see text.

(i.e. color) and their characteristic "slopes" between the measurements, as indicated by the arrows. At storage times where a signal is not visible in the spectrum, the ions are located in the MR-ToF mirror potentials or in the in-trap lift with a direction of motion away from the detector at the time of ejection. For more information about these effects and the behavior of ions of different m/q in an *N*-versus-ToF plot, the reader is referred to [22].

The top of Fig. 7 shows the same measurements, however with the second capture pulse enabled. The Δt_{down} and Δt_{up} times are optimized to retain Bi_4^- in the exit-side mirror (see Fig. 6), the Bi_3^- and Bi_5^- ion species are lost. However, Bi_{11}^- is captured during the second capture pulse, as indicated by the ion signal at identical τ-values throughout the measurements. According to (2), it is clearly not possible to capture Bi_4^- and Bi_{11}^- in the present setup with single-capture-pulse operation. However, utilizing the technique of multiple capture pulses, this can be achieved.

Although it is possible to also capture Bi_{10}^- and Bi_{12}^- to the already-stored Bi_4^- ions (see above), the timing of the second capture was chosen to only inject Bi_{11}^-. The lift potential is raised at $t_{\mathrm{cap1}} + \Delta t_{\mathrm{down}} = 77\,\mu s$, which is too late to not disturb the Bi_{10}^- ions. The actual second capture time amounts to $t_{\mathrm{cap2}} = t_{\mathrm{cap1}} + \Delta t_{\mathrm{down}} + \Delta t_{\mathrm{up}} = 84\,\mu s$, which is viable for Bi_{11}^- but not for Bi_{12}^- ($t_{\mathrm{cap,min}} = 85.7\,\mu s$). Such a preselection cannot always be performed however, as the relative mass difference between cluster sizes decreases with increasing n. Additionally, contaminant ion

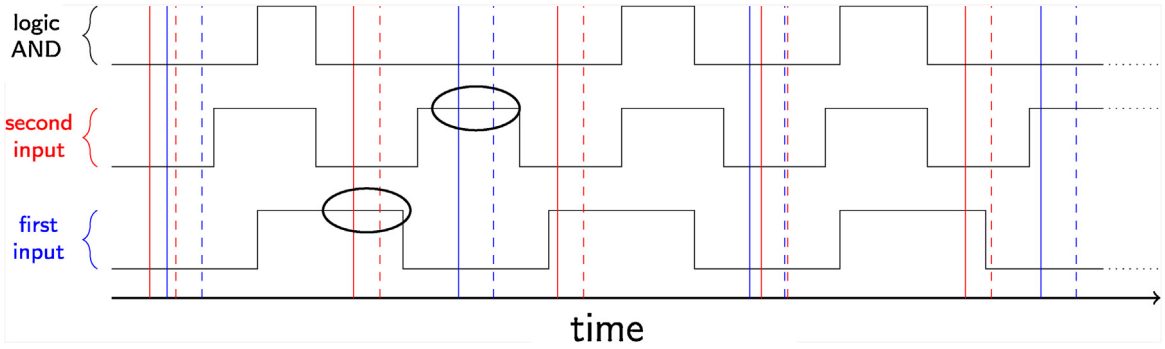

Fig. 8. (color online) Schematic of transversal ion ejection [23a] with two individual deflector functions and a single output determined by a logical AND gate. The red and blue vertical lines indicate two ion species passing the deflector electrode before (solid) and after (dashed) their reflection in the exit-side mirror potential. Ellipses mark where ions would first sample a "high" state of the other deflector function.

species with masses close to the ions of interest cannot be selectively excluded from the capture.

For a precise control over the retained ion species, however, an in-trap selection can be performed after the repeated capture to specifically retain ions of interest from both capture pulses (see following section). Thus, it is not necessary to precisely tune the timings of the repeated capture itself for ion selection.

5. Transversal ejection at multiple frequencies

The technique of transversal ion ejection from MR-ToF devices by means of synchronized deflector pulses has been previously reported for several setups. To this end, either a set of deflector electrodes located within the MR-ToF device [35,42] or one of its mirror electrodes [33] is switched between deflecting and non-deflecting states. For the present setup, an in-depth study has been performed to characterize the technique's efficiency and selection resolving power, as well as typical operational parameters [23]: The retained mass range was demonstrated to be adjustable by changing the frequency, phase, and duty cycle of the rectangular deflector function. Ion species matching a given set of conditions pass a deflector electrode located between the in-trap lift and stack of mirror electrodes (see Fig. 1) at ground potential, while all other ions sample a transversally-deflecting electric field from some voltages $\pm U_D$ applied to opposing parts of the electrode. A voltage of $\pm U_D = 10\,V$ is sufficient to eject ions over the course of a few revolution periods [23].

In the following, the technique is extended to allow for the simultaneous isolation of ion species with large m/q differences. Rather than widening the "window" for undisturbed passage to a larger mass range, i.e. without deflecting any ion species with an m/q value between two species to be retained, an advanced function for the time windows is constructed by use of an AND gate, which allows two ions of interest to pass. The vertical lines in Fig. 8 indicate the two ion species revolving in the analyzer with frequencies matching those of the two input deflector functions. As described in [23], each species has to pass the deflector electrode twice in quick succession: before (solid lines) and after (dashed lines) their reflection in the mirror potential. Note that, while the individual input functions would each disturb the other ion, respectively (ion passage during "high" state, marked by ellipses), the resulting AND-function is on a "low" state whenever either species passes. With this approach, the frequency, phase, and duty cycle for the selection of each species of interest can be individually tuned. This is of special interest for investigations as performed in the present study, where ion species with large m/q-differences are simultaneously stored. Typically, ion selection will need to be more complex than the restriction to a single mass range of interest.

To extend the technique from the one implemented for a single ion species, only the (multiple) AND gate itself and—depending on the number of input signals—additional function generators are needed. The general operational parameters found in [23], such as duty-cycle restrictions, $\pm U_D$-values, and number of pulses needed for ejection, are still valid. When several input functions are involved, the deflection of contaminants becomes slower in terms of revolution periods due to the fact that a decreasing amount of deflector pulses will actually be applied to the electrode.

Fig. 9 shows N-versus-ToF plots for a sequential capture scheme similar to that of Fig. 7, however with the parameters $t_{cap1} = 62\,\mu s$, $\Delta t_{down} = 37\,\mu s$, and $\Delta t_{up} = 11\,\mu s$. This results in a capture of the cluster sizes $n = 4$ to 6 in the first and $n = 18$ and 19 in the second capture pulse. Contrary to the previous measurement, the Bi_4^- ion species is retained in the in-trap lift electrode instead of the exit-side mirror. The N-versus-ToF plots' incremental time closely matches the Bi_{19}^- revolution period $T(19) = 211.1\,\mu s$.

When no transversal ion ejection is employed (bottom of Fig. 9), a number of ion species are visible in the spectra, most prominently Bi_4^-, Bi_6^-, Bi_{18}^-, and Bi_{19}^- (Bi_5^- is lost during the second capture pulse). As the measurement was performed with a larger number of iterations compared to the one shown in Fig. 7, additional contaminant ion species are also visible. These can be traced to low-abundance Bi-Pb compound clusters resulting from target impurities. Since the difference in m/q values between the light ions and the target reference species for the N-versus-ToF plot, Bi_{19}^-, is larger, the patterns formed in the range of low τ-values are less obvious, making the identification and tracking of individual ion species somewhat more difficult.

The upper part of Fig. 9 shows the same measurement with the transversal ejection enabled. Two deflector functions are used, matching the revolution frequencies of Bi_4^- and Bi_{19}^-. Consequently, all other ion species are ejected from the analyzer over the course of the storage time of roughly 21 ms. The deflection with the Bi_4^--frequency is started on the second (Bi_4^-) period ($-340°$ starting phase, see [23] for definition), the deflection with the Bi_{19}^--frequency is started with a phase of $-193°$ to adjust for this species' capture close to the entry-side of the lift electrode. Both deflector functions exhibit duty cycles of 60%, the Bi_4^- one consists of 200, the Bi_{19}^- one of 100 deflector pulses.

The most prominent change between the measurements is the ejection of the Bi_{18}^- signal after four revolution periods, however, the ejection of the light ion species can also be observed. A large number of ions are removed from the spectra early on, allowing a clearer tracking of Bi_4^-. The deformed Bi_4^- signal shapes at (Bi_{19}^-) revolution numbers 2, 41, and 80 result from the Bi_4^- signal sampling the lift switching pulse during ejection due to being located close to the end of the drift tube. In the range from 8 to 41 (Bi_{19}^-) revolution periods, the Bi-Pb compound clusters preceding the Bi_4^-

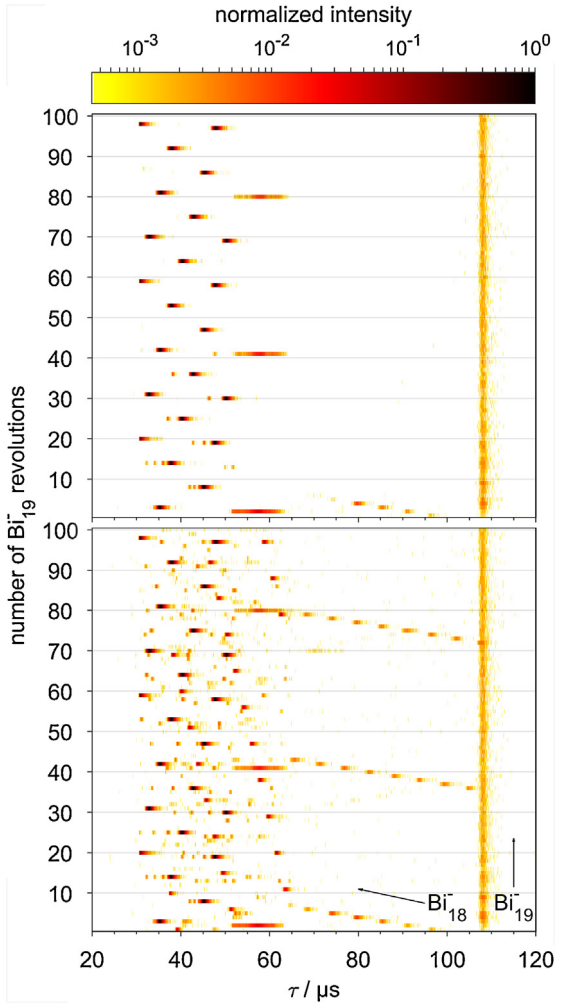

Fig. 9. (color online) *N*-versus-ToF plots after repeated capture with $t_{cap1} = 62\,\mu s$, $\Delta t_{down} = 37\,\mu s$, and $\Delta t_{up} = 11\,\mu s$. Bottom: without transversal ejection. Top: transversal ejection enabled to retain Bi_4^- (10.324 kHz, −340° starting phase, 60% duty cycle) and Bi_{19}^- (4.737 kHz, −193° starting phase, 60% duty cycle).

ion species can be observed. They become increasingly separated from the ion of interest until their eventual ejection. For illustration, Fig. 10 shows the individual spectra after 58 Bi_{19}^- revolutions: While the Bi_4^- and Bi_{19}^- ions show no change between the spectra, all other ion species are no longer present in the trap when the transversal ejection is enabled. The corresponding selection resolving power (for the selection of Bi_4^-) is around 840. The Bi-Pb compound clusters around Bi_{19}^- are not visible in the current measurement due to the low abundance of that cluster size, however, the selection resolving power needed for their ejection is around 4000, which is still well within the capabilities of the technique for the present system [23].

6. Summary and outlook

The present study illustrates new approaches for the operation of an electrostatic ion beam trap for simultaneous storage of ions with large *m*/*q*-differences. To this end, multiple capture pulses are applied to store ions that could not be captured with a single switching. The timing requirements of the capture pulses are investigated and the mass range that can be captured in both single-capture- and multiple-capture-pulse operation is determined for the present system. A maximum mass ratio of 1.9 is found for regular, single-pulse capture. Employing multiple-capture-pulse

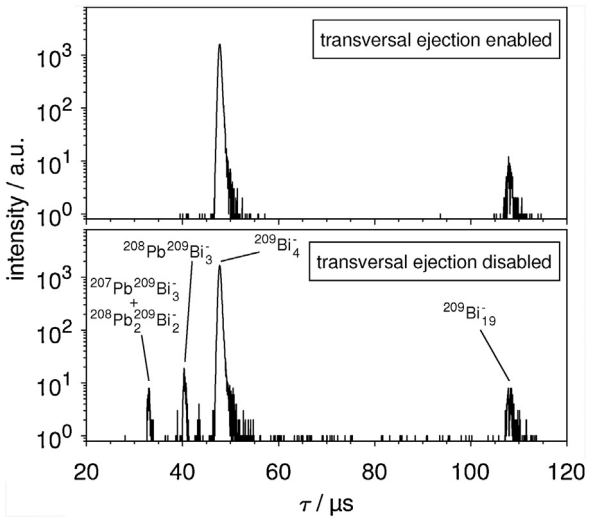

Fig. 10. Individual spectra from the *N*-versus-ToF plots of Fig. 9 after 58 Bi_{19}^- revolutions. The (compound) clusters visible at low τ-values have completed 127 revolution periods.

operation, the cluster ions Bi_4^- and Bi_{19}^- are successfully stored sequentially, surpassing this limit by more than a factor of two.

Since the sequential operation implies a large number of ion species in the trap, the technique of transversal ion ejection is used to perform a simultaneous in-trap selection of different ions of interest. For single-species selection, this technique has already been characterized in-depth (see [23] and references therein). In the present study, it is shown that with the previously-found parameters, the operation can be expanded to select two ion species of interest simultaneously. Utilizing an AND-gate logic, two individually-tuned functions are used to form a deflector function that disturbs neither ion of interest but leads to the ejection of all other species.

The combination of both techniques offers the possibility of a broad and yet precisely-controlled mass range for cluster and molecular experiments in an electrostatic ion beam trap. For investigations based on, e.g., the interaction of stored ions with photons [14,26] or electrons [12,45], the EIBT can double as both a high-precision selection device and reaction chamber. Its high mass resolving powers enable the detection—and selective ejection—of contaminant species like the bismuth-lead compound clusters found in the present measurements. The general principle of injecting additional ions to an already-stored bunch also offers possibilities like the introduction of same-species reference ions at specific phases of the ions' revolution period.

Acknowledgements

This work has been supported by the German Ministry for Education and Research (BMBF).

References

[1] H. Wollnik, M. Przewloka, Time-of-flight mass spectrometers with multiply reflected ion trajectories, Int. J. Mass Spectrom. Ion Processes 96 (3) (1990) 267–274, ISSN 0168-1176, doi:https://doi.org/10.1016/0168-1176(90)85127-N.
[2] D. Zajfman, O. Heber, L. Vejby-Christensen, I. Ben-Itzhak, M. Rappaport, R. Fishman, M. Dahan, Electrostatic bottle for long-time storage of fast ion beams, Phys. Rev. A 55 (1997) R1577–R1580, doi:10.1103/PhysRevA.55.R1577.
[3] M. Dahan, R. Fishman, O. Heber, M. Rappaport, N. Altstein, D. Zajfman, W.J. van der Zande, A new type of electrostatic ion trap for storage of fast ion beams, Rev. Sci. Instrum. 69 (1) (1998) 76–83, http://dx.doi.org/10.1063/1.1148481.
[4] Y. Ito, P. Schury, M. Wada, S. Naimi, T. Sonoda, H. Mita, F. Arai, A. Takamine, K. Okada, A. Ozawa, H. Wollnik, Single-reference high-precision mass

measurement with a multireflection time-of-flight mass spectrograph, Phys. Rev. C 88 (2013) 011306, http://dx.doi.org/10.1103/PhysRevC.88.011306.
[5] F. Wienholtz, D. Beck, K. Blaum, C. Borgmann, M. Breitenfeldt, R.B. Cakirli, S. George, F. Herfurth, J.D. Holt, M. Kowalska, S. Kreim, D. Lunney, V. Manea, J. Menendez, D. Neidherr, M. Rosenbusch, L. Schweikhard, A. Schwenk, J. Simonis, J. Stanja, R.N. Wolf, K. Zuber, Masses of exotic calcium isotopes pin down nuclear forces, Nature 498 (7454) (2013) 346–349, ISSN 0028-0836, doi:https://doi.org/10.1038/nature12226, letter.
[6] D. Atanasov, P. Ascher, K. Blaum, R.B. Cakirli, T.E. Cocolios, S. George, S. Goriely, F. Herfurth, H.-T. Janka, O. Just, M. Kowalska, S. Kreim, D. Kisler, Y.A. Litvinov, D. Lunney, V. Manea, D. Neidherr, M. Rosenbusch, L. Schweikhard, A. Welker, F. Wienholtz, R.N. Wolf, K. Zuber, Precision Mass Measurements of $^{129-131}$Cd and Their Impact on Stellar Nucleosynthesis via the Rapid Neutron Capture Process, Phys. Rev. Lett. 115 (2015) 232501, http://dx.doi.org/10.1103/PhysRevLett.115.232501.
[7] M. Rosenbusch, P. Ascher, D. Atanasov, C. Barbieri, D. Beck, K. Blaum, C. Borgmann, M. Breitenfeldt, R.B. Cakirli, A. Cipollone, S. George, F. Herfurth, M. Kowalska, S. Kreim, D. Lunney, V. Manea, P. Navrátil, D. Neidherr, L. Schweikhard, V. Somà, J. Stanja, F. Wienholtz, R.N. Wolf, K. Zuber, Probing the $N = 32$ Shell Closure below the Magic Proton Number $Z = 20$: Mass Measurements of the Exotic Isotopes ^{52,53}K, Phys. Rev. Lett. 114 (2015) 202501, http://dx.doi.org/10.1103/PhysRevLett.114.202501.
[8] A. de Roubin, D. Atanasov, K. Blaum, S. George, F. Herfurth, D. Kisler, M. Kowalska, S. Kreim, D. Lunney, V. Manea, E. Minaya Ramirez, M. Mougeot, D. Neidherr, M. Rosenbusch, L. Schweikhard, A. Welker, F. Wienholtz, R.N. Wolf, K. Zuber, Nuclear deformation in the $A \approx 100$ region: Comparison between new masses and mean-field predictions, Phys. Rev. C 96 (2017) 014310, http://dx.doi.org/10.1103/PhysRevC.96.014310.
[9] A. Welker, N.A.S. Althubiti, D. Atanasov, K. Blaum, T.E. Cocolios, F. Herfurth, S. Kreim, D. Lunney, V. Manea, M. Mougeot, D. Neidherr, F. Nowacki, A. Poves, M. Rosenbusch, L. Schweikhard, F. Wienholtz, R.N. Wolf, K. Zuber, Binding Energy of ^{79}Cu: Probing the Structure of the Doubly Magic ^{78}Ni from Only One Proton Away, Phys. Rev. Lett. 119 (2017) 192502, http://dx.doi.org/10.1103/PhysRevLett.119.192502.
[10] M. Mougeot, D. Atanasov, K. Blaum, K. Chrysalidis, T.D. Goodacre, D. Fedorov, V. Fedosseev, S. George, F. Herfurth, J.D. Holt, D. Lunney, V. Manea, B. Marsh, D. Neidherr, M. Rosenbusch, S. Rothe, L. Schweikhard, A. Schwenk, C. Seiffert, J. Simonis, S.R. Stroberg, A. Welker, F. Wienholtz, R.N. Wolf, K. Zuber, Precision Mass Measurements of $^{58-63}$Cr: Nuclear Collectivity Towards the $N = 40$ Island of Inversion, Phys. Rev. Lett. 120 (2018) 232501, http://dx.doi.org/10.1103/PhysRevLett.120.232501.
[11] M. Rosenbusch, Y. Ito, P. Schury, M. Wada, D. Kaji, K. Morimoto, H. Haba, S. Kimura, H. Koura, M. MacCormick, H. Miyatake, J.Y. Moon, K. Morita, I. Murray, T. Niwase, A. Ozawa, M. Reponen, A. Takamine, T. Tanaka, H. Wollnik, New mass anchor points for neutron-deficient heavy nuclei from direct mass measurements of radium and actinium isotopes, Phys. Rev. C 97 (2018) 064306, http://dx.doi.org/10.1103/PhysRevC.97.064306.
[12] O. Heber, P.D. Witte, A. Diner, K.G. Bhushan, D. Strasser, Y. Toker, M.L. Rappaport, I. Ben-Itzhak, N. Altstein, D. Schwalm, A. Wolf, D. Zajfman, Electrostatic ion beam trap for electron collision studies, Rev. Sci. Instrum. 76 (1) (2005) 013104, http://dx.doi.org/10.1063/1.1832192.
[13] R. Antoine, T. Doussineau, P. Dugourd, F. Calvo, Multiphoton dissociation of macromolecular ions at the single-molecule level, Phys. Rev. A 87 (2013) 013435, http://dx.doi.org/10.1103/PhysRevA.87.013435.
[14] B. Kafle, O. Aviv, V. Chandrasekaran, O. Heber, M.L. Rappaport, H. Rubinstein, D. Schwalm, D. Strasser, D. Zajfman, Electron detachment and fragmentation of laser-excited rotationally hot Al_4^-, Phys. Rev. A 92 (2015) 052503, http://dx.doi.org/10.1103/PhysRevA.92.052503.
[15] C. Breitenfeldt, K. Blaum, S. George, J. Göck, G. Guzmán-Ramírez, J. Karthein, T. Kolling, M. Lange, S. Menk, C. Meyer, J. Mohrbach, G. Niedner-Schatteburg, D. Schwalm, L. Schweikhard, A. Wolf, Long-Term Monitoring of the Internal Energy Distribution of Isolated Cluster Systems, Phys. Rev. Lett. 120 (2018) 253001, http://dx.doi.org/10.1103/PhysRevLett.120.253001.
[16] E.T. Dziekonski, J.T. Johnson, K.W. Lee, S.A. McLuckey, Determination of Collision Cross Sections Using a Fourier Transform Electrostatic Linear Ion Trap Mass Spectrometer, J. Am. Soc. Mass Spectrom. 29 (2) (2018) 242–250, ISSN 1879-1123, doi:10.1007/s13361-017-1720-1.
[17] R.N. Wolf, D. Beck, K. Blaum, C. Böhm, C. Borgmann, M. Breitenfeldt, N. Chamel, S. Goriely, F. Herfurth, M. Kowalska, S. Kreim, D. Lunney, V. Manea, E. Minaya Ramirez, S. Naimi, D. Neidherr, M. Rosenbusch, L. Schweikhard, J. Stanja, F. Wienholtz, K. Zuber, Plumbing neutron stars to new depths with the binding energy of the exotic nuclide ^{82}Zn, Phys. Rev. Lett. 110 (2013) 041101, http://dx.doi.org/10.1103/PhysRevLett.110.041101.
[18] N.A. Althubiti, D. Atanasov, K. Blaum, T.E. Cocolios, T. Day Goodacre, G.J. Farooq-Smith, D.V. Fedorov, V.N. Fedosseev, S. George, F. Herfurth, K. Heyde, S. Kreim, D. Lunney, K.M. Lynch, V. Manea, B.A. Marsh, D. Neidherr, M. Rosenbusch, R.E. Rossel, S. Rothe, L. Schweikhard, M.D. Seliverstov, A. Welker, F. Wienholtz, R.N. Wolf, K. Zuber, Spectroscopy of the long-lived excited state in the neutron-deficient nuclides ^{195,197,199}Po by precision mass measurements, Phys. Rev. C 96 (2017) 044325, http://dx.doi.org/10.1103/PhysRevC.96.044325.
[19] D. Atanasov, D. Beck, K. Blaum, C. Borgmann, R. B. Cakirli, T. Eronen, S. George, F. Herfurth, A. Herlert, M. Kowalska, S. Kreim, Y. A. Litvinov, D. Lunney, V. Manea, D. Neidherr, M. Rosenbusch, L. Schweikhard, F. Wienholtz, R. N. Wolf, K. Zuber, Precision mass measurements of cesium isotopes-new entries in the ISOLTRAP chronicles, Journal of Physics G: Nuclear and Particle Physics 44 (4) (2017) 044004.
[20] V. Manea, P. Ascher, D. Atanasov, A.E. Barzakh, D. Beck, K. Blaum, C. Borgmann, M. Breitenfeldt, R.B. Cakirli, T.E. Cocolios, T. Day Goodacre, D.V. Fedorov, V.N. Fedosseev, S. George, F. Herfurth, M. Kowalska, S. Kreim, Y.A. Litvinov, D. Lunney, B. Marsh, D. Neidherr, M. Rosenbusch, R.E. Rossel, S. Rothe, L. Schweikhard, F. Wienholtz, R.N. Wolf, K. Zuber, Penning-trap mass spectrometry and mean-field study of nuclear shape coexistence in the neutron-deficient lead region, Phys. Rev. C 95 (2017) 054322, http://dx.doi.org/10.1103/PhysRevC.95.054322.
[21] P. Schury, Y. Ito, M. Wada, H. Wollnik, Wide-band mass measurements with a multi-reflection time-of-flight mass spectrograph, Int. J. Mass spectrom. 359 (2014) 19–25, ISSN 1387-3806, http://dx. doi.org/10.1016/j.ijms.2013.11.005.
[22] S. Knauer, P. Fischer, G. Marx, B. Schabinger, L. Schweikhard, R. Wolf, Multi-reflection time-of-flight mass spectrometry with combined in-trap lift capture and mirror-switch ejection, Int. J. Mass spectrom. 423 (2017) 46–53, ISSN 1387-3806, https://doi.org/10.1016/j.ijms.2017.10.007.
[23] P. Fischer, S. Knauer, G. Marx, L. Schweikhard, In-depth study of in-trap high-resolution mass separation by transversal ion ejection from a multi-reflection time-of-flight device, Rev. Sci. Instrum. 89 (1) (2018) 015114, http://dx.doi.org/10.1063/1.5009167.
[24] A. Naaman, K.G. Bhushan, H.B. Pedersen, N. Altstein, O. Heber, M.L. Rappaport, R. Moalem, D. Zajfman, Metastable states of negative carbon clusters: Cn-, n=2-6, The Journal of Chemical Physics 113 (11) (2000) 4662–4667, http://dx.doi.org/10.1063/1.1286978.
[25] O. Aviv, Y. Toker, M. Errit, K.G. Bhushan, H.B. Pedersen, M.L. Rappaport, O. Heber, D. Schwalm, D. Zajfman, A bent electrostatic ion beam trap for simultaneous measurements of fragmentation and ionization of cluster ions, Rev. Sci. Instrum. 79 (8) (2008) 083110, http://dx.doi.org/10.1063/1.2972151.
[26] O. Aviv, B. Kafle, V. Chandrasekaran, O. Heber, M.L. Rappaport, H. Rubinstein, D. Schwalm, D. Strasser, Y. Toker, D. Zajfman, Absolute photo-destruction and photo-fragmentation cross section measurements using an electrostatic ion beam trap, Rev. Sci. Instrum. 84 (5) (2013) 053106, http://dx.doi.org/10.1063/1.4804646.
[27] E.E. Pierson, D.Z. Keifer, N.C. Contino, M.F. Jarrold, Probing higher order multimers of pyruvate kinase with charge detection mass spectrometry, Int. J. Mass spectrom. 337 (2013) 50–56, ISSN 1387-3806, https://doi.org/10.1016/j.ijms.2013.01.002.
[28] R.T. Hilger, E.T. Dziekonski, R.E. Santini, S.A. McLuckey, Injecting electrospray ions into a Fourier transform electrostatic linear ion trap, Int. J. Mass spectrom. 378 (2015) 281–287, ISSN 1387-3806, doi:https://doi.org/10.1016/j.ijms.2014.09.005.
[29] W.H. Benner, A gated electrostatic ion trap to repetitiously measure the charge and m/z of large electrospray ions, Anal. Chem. 69 (20) (1997) 4162–4168, http://dx.doi.org/10.1021/ac970163e.
[30] S. Ring, H.B. Pedersen, O. Heber, M.L. Rappaport, P.D. Witte, K.G. Bhushan, N. Altstein, Y. Rudich, I. Sagi, D. Zajfman, Fourier transform time-of-flight mass spectrometry in an electrostatic ion beam trap, Anal. Chem. 72 (17) (2000) 4041–4046, http://dx.doi.org/10.1021/ac000317h.
[31] K.G. Bhushan, S.C. Gadkari, J.V. Yakhmi, V.C. Sahni, Electrostatic ion trap and Fourier transform measurements for high-resolution mass spectrometry, Rev. Sci. Instrum. 78 (8) (2007) 083302, http://dx.doi.org/10.1063/1.2777195.
[32] R.T. Hilger, P.J. Wyss, R.E. Santini, S.A. McLuckey, Absorption mode Fourier transform electrostatic linear ion trap mass spectrometry, Anal. Chem. 85 (17) (2013) 8075–8079, http://dx.doi.org/10.1021/ac401935e.
[33] R. T. Hilger, R. Santini, S. Mcluckey, Square Wave Modulation of a Mirror Lens for Ion Isolation in a Fourier Transform Electrostatic Linear Ion Trap Mass Spectrometer, International Journal of Mass Spectrometry 362, doi:https://doi.org/10.1016/j.ijms.2014.02.003.
[34] W.R. Plaß, T. Dickel, U. Czok, H. Geissel, M. Petrick, K. Reinheimer, C. Scheidenberger, M.I. Yavor, Isobar separation by time-of-flight mass spectrometry for low-energy radioactive ion beam facilities, Nucl. Instrum. Methods Phys. Res. Section B 266 (19) (2008) 4560–4564, ISSN 0168-583X, doi: http://dx. doi.org/10.1016/j.nimb.2008.05.079.
[35] T. Dickel, W. Plaß, A. Becker, U. Czok, H. Geissel, E. Haettner, C. Jesch, W. Kinsel, M. Petrick, C. Scheidenberger, A. Simon, M. Yavor, A high-performance multiple-reflection time-of-flight mass spectrometer and isobar separator for the research with exotic nuclei, Nuclear Instruments and Methods in Physics Research Section A: Accelerators, Spectrometers, Detectors and Associated Equipment 777 (2015) 172–188, ISSN 0168-9002, https://doi.org/10.1016/j.nima.2014.12.094.
[36] R.N. Wolf, G. Marx, M. Rosenbusch, L. Schweikhard, Static-mirror ion capture and time focusing for electrostatic ion-beam traps and multi-reflection time-of-flight mass analyzers by use of an in-trap potential lift, Int. J. Mass spectrom. 313 (2012) 8–14, ISSN 1387-3806, doi: http://dx. doi.org/10.1016/j.ijms.2011.12.006.
[37] M. Rosenbusch, S. Kemnitz, R. Schneider, L. Schweikhard, R. Tschiersch, R.N. Wolf, Towards systematic investigations of space-charge phenomena in multi-reflection ion traps, AIP Conference Proceedings 1521 (1) (2013) 53–62, http://dx.doi.org/10.1063/1.4796061.
[38] P. Chauveau, P. Delahaye, G.D. France, S.E. Abir, J. Lory, Y. Merrer, M. Rosenbusch, L. Schweikhard, R. Wolf, PILGRIM, a Multi-Reflection Time-of-Flight Mass Spectrometer for Spiral2-S3 at GANIL, Nucl. Instrum. Methods Phys. Res. Section B 376 (2016) 211–215, http://dx.doi.org/10.1016/j.nimb.2016.01.025.

[39] E.T. Dziekonski, R.E. Santini, S.A. McLuckey, A dual detector Fourier transform electrostatic linear ion trap utilizing in-trap potential lift, Int. J. Mass spectrom. 405 (2016) 1–8, ISSN 1387-3806, https://doi.org/10.1016/j.ijms.2016.05.010.
[40] T.Y. Hirsh, N. Paul, M. Burkey, A. Aprahamian, F. Buchinger, S. Caldwell, J.A. Clark, A.F. Levand, L.L. Ying, S.T. Marley, G.E. Morgan, A. Nystrom, R. Orford, A.P. Galván, J. Rohrer, G. Savard, K.S. Sharma, K. Siegl, First operation and mass separation with the CARIBU MR-TOF, Nucl. Instrum. Methods Phys. Res. Section B 376 (2016) 229–232, ISSN 0168-583X, doi:https://doi.org/10.1016/j.nimb.2015.12.037.
[41] C. Stoermer, J. Friedrich, M.M. Kappes, Observation of multiply charged cluster anions upon pulsed UV laser ablation of metal surfaces under high vacuum, Int. J. Mass spectrom. 206 (1) (2001) 63–78, ISSN 1387-3806, doi:https://doi.org/10.1016/S1387-3806(00)00390-0.
[42] Y. Toker, N. Altstein, O. Aviv, M.L. Rappaport, O. Heber, D. Schwalm, D. Strasser, D. Zajfman, The kick-out mass selection technique for ions stored in an Electrostatic Ion Beam Trap, J. Instrum. 4 (09) (2009) P09001.
[43] P. Fischer, S. Knauer, G. Marx, L. Schweikhard, Non-isobaric time-of-flight correction for isobar resolving in MR-ToF mass spectrometry, Int. J. Mass spectrom. 432 (2018) 44–51, ISSN 1387-3806, doi:https://doi.org/10.1016/j.ijms.2018.07.004.
[44] D. Beck, K. Blaum, H. Brand, F. Herfurth, S. Schwarz, A new control system for ISOLTRAP, Nuclear Instruments and Methods in Physics Research Section A: Accelerators, Spectrometers, Detectors and Associated Equipment 527 (3) (2004) 567–579, ISSN 0168-9002, doi:https://doi.org/10.1016/j.nima.2004.02.043.
[45] A. Diner, Y. Toker, D. Strasser, O. Heber, I. Ben-Itzhak, P.D. Witte, A. Wolf, D. Schwalm, M.L. Rappaport, K.G. Bhushan, D. Zajfman, Size-Dependent Electron-Impact Detachment of Internally Cold C_n^- and Al_n^- Clusters, Phys. Rev. Lett. 93 (2004) 063402, http://dx.doi.org/10.1103/PhysRevLett.93.063402.

7.3 Non-isobaric time-of-flight correction for isobar resolving in MR-ToF mass spectrometry

International Journal of Mass Spectrometry 432 (2018) 44–51

Contents lists available at ScienceDirect

International Journal of Mass Spectrometry

journal homepage: www.elsevier.com/locate/ijms

Full Length Article

Non-isobaric time-of-flight correction for isobar resolving in MR-ToF mass spectrometry

Paul Fischer*, Stefan Knauer, Gerrit Marx, Lutz Schweikhard

Institut für Physik, Universität Greifswald, 17489 Greifswald, Germany

ARTICLE INFO

Article history:
Received 17 May 2018
Received in revised form 10 July 2018
Accepted 17 July 2018
Available online 18 July 2018

Keywords:
Multi-reflection time-of-flight mass spectrometry
MR-ToF MS
Offline correction
Isobar separation

ABSTRACT

A development in multi-reflection time-of-flight (MR-ToF) mass spectrometry is presented with which isobars are resolved by means of an offline correction with the signal of a non-isobaric ion species. The method is demonstrated for a pair of Cr_2^+ isobars with a relative mass difference of $1.8 \cdot 10^{-5}$, with either an additional, non-isobaric Cr_2^+ or a CrO^+ ion appearing in the same time-of-flight spectrum, although at a different number of revolutions during the same storage time. This is in contrast to earlier applications where ToF shift corrections are performed with ions at identical revolution numbers, typically isobars that are also acting as mass-reference ions. It is shown that ions of virtually any mass simultaneously stored in the MR-ToF analyzer can be employed. This is particularly useful in situations where both the ions of interest and the reference ions for mass calibration have only small count rates not sufficient for the ToF-shift corrections. For the present system, the resolving power increases by more than a factor of two when the offline drift correction is applied.

1. Introduction and motivation

Multi-reflection time-of-flight mass spectrometers (MR-ToF MS), also referred to as electrostatic ion beam traps/EIBTs [1,2] or electrostatic linear ion traps/ELITs [3–5] are powerful tools for the investigation of charged particles, in particular as they are reaching mass resolving powers exceeding 10^5 in just a few tens of milliseconds [6–10]. This allows investigations such as precision mass measurements [11–17] as well as fast ion beam analysis [18] or ion separation for further investigations, e.g. in Penning traps [12,14,15,17,19–21] or devices for nuclear decay studies [22]. In their function as ion traps, MR-ToF devices are also used for the study of the properties of clusters and molecules [2,23,24].

For applications based on mass spectrometry, where ion species are retained as individual bunches revolving between the trap's electrostatic mirrors, the stability of the trap parameters, including said mirror potentials, is of significant importance, specifically for the separation of isobars [6,25,26]. Short-term drifts lead to a loss of resolving power, thus, the voltages applied should be as stable as possible. Passive and active voltage stabilization by means of temperature control, low-pass filtering, and feedback circuitry to ensure ideal storage conditions have been reported [4,8,9,26].

If drifts cannot be avoided, they may, however, be remediated by use of an additional correction-ion species [9,27–29]: In cases where both the ion species of interest and the correction species show systematic, identical time-of-flight shifts between measurement iterations, a retrospective offline correction is possible [27]. Such a drift correction entails fitting the correction-ion signal in each measurement iteration and retrospectively shifting each ToF axis, before all spectra are summed for further evaluation. It follows that the correction ion has to be present in high abundance to allow for a sufficient accuracy of the fitting routine. However, there is not always such an abundant ion available at the same revolution number.

We show that the correction of short-term drifts in this manner can be performed employing virtually any ion species stored simultaneously with the ions of interest, regardless of their difference in mass and, thus, their numbers of revolutions during the storage time. Instead of using an isobaric species as both reference and correction ion, an ion species with a larger mass difference is employed for correction to resolve both isobars of an ion pair of interest. Only then is it possible to employ one of them as a reference ion species, i.e. to determine the relative mass difference between the two.

The method is demonstrated for the pair of Cr_2^+ isobars with mass number 106. Since there are no high-abundance correction-ion species at $A = 106$, either the signals of a chromium dimer Cr_2^+ with $A = 104$ or a CrO^+ molecule with $A = 68$ are used for the drift correction.

* Corresponding author at: Institut für Physik, Universität Greifswald, Felix-Hausdorff-Str. 6, 17489 Greifswald, Germany.
E-mail address: paul.fischer@uni-greifswald.de (P. Fischer).

https://doi.org/10.1016/j.ijms.2018.07.004
1387-3806/

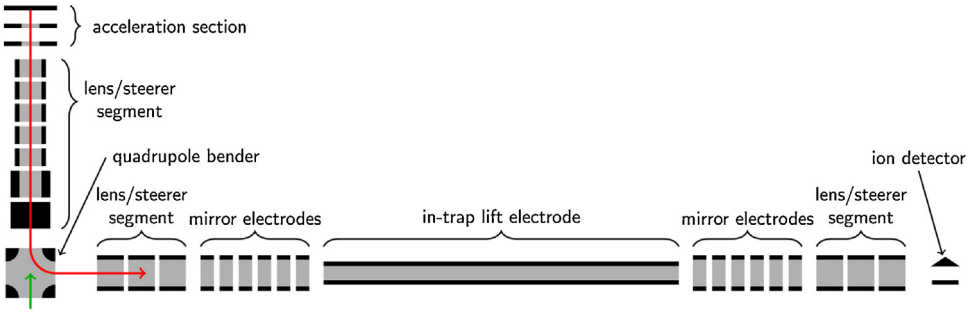

Fig. 1. Schematic of the experimental setup. Ions are created at the back of the acceleration section and guided towards the MR-ToF analyzer consisting of an in-trap lift and two stacks of mirror electrodes (red arrow). The direction of the laser beam is indicated as a green arrow.

Table 1
Voltages applied to the MR-ToF electrodes M1-M6 and in-trap lift electrode for cation storage. The in-trap lift is switched to ground for ion capture.

electrode	voltage / V
M1	−1315
M2	−1570
M3	585.2
M4	1063.4
M5	1282.73
M6	1668.9
in-trap lift	808 / 0

2. Experimental setup

The experimental setup (Fig. 1) combines a laser ablation source [30] with an MR-ToF analyzer. Ions of both polarities as well as neutral particles are produced by laser irradiation of metal targets in UHV conditions and charged atoms and clusters are subsequently guided towards the analyzer. Ion optical elements include several lenses and steerers as well as a quadrupole deflector for a 90° turn.

The laser (Continuum, MiniLite) provides a pulse energy of up to 15 mJ at the second harmonic ($\lambda = 532$ nm) with pulse lengths of about 6 ns. The laser's repetition rate of 10 Hz defines the experiment's cycle rate. The pulse energy is typically set to ∼3 mJ for the present measurements.

Ion acceleration is performed by applying a voltage of 2.01 kV to the target plate. The first electrode of the acceleration section following the target (distance: 10 mm, bore diameter: 5 mm) is set to 1.78 kV while the second electrode (distance: 10 mm, bore diameter: 3 mm) is grounded. This forms a Wiley/McLaren-type two-stage acceleration [31]. Subsequent to their focusing and 90° deflection, the ions pass through the MR-ToF analyzer, where they can be captured by lowering their total energy via an in-trap lift electrode [5,26,32].

The voltages applied to the mirror electrodes (Table 1) are low enough that the 2 - keV ions traverse the analyzer when no potential switching is employed (single-path operation). If the lift electrode is switched to ground potential, however, ions located therein lose some of their potential energy, resulting in their reflection at the mirror potentials. The innermost two mirror electrodes, M1 and M2, form a radially refocusing potential, the outer four electrodes, M3 through M6, ensure the ions' axial confinement. Ion ejection is analogously performed by reapplying the lift potential. Both the shape of the mirror potentials as well as the in-trap lift voltage determining the ions' total energy during storage are tuned to yield mass resolving powers exceeding 10^5.

To ensure a high stability of the applied mirror voltages, they are provided by precision power supplies (Stahl Electronics, HV 400) which are floated to reach the relevant voltage ranges (floating power supply: iseg Spezialelektronik GmbH, EHS 8240). The floating voltages themselves are buffered by individual low-pass filters consisting of 40 μF capacitors (General Electric, Geconol 28F2039) and 1 MΩ resistors (TT Electronics, Welwyn VRW68). Each capacitor is connected to ground potential. This setup provides very low-noise voltages that can still be tuned to optimize the storage conditions for individual measurements.

Ion detection is performed with a channeltron detector with a −5 kV conversion dynode. The detector signals are amplified (ORTEC, VT120a, 46 dB) and digitalized with a computer-mounted multiscaler card (Becker & Hickl GmbH, MSA-300). The control of the experimental timing pattern is performed with a LabVIEW-based control software [33] and a Field-Programmable-Gate-Array (FPGA) card (National Instruments, PCI-7811R).

The experiment cycle for MR-ToF operation consists of three parts:

1) The capture time t_{cap}, during which the ions travel from the source to the MR-ToF analyzer after their production by laser ablation/ionization. By tuning t_{cap}, the mass range of stored ions can be somewhat preselected.
2) The storage time t_s between switching down the lift potential for ion capture and reapplying it for ion ejection, during which the stored ions revolve between the MR-ToF mirrors. Different ion species have correspondingly different revolution periods T according to their mass-to-charge ratios. For observation of an ion species after N revolution periods, the storage time has to match $N \cdot T$. More information concerning the range of viable ejection times can be found in [34]. In addition, during the storage time, a pulsed deflector potential can be applied to a segmented ring electrode located between the in-trap lift and mirror electrodes. The frequency of the deflection pulses is matched to the revolution period of an ion species of interest (more precisely a mass-over-charge range). All ions not in sync are transversally ejected from the trap. Thus, the ions of interest can be isolated during (the beginning of) their storage. For more information about this technique of transversal ion ejection see Refs. [1,35].
3) The measured time-of-flight τ after the ion ejection. Since t_{cap} and t_s are known with the accuracy of the control system (negligible uncertainty: 80 MHz clock, 100 ppm accuracy), only this portion of the total flight time $t_{cap} + t_s + \tau$ has to be measured.

3. The Cr_2 isotopologue distribution

The single-path ToF spectrum from the laser ablation of a chromium target (Fig. 2) shows the cluster sizes $n = 1$, 2, and 3 (red labels) together with a number of oxide compounds (black labels) and additional contaminant ion species such as sodium, aluminum, potassium, and calcium (blue labels). Note that there are four stable chromium isotopes (Table 2), i.e. there are a number of possible isotopic compositions (so-called isotopologues) making up the signals involving chromium atoms. The mass resolving

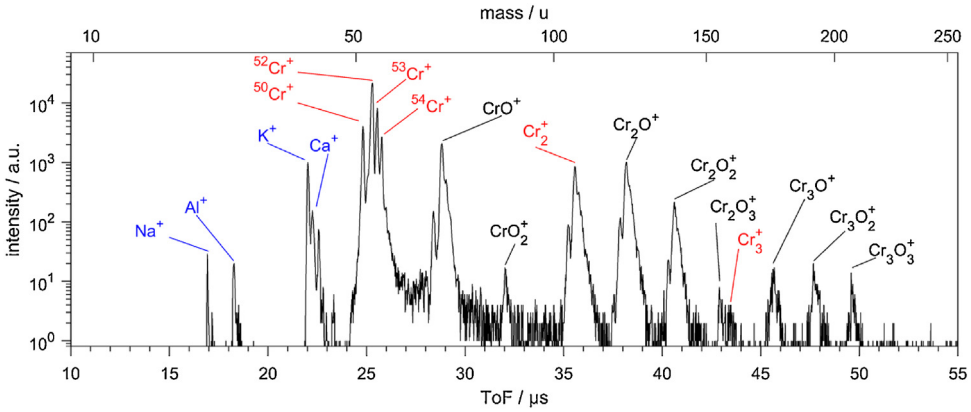

Fig. 2. Single-path spectrum resulting from laser ablation of a chromium target (3 mJ laser pulse energy). Next to the clusters Cr_1^+ through Cr_3^+ (red labels), a number of oxide compounds can be observed (black labels). Additional ion species observed include Na^+, Al^+, K^+, and Ca^+ (blue labels) (For interpretation of the references to colour in the text, the reader is referred to the web version of this article.).

Table 2
Mass numbers and relative abundances of all naturally occurring chromium isotopes [39].

mass number	50	52	53	54
rel. abundance	0.04345	0.83789	0.09501	0.02365

power in this single-path operation is sufficient to resolve the Cr^+ isotopes, for resolving the isotopologues however, MR-ToF operation is required.

From the values given in Table 2, the expected relative abundance of Cr_2^+ isotopologues can be calculated by summing the probabilities of all possible permutations for a given mass number (Table 3). These values can then be compared to the measured distribution of ion counts for already resolved Cr_2^+ isotopologues after four revolutions in the MR-ToF analyzer (Fig. 3).

The upper part of Fig. 3 shows a ToF spectrum of the resolved Cr_2^+ isotopologues that were not resolved in single-path mode. The capture time between the pulse of the ablation laser and the capture switching is $t_{cap} = 21\,\mu s$ and the storage time is $t_s = 136.7\,\mu s$, which amounts to four revolution periods for all ion species observed. By evaluating the number of detected ion counts for each signal, the ion species' relative abundances can be compared to the expected ones given in Table 3 as illustrated in the bottom of Fig. 3. For this purpose, both the expected and measured abundances have been normalized to the highest signal (which is that of $A = 104$ in both cases).

Obviously, all isotopologues with mass numbers between 100 and 107 show good agreement with the theory, whereas the $A = 108$ isotopologue shows a higher-than-expected abundance. Additionally, a signal with mass number 109 can be observed, which cannot be constructed from chromium atoms only. Both of these discrepancies can be traced back to contaminant ions, namely different isotopic compositions of the $CaCrO^+$ molecule. Since there are multiple isobaric compositions that cannot be resolved at this revolution number, an exact investigation of the contaminants is not performed. However, compared to the most abundant molecule, $^{40}Ca^{52}Cr^{16}O$, other isotopologues are less abundant by about an order of magnitude or more.

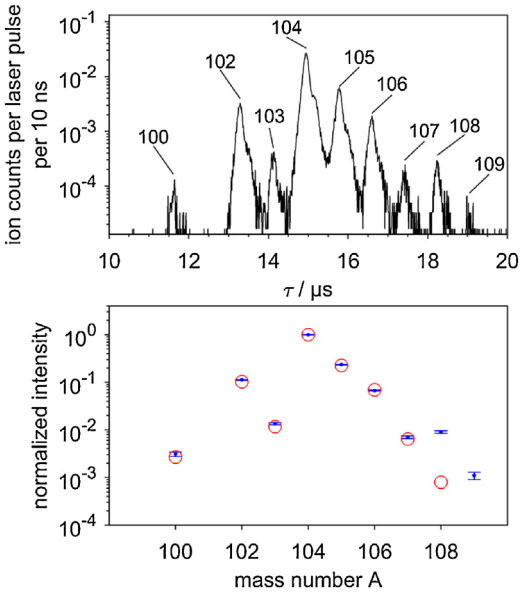

Fig. 3. Top: ToF spectrum of Cr_2^+ isotopologue distribution after 4 revolutions in the MR-ToF analyzer, summed over 60 700 laser pulses. Signals are marked by their mass numbers A. Bottom: total number of detected ions in each isotopologue signal (blue) and expected isotopologue abundances (Table 3), as indicated by red circles (For interpretation of the references to colour in the text, the reader is referred to the web version of this article.).

Note that the individual signal shapes deviate from those of pure Gaussian functions. This is due to the specific present settings of the acceleration section that have to be adopted to ensure a minimum signal FWHM. Particularly, the rightwards slope (longer flight-time) of the signals exhibits a slight bend. This will also be observed for signals investigated at higher revolution numbers in the following section, and is, in fact, already visible in the single path spectrum of Fig. 2.

For resolving the isobar pair of Cr_2^+ at mass number $A = 106$ (see Table 4), the storage time is increased to yield higher resolving powers. The count rate for the sum of isobars with $A = 106$ is

Table 3
Mass numbers, relative abundances [39], and number of "molecular isobars" for all naturally occurring Cr_2^+ isotopologues.

mass number	100	102	103	104	105	106	107	108
rel. abundance	0.0019	0.0728	0.0083	0.7041	0.1592	0.0487	0.0045	0.0006
no. of isobars	1 (50 + 50)	1 (50 + 52)	1 (50 + 53)	2 (50 + 54, 52 + 52)	1 (52 + 53)	2 (52 + 54, 53 + 53)	1 (53 + 54)	1 (54 + 54)

Table 4
Ion Masses [40] and natural abundance ratios (calculated from the isotope abundances of Table 2 [39] for the Cr_2^+ isobar pair with mass number 106, as well as corresponding relative mass differences.

mass number	mass / u	rel. mass difference	rel. abundance	abundance ratio
106 (52 + 54)	105.878834	$180 \cdot 10^{-7}$	0.903 %	0.23
106 (53 + 53)	105.880745		3.963 %	

approximately 0.06 per laser pulse. This implies that the number of iterations will be large for a measurement yielding sufficient ion counts, i.e. the measurement time will be long. Thus, drifts in the system can significantly affect the resolving power in this timeframe. However, there is no $A = 106$ ion species with high enough abundance for an offline drift correction.

Typically, an isobaric ion would be used to both correct drifts in the signal ToF and act as reference ion for the calibration of the time-of-flight spectrum, i.e. for the determination of the mass of the ion or ions of interest [27]. However, no such ion species is readily available in the present case. Therefore, the correction is performed by employing a non-isobaric species. To this end, the storage time t_s is chosen such that both the correction-ion signal and the signals of the ions of interest (both the reference and the ion to be determined) appear in the same ToF spectrum [34], i.e. t_s has to closely match an integer multiple of the revolution periods of all ions involved. In the present case of the demonstration of this new method, the additional ion is employed for the correction of the ToF drifts of both isobaric ion species of interest so that one of them can act as a reference ion.

4. Resolving the Cr_2 isobar pair by non-isobar reference

For the present study on the $A = 106$ isobars of Cr_2^+, the most readily-available candidate for a non-isobaric Cr_2^+ reference is the high-abundance isotopologue consisting of two ^{52}Cr atoms at $A = 104$, with a relative abundance of more than 70%. A measurement has been performed (Fig. 4) where $t_s = 82.573$ ms. This amounts to 2393 revolutions for both $A = 106$ isobars ($T = 34.5054\,\mu s$) and 2416 revolutions for the $A = 104$ correction-ion species ($T = 34.1783\,\mu s$). The bottom part of Fig. 4 shows the ToF spectrum, recorded by repeating the measurement cycle 120, 000 times over the course of roughly 3.5 hours. The signal on the left belongs to the pair of $A = 106$ isobars, the signal on the right to the $A = 104$ ion species. During the first five revolution periods, the technique of transversal ion ejection [35] is employed to remove contaminant ions with mass numbers which are not in the range from $A = 104$ to 106.

As is readily apparent, the mass resolving power is not sufficient to separate the isobar pairs. If the measurement is viewed in terms of its individual iterations however (top part of Fig. 4), it becomes obvious that this is primarily due to fluctuations of the ions' flight times. Each slice represents the signal sum of 100 measurement cycles (10 s) to gain sufficient fit accuracy for the correction (see below). It is also visible that—even though the ion species have completed different numbers of revolutions in the MR-ToF analyzer—the shifts for all species follow the same pattern. As is obvious from the measurement and further explained below, these short- and longer-term ToF shifts are systematic in the sense that they affect all four ion species in the same way.

To perform a shift correction (Fig. 5), the correction-ion signal $^{52}Cr^{52}Cr^+$ is fitted with a Gaussian function in each measurement slice. The individual spectra are then shifted to match the mean time-of-flight of this signal before they are summed to the total ToF spectrum. Thus, ToF shifts are corrected on the basis of 10 s steps (each slice represents 100 iterations measured at a 10 Hz cycle rate).

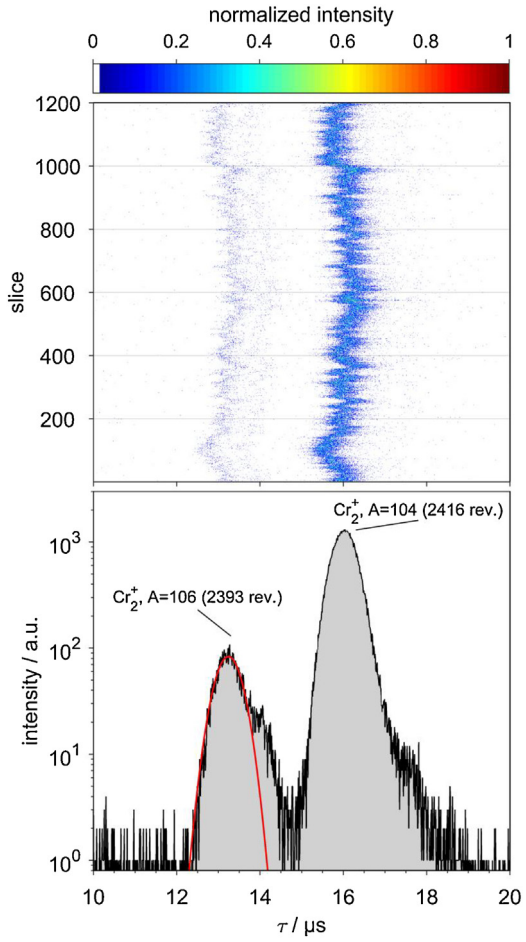

Fig. 4. Top: 2D color intensity plot of horizontal slices of ToF spectra of Cr_2^+ for t_s = 82.573 ms from adding the ion signals of 100 measurement cycles each. Bottom: ToF spectrum summed over all data shown above. The left (right) signal is due to isobaric ion species of mass number $A = 106$ ($A = 104$) after the number of revolutions stated in the figure.

When comparing the bottom parts of Figs. 4 and 5, the effect of the ToF-shift correction is readily apparent as an increase in mass resolving power: The previously unresolved pair of $A = 106$ isobars is now resolved. Additionally, a low-abundance $A = 104$ isotopologue, $^{50}Cr^{54}Cr^+$, becomes apparent, too. The (FWHM) mass resolving power of the summed signal of the corrected $A = 106$ isotopologues is $126(7) \cdot 10^3$, while for the uncorrected signal (determined by a fit to the more abundant $A = 106$ isotopologue) it is $57(2) \cdot 10^3$, i.e. lower by more than a factor of two. According to the relative mass difference given in Table 4, a FWHM mass resolving power of about 56, 000 would be sufficient for the separation of species of identical abundance. For the present abundance difference however, it has to be increased by about 50% (see Fig. 9 in [27]).

We note that the total number of detected $^{50}Cr^{54}Cr^+$ ions in the present measurement is roughly 95, 500, resulting in an average 0.8 events per cycle. We therefore conclude that space-charge effects such as self-bunching [1,36,37] of the ions of interest can be neglected for this study.

From the Gaussian fits performed in the corrected ToF spectrum, the abundance ratio of the $A = 106$ isobars results in

$$\frac{A\left(^{53}Cr^{53}Cr^+\right)}{A\left(^{52}Cr^{54}Cr^+\right)} = 0.24(2),$$

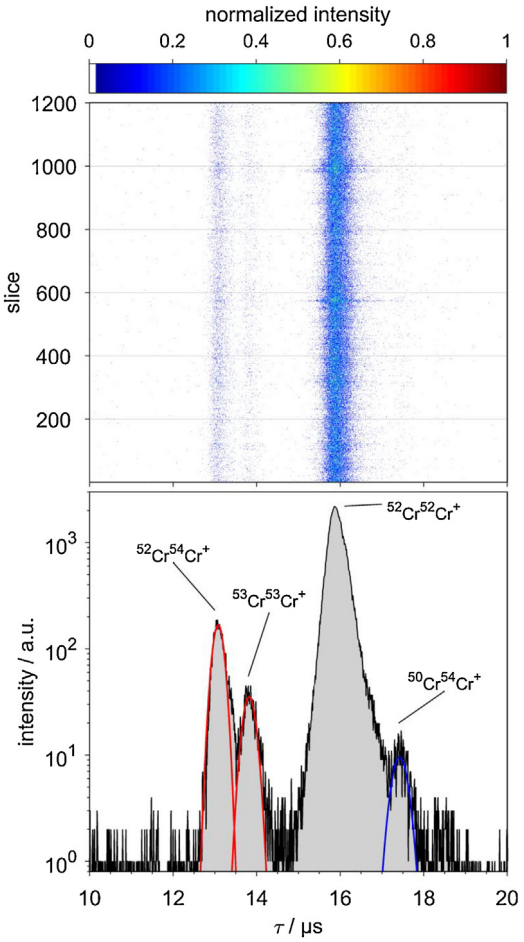

Fig. 5. As Fig. 4, but now with ToF shifts corrected via the $^{52}Cr^{52}Cr^+$ signal. The red (blue) lines for the $A = 106$ (104) signals are fits of Gaussian functions (where the data fitted has been restricted to the upper two thirds of the signals) (For interpretation of the references to colour in the text, the reader is referred to the web version of this article.).

thus matching the predicted value of 0.23 (see Table 4). The experimental relative mass difference

$$1 - \left(\frac{t_{cap} + t_s + \tau(^{52}Cr^{54}Cr^+)}{t_{cap} + t_s + \tau(^{53}Cr^{53}Cr^+)}\right)^2 = 179(2).10^{-7}$$

also agrees with the expected value of $180 \cdot 10^{-7}$.

In the following, the reason for the identical shifts of time-of-flight despite the difference in revolution numbers is further discussed: Consider two ion species of masses m_1 and m_2 (more precisely ratios of mass-over-charge state; masses are used for simplicity) with corresponding revolution periods T_1 and T_2. The ratio of these periods is then given by

$$\frac{T_1}{T_2} = \sqrt{\frac{m_1}{m_2}}.$$

When the storage parameters (potentials or spatial dimensions of the MR-ToF electrodes) change, the corresponding revolution periods shift by some time ΔT_i to new values $T_i' = T_i + \Delta T_i$, where again $T_1'/T_2' = \sqrt{m_1/m_2}$. Consequently, the same relation holds for the shifts of the periods, i.e.

$$\frac{\Delta T_1}{\Delta T_2} = \sqrt{\frac{m_1}{m_2}} = \frac{T_1}{T_2}.$$

While the time between the switching of the in-trap lift for capture and ejection, i.e. the storage time t_s, is fixed, the ions' time-of-flight ToF_i for the completion of N_i revolutions shifts to

$$\mathrm{ToF}_i' = N_i \cdot T_i'.$$

This leads to different ion positions in the lift electrode at the time of the ejection switching and, consequently, to a shift in the measured flight times to the detector, τ_i. The observed shift $\Delta\mathrm{ToF}_i$ can therefore be understood as the shift in time-of-flight for N_i revolutions. It follows readily that

$$\Delta\mathrm{ToF}_i = N_i \cdot \Delta T_i.$$

The number of revolutions the ion species perform during their storage are given by

$$N_i \approx \frac{t_s}{T_i}.$$

The storage time t_s is specifically chosen to closely match integer multiples of the revolution periods. The ion trajectory is invariant to the exact time of the switching of the in-trap lift in relation to ToF_i, as long as the ion species are fully within the drift tube, i.e. far enough to not be affected by the switching process. The ratio of revolution numbers for the two species

$$\frac{N_1}{N_2} = \frac{T_2}{T_1}$$

is therefore fixed to the inverse ratio of the revolution periods. Consequently, the ratio of the shifts in the time-of-flights is

$$\frac{\Delta\mathrm{ToF}_1}{\Delta\mathrm{ToF}_2} = \frac{N_1 \cdot \Delta T_1}{N_2 \cdot \Delta T_2} = \frac{T_2}{T_1} \cdot \frac{T_1}{T_2} = 1.$$

In other words, the measured shift of the time-of-flight is identical,

$$\Delta\mathrm{ToF}_1 = \Delta\mathrm{ToF}_2 = \Delta\mathrm{ToF}_3 = \ldots,$$

for any ion species measured simultaneously with the same storage time t_s, regardless of its mass-over-charge ratio. While lighter/faster ion species complete higher numbers of revolutions, heavier/slower species exhibit a correspondingly larger shift in their revolution periods. These two factors lead to the same ToF shift, which allows the offline correction.

While this result may be counterintuitive, note that the approach of investigating all ion species at identical flight times leads to differently-long flight paths in the MR-ToF analyzer. The ions are therefore not investigated with a "fixed-length" spectrometer in which time-of-flight fluctuations would be mass-dependent. However, the remaining, absolute time-of-flight difference of 3 μs between the reference ion species and the ion species of interest leads to a portion of the drifts scaling with the square root of the ions' mass ratio. For the present measurement (total flight time 82.5 ms), this amounts to a relative error of about $3.6 \cdot 10^{-5}$ in the ToF-drift correction. For cases where this cannot be neglected, a correction taking into account scaling ToF-drifts can be employed [29].

It should be noted that this approach does not include changes of the single-path time-of-flight, i.e. the flight time from the ion source to the MR-ToF analyzer and from the analyzer to the detector. However, these flight times are usually short compared to the storage time, and deviations thereof are correspondingly smaller. Furthermore, the present derivation is based on the assumption that the changes of the MR-ToF parameters occur between the measurement cycles (more precisely the number of measurement cycles needed for sufficient statistics for correction), i.e. that they are slow with respect to the length of the measurement cycles. A single measurement is performed at effectively constant conditions. Fast random fluctuations on the other hand are not expected to lead to largely different shifts, as they are averaged out during the storage time. Only variations with some coherent correlation

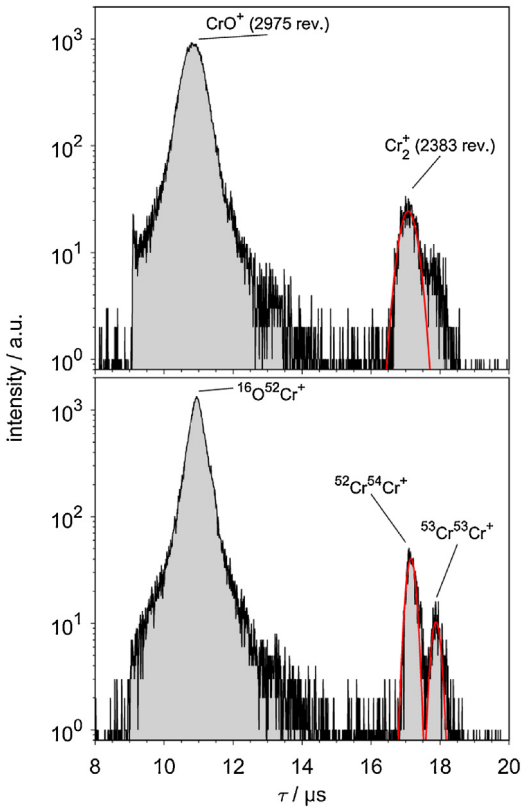

Fig. 6. Top: ToF spectrum for a storage time of $t_s = 82.228$ms. The left signal is due to CrO^+ ($A = 68$), the right due to Cr_2^+ ($A = 106$) after the number of revolution periods stated in the figure. Bottom: ToF spectrum after correction by use of CrO^+ as correction ion.

with respect to the revolution period of an ion species would lead to noticeable systematic deviations.

Note that, in addition to variations of the MR-ToF parameters like electrode potentials or spatial dimensions (both possibly due to temperature effects), drifts of the offset of the data acquisition, i.e. the starting of the time-of-flight recording, are also corrected by the present method.

To further demonstrate the applicability of non-isobaric ions for drift corrections, the experiment has been repeated with the CrO^+ molecule at mass number $A = 68$ as correction ion, i.e. an ion far away in mass from the ion(s) of interest (Fig. 6). For the present setup, this represents the available ion species with the largest mass difference to the pair of Cr_2^+ isobars that can still be simultaneously captured in the MR-ToF analyzer.

As can be seen, the method of correcting the ToF shifts again yields the desired results. The pair of Cr_2^+ isobars can be fitted in the corrected spectrum, resulting in an abundance ratio of 0.26 (6) and a relative mass difference of $177\,(4) \cdot 10^{-7}$. Again, both numbers match their expected values. The slightly-larger uncertainties are due to the fact that the measurement has been performed for only 930 slices, as opposed to the 1200 in Fig. 4 and 5. The mass resolving power increases from $73\,(4) \cdot 10^3$ without to $134\,(3) \cdot 10^3$ with the correction.

For completeness, we note that due to the increased difference in mass—and therefore revolution period—between the correction ion and the ions of interest, no transversal ion ejection has been employed in the CrO^+-correction measurement. All ion species captured by the switching of the in-trap lift electrode are retained in the MR-ToF analyzer. We further note that the correction signal's left flank is not entirely visible in the ToF spectrum of Fig. 6 due to part of it being beyond the system's ToF ejection window [34]. This is of no consequence however, as the fitting ranges of the relevant signals are unaffected.

5. Summary and conclusion

A development in the separation of isobaric ion species with an MR-ToF device has been presented. The technique of the correction of short-term drifts in the ions' time-of-flight with a correction-ion species has been extended: it has been shown that such a correction is not only possible—as is the typical approach—using an isobaric species itself, but also using correction ions with larger mass differences.

A pair of Cr_2^+ isobars with a relative mass difference of $1.8 \cdot 10^{-5}$ has been stored in the MR-ToF analyzer for ~82 ms. For the present experimental conditions, resolving of the individual species is not possible at this storage time due to drifts in the time-of-flight values over the course of the measurement. It has been shown, however, that an offline correction of these drifts is possible using virtually any other simultaneously-stored ion species, in this case another Cr_2^+ isotopologue (rel. mass difference 1.9 %) or a CrO^+ molecule (rel. mass difference 36%). For both cases, the measured relative mass difference and abundance ratio of the target isobar pair agree with their expected values.

The viability of the offline correction is dependent on the type and severity of the drifts in the individual system, and we expect it to differ for different MR-ToF setups. It is not possible to correct fluctuations somewhat shorter than the storage time, as in this case the assumption of identical absolute shifts in the ions' time-of-flight may not hold. Fast random fluctuations should, however, average out over the duration of the storage time. The systematic drifts have to be slow enough to allow for the collection of sufficient measurement statistics under (close to) identical conditions. For applications as the one presented in this study, where ToF shifts are mostly due to slow, systematic drifts of the MR-ToF analyzer's parameters, a significant gain in mass resolving power, in this case by a factor exceeding two and thus reaching up to $R = 130\,000$, can be achieved without any need for online corrections or adjustments.

Even in cases where the target isobar pair can be resolved at higher revolution numbers without an additional correction-ion species, the latter may still be useful as it allows the minimization of the necessary number of revolutions, i.e. the storage and, thus, experiment time. This can lead to a gain in the number of detected ions in a given experimental timeframe, fewer losses from residual gas impacts during the MR-ToF storage, and, in the case of short-lived isotopes, fewer losses due to nuclear decays.

Acknowledgements

This work has been supported by the German Ministry for Education and Research (BMBF) and the Collaborative Research Centre of the DFG (SFB 652, TP A03).

References

[1] Y. Toker, N. Altstein, O. Aviv, M.L. Rappaport, O. Heber, D. Schwalm, D. Strasser, D. Zajfman, The kick-out mass selection technique for ions stored in an Electrostatic Ion Beam Trap, J. Instrum. 4 (09) (2009), P09001 http://stacks.iop.org/1748-0221/4/i=09/a=P09001.

[2] B. Kafle, O. Aviv, V. Chandrasekaran, O. Heber, M.L. Rappaport, H. Rubinstein, D. Schwalm, D. Strasser, D. Zajfman, Electron detachment and fragmentation of laser-excited rotationally hot Al_4^-, Phys. Rev. A (Coll Park) 92 (5) (2015), 052503, http://dx.doi.org/10.1103/PhysRevA.92.052503.

[3] T. Suzuki, Y. Yamauchi, Electrostatic linear ion trap for low-energy ion beam storage, Nucl. Instrum. Methods Phys. Res. A 562 (1) (2006) 53–56, http://dx.doi.org/10.1016/j.nima.2006.02.196.

[4] R.T. Hilger, R.E. Santini, S.A. McLuckey, Square wave modulation of a mirror lens for ion isolation in a Fourier transform electrostatic linear ion trap mass

spectrometer, Int. J. Mass Spectrom. 362 (2014) 1–8, http://dx.doi.org/10.1016/j.ijms.2014.02.003.
[5] E.T. Dziekonski, R.E. Santini, S.A. McLuckey, A dual detector Fourier transform electrostatic linear ion trap utilizing in-trap potential lift, Int. J. Mass Spectrom. 405 (2016) 1–8, http://dx.doi.org/10.1016/j.ijms.2016.05.010.
[6] R.N. Wolf, D. Beck, K. Blaum, Ch. Böhm, Ch. Borgmann, M. Breitenfeldt, F. Herfurth, A. Herlert, M. Kowalska, S. Kreim, D. Lunney, S. Naimi, D. Neidherr, M. Rosenbusch, L. Schweikhard, J. Stanja, F. Wienholtz, K. Zuber, On-line separation of short-lived nuclei by a multi-reflection time-of-flight device, Nucl. Instrum. Methods Phys. Res. A 686 (2012) 82–90, http://dx.doi.org/10.1016/j.nima.2012.05.067.
[7] Y. Ito, P. Schury, M. Wada, S. Naimi, T. Sonoda, H. Mita, F. Arai, A. Takamine, K. Okada, A. Ozawa, H. Wollnik, Single-reference high-precision mass measurement with a multireflection time-of-flight mass spectrograph, Phys. Rev. C 88 (1) (2013), 011306, http://dx.doi.org/10.1103/PhysRevC.88.011306.
[8] P. Schury, M. Wada, Y. Ito, F. Arai, S. Naimi, T. Sonoda, H. Wollnik, V.A. Shchepunov, C. Smorra, C. Yuan, A high-resolution multi-reflection time-of-flight mass spectrograph for precision mass measurements at RIKEN/SLOWRI, Nucl. Instrum. Methods Phys. Res. B 335 (2014) 39–53, http://dx.doi.org/10.1016/j.nimb.2014.05.016.
[9] T. Dickel, W.R. Plaß, A. Becker, U. Czok, H. Geissel, E. Haettner, C. Jesch, W. Kinsel, M. Petrick, C. Scheidenberger, A. Simon, M.I. Yavor, A high-performance multiple-reflection time-of-flight mass spectrometer and isobar separator for the research with exotic nuclei, Nucl. Instrum. Methods Phys. Res. A 777 (2015) 172–188, http://dx.doi.org/10.1016/j.nima.2014.12.094.
[10] F. Wienholtz, D. Atanasov, S. Kreim, V. Manea, M. Rosenbusch, L. Schweikhard, A. Welker, R.N. Wolf, Towards ultrahigh-resolution multi-reflection time-of-flight mass spectrometry at ISOLTRAP, Phys. Scripta 2015 (T166) (2015), 014068, http://dx.doi.org/10.1088/0031-8949/2015/T166/014068.
[11] F. Wienholtz, D. Beck, K. Blaum, Ch. Borgmann, M. Breitenfeldt, R.B. Cakirli, S. George, F. Herfurth, J.D. Holt, M. Kowalska, S. Kreim, D. Lunney, V. Manea, J. Menéndez, D. Neidherr, M. Rosenbusch, L. Schweikhard, A. Schwenk, J. Simonis, J. Stanja, R.N. Wolf, K. Zuber, Masses of exotic calcium isotopes pin down nuclear forces, Nature 498 (2013) 346, http://dx.doi.org/10.1038/nature12226.
[12] D. Atanasov, P. Ascher, K. Blaum, R.B. Cakirli, T.E. Cocolios, S. George, S. Goriely, F. Herfurth, H.-T. Janka, O. Just, M. Kowalska, S. Kreim, D. Kisler, Yu.A. Litvinov, D. Lunney, V. Manea, D. Neidherr, M. Rosenbusch, L. Schweikhard, A. Welker, F. Wienholtz, R.N. Wolf, K. Zuber, Precision mass measurements of 129-131Cd and their impact on stellar nucleosynthesis via the rapid neutron capture process, Phys. Rev. Lett. 115 (23) (2015), http://dx.doi.org/10.1103/PhysRevLett.115.232501, 232501.
[13] M. Rosenbusch, P. Ascher, D. Atanasov, C. Barbieri, D. Beck, K. Blaum, Ch. Borgmann, M. Breitenfeldt, R.B. Cakirli, A. Cipollone, S. George, F. Herfurth, M. Kowalska, S. Kreim, D. Lunney, V. Manea, P. Navrátil, D. Neidherr, L. Schweikhard, V. Somà, J. Stanja, F. Wienholtz, R.N. Wolf, K. Zuber, Probing the N=32 shell closure below the magic proton number z=20: mass measurements of the exotic isotopes 52,53K, Phys. Rev. Lett. 114 (20) (2015), http://dx.doi.org/10.1103/PhysRevLett.114.202501, 202501.
[14] A. de Roubin, D. Atanasov, K. Blaum, S. George, F. Herfurth, D. Kisler, M. Kowalska, S. Kreim, D. Lunney, V. Manea, E. Minaya Ramirez, M. Mougeot, D. Neidherr, M. Rosenbusch, L. Schweikhard, A. Welker, F. Wienholtz, R.N. Wolf, K. Zuber, Nuclear deformation in the A≈100 region: comparison between new masses and mean-field predictions, Phys. Rev. C 96 (1) (2017), 014310, http://dx.doi.org/10.1103/PhysRevC.96.014310.
[15] A. Welker, N.A.S. Althubiti, D. Atanasov, K. Blaum, T.E. Cocolios, F. Herfurth, S. Kreim, D. Lunney, V. Manea, M. Mougeot, D. Neidherr, F. Nowacki, A. Poves, M. Rosenbusch, L. Schweikhard, F. Wienholtz, R.N. Wolf, K. Zuber, Binding energy of ^{79}Cu: probing the structure of the doubly magic ^{78}Ni from only one proton away, Phys. Rev. Lett. 119 (19) (2017), 192502, http://dx.doi.org/10.1103/PhysRevLett.119.192502.
[16] Y. Ito, P. Schury, M. Wada, F. Arai, H. Haba, Y. Hirayama, S. Ishizawa, D. Kaji, S. Kimura, H. Koura, M. MacCormick, H. Miyatake, J.Y. Moon, K. Morimoto, K. Morita, M. Mukai, I. Murray, T. Niwase, K. Okada, A. Ozawa, M. Rosenbusch, A. Takamine, T. Tanaka, Y.X. Watanabe, H. Wollnik, S. Yamaki, First direct mass measurements of nuclides around z=100 with a multireflection time-of-flight mass spectrograph, Phys. Rev. Lett. 120 (15) (2018), 152501, http://dx.doi.org/10.1103/PhysRevLett.120.152501.
[17] M. Mougeot, D. Atanasov, K. Blaum, K. Chrysalidis, T. Day Goodacre, D. Fedorov, V. Fedosseev, S. George, F. Herfurth, J.D. Holt, D. Lunney, V. Manea, B. Marsh, D. Neidherr, M. Rosenbusch, S. Rothe, L. Schweikhard, A. Schwenk, C. Seiffert, J. Simonis, S.R. Stroberg, A. Welker, F. Wienholtz, R.N. Wolf, K. Zuber, Precision mass measurements of 58-63Cr: nuclear collectivity towards the N=40 island of inversion, Phys. Rev. Lett. (2018), in print https://journals.aps.org/prl/accepted/15078Y20Y281e05ff9a16c3174b14a43ad475befd.
[18] B.A. Marsh, B. Andel, A.N. Andreyev, S. Antalic, D. Atanasov, A.E. Barzakh, B. Bastin, Ch. Borgmann, L. Capponi, T.E. Cocolios, T. Day Goodacre, M. Dehairs, X. Derkx, H. De Witte, D.V. Fedorov, V.N. Fedosseev, G.J. Focker, D.A. Fink, K.T. Flanagan, S. Franchoo, L. Ghys, M. Huyse, N. Imai, Z. Kalaninova, U. Köster, S. Kreim, N. Kesteloot, Yu. Kudryavtsev, J. Lane, N. Lecesne, V. Liberati, D. Lunney, K.M. Lynch, V. Manea, P.L. Molkanov, T. Nicol, D. Pauwels, L. Popescu, D. Radulov, E. Rapisarda, M. Rosenbusch, R.E. Rossel, S. Rothe, L. Schweikhard, M.D. Seliverstov, S. Sels, A.M. Sjödin, V. Truesdale, C. Van Beveren, P. Van Duppen, K. Wendt, F. Wienholtz, R.N. Wolf, S.G. Zemlyanoy, New developments of the in-source spectroscopy method at RILIS/ISOLDE, Nucl. Instrum. Methods Phys. Res. B 317(B (2013) 550–556, http://dx.doi.org/10.1016/j.nimb.2013.07.070.
[19] R.N. Wolf, D. Beck, K. Blaum, Ch. Böhm, Ch. Borgmann, M. Breitenfeldt, N. Chamel, S. Goriely, F. Herfurth, M. Kowalska, S. Kreim, D. Lunney, V. Manea, E. Minaya Ramirez, S. Naimi, D. Neidherr, M. Rosenbusch, L. Schweikhard, J. Stanja, F. Wienholtz, K. Zuber, Plumbing neutron stars to new depths with the binding energy of the exotic nuclide ^{82}Zn, Phys. Rev. Lett. 110 (4) (2013), 041101, http://dx.doi.org/10.1103/PhysRevLett.110.041101.
[20] D. Atanasov, D. Beck, K. Blaum, Ch. Borgmann, R.B. Cakirli, T. Eronen, S. George, F. Herfurth, A. Herlert, M. Kowalska, S. Kreim, Yu.A. Litvinov, D. Lunney, V. Manea, D. Neidherr, M. Rosenbusch, L. Schweikhard, F. Wienholtz, R.N. Wolf, K. Zuber, Precision mass measurements of cesium isotopes—new entries in the ISOLTRAP chronicles, J. Phys. G Nucl. Part. Phys. 44 (4) (2017), 044004 http://stacks.iop.org/0954-3899/44/i=4/a=044004.
[21] V. Manea, P. Ascher, D. Atanasov, A.E. Barzakh, D. Beck, K. Blaum, Ch. Borgmann, M. Breitenfeldt, R.B. Cakirli, T.E. Cocolios, T. Day Goodacre, D.V. Fedorov, V.N. Fedosseev, S. George, F. Herfurth, M. Kowalska, S. Kreim, Yu.A. Litvinov, D. Lunney, B. Marsh, D. Neidherr, M. Rosenbusch, R.E. Rossel, S. Rothe, L. Schweikhard, F. Wienholtz, R.N. Wolf, K. Zuber, Penning-trap mass spectrometry and mean-field study of nuclear shape coexistence in the neutron-deficient lead region, Phys. Rev. C 95 (5) (2017), 054322, http://dx.doi.org/10.1103/PhysRevC.95.054322.
[22] N.A. Althubiti, D. Atanasov, K. Blaum, T.E. Cocolios, T. Day Goodacre, G.J. Farooq-Smith, D.V. Fedorov, V.N. Fedosseev, S. George, F. Herfurth, K. Heyde, S. Kreim, D. Lunney, K.M. Lynch, V. Manea, B.A. Marsh, D. Neidherr, M. Rosenbusch, R.E. Rossel, S. Rothe, L. Schweikhard, M.D. Seliverstov, A. Welker, F. Wienholtz, R.N. Wolf, K. Zuber, Spectroscopy of the long-lived excited state in the neutron deficient nuclides ^{195,197,199}Po by precision mass measurement, Phys. Rev. C 96 (2017), 044325, http://dx.doi.org/10.1103/PhysRevC.96.044325.
[23] C. Breitenfeldt, K. Blaum, M.W. Froese, S. George, G. Guzmán-Ramírez, M. Lange, S. Menk, L. Schweikhard, A. Wolf, Decay processes and radiative cooling of small anionic copper clusters, Phys. Rev. A (Coll Park) 94 (3) (2016), 033407, http://dx.doi.org/10.1103/PhysRevA.94.033407.
[24] E.T. Dziekonski, J.T. Johnson, K.W. Lee, S.A. McLuckey, Determination of collision cross sections using a fourier transform electrostatic linear ion trap mass spectrometer, J. Am. Soc. Mass Spectrom. 29 (2) (2018) 242–250, http://dx.doi.org/10.1007/s13361-017-1720-1.
[25] W.R. Plaß, T. Dickel, U. Czok, H. Geissel, M. Petrick, K. Reinheimer, C. Scheidenberger, M.I. Yavor, Isobar separation by time-of-flight mass spectrometry for low-energy radioactive ion beam facilities, Nucl. Instrum. Methods Phys. Res. B 266 (19–20) (2008) 4560–4564, http://dx.doi.org/10.1016/j.nimb.2008.05.079.
[26] T.Y. Hirsh, N. Paul, M. Burkey, A. Aprahamian, F. Buchinger, S. Caldwell, J.A. Clark, A.F. Levand, L. Ling Ying, S.T. Marley, G.E. Morgan, A. Nystrom, R. Orford, A. Pérez Galván, J. Rohrer, G. Savard, K.S. Sharma, K. Siegl, First operation and mass separation with the CARIBU MR-TOF, Nucl. Instrum. Methods Phys. Res. B 376 (2016) 229–232, http://dx.doi.org/10.1016/j.nimb.2015.12.037.
[27] R.N. Wolf, F. Wienholtz, D. Atanasov, D. Beck, K. Blaum, Ch. Borgmann, F. Herfurth, M. Kowalska, S. Kreim, Yu.A. Litvinov, D. Lunney, V. Manea, D. Neidherr, M. Rosenbusch, L. Schweikhard, J. Stanja, K. Zuber, ISOLTRAP's multi-reflection time-of-flight mass separator/spectrometer, Int. J. Mass Spectrom. 349–350 (2013) 123–133, http://dx.doi.org/10.1016/j.ijms.2013.03.020.
[28] E. Leistenschneider, M.P. Reiter, S. Ayet San Andrés, B. Kootte, J.D. Holt, P. Navrátil, C. Babcock, C. Barbieri, B.R. Barquest, J. Bergmann, J. Bollig, T. Brunner, E. Dunling, A. Finlay, H. Geissel, L. Graham, F. Greiner, H. Hergert, C. Hornung, C. Jesch, R. Klawitter, Y. Lan, D. Lascar, K.G. Leach, W. Lippert, J.E. McKay, S.F. Paul, A. Schwenk, D. Short, J. Simonis, V. Somà, R. Steinbrügge, S.R. Stroberg, R. Thompson, M.E. Wieser, C. Will, M. Yavor, C. Andreoiu, T. Dickel, I. Dillmann, G. Gwinner, W.R. Plaß, C. Scheidenberger, A.A. Kwiatkowski, J. Dilling, Dawning of the N=32 shell closure seen through precision mass measurements of neutron-rich titanium isotopes, Phys. Rev. Lett. 120 (6) (2018), 062503, http://dx.doi.org/10.1103/PhysRevLett.120.062503.
[29] M. Rosenbusch, Y. Ito, P. Schury, M. Wada, D. Kaji, K. Morimoto, H. Haba, S. Kimura, H. Koura, M. MacCormick, H. Miyatake, J.Y. Moon, K. Morita, I. Murray, T. Niwase, A. Ozawa, M. Reponen, A. Takamine, T. Tanaka, H. Wollnik, New mass anchor points for neutron-deficient heavy nuclei from direct mass measurements of radium and actinium isotopes, Phys. Rev. C 97 (6) (2018), 064306, http://dx.doi.org/10.1103/PhysRevC.97.064306.
[30] C. Stoermer, J. Friedrich, M.M. Kappes, Observation of multiply charged cluster anions upon pulsed UV laser ablation of metal surfaces under high vacuum, Int. J. Mass Spectrom. 206 (1-2) (2001) 63–78, http://dx.doi.org/10.1016/S1387-3806(00)00390-0.
[31] W.C. Wiley, I.H. McLaren, Time-of-Flight mass spectrometer with improved resolution, Rev. Sci. Instrum. 26 (12) (1955) 1150–1157, http://dx.doi.org/10.1063/1.1715212.
[32] R.N. Wolf, G. Marx, M. Rosenbusch, L. Schweikhard, Static-mirror ion capture and time focusing for electrostatic ion-beam traps and multireflection time-of-flight mass analyzers by use of an in-trap potential lift, Int. J. Mass Spectrom. 313 (2012) 8–14, http://dx.doi.org/10.1016/j.ijms.2011.12.006.
[33] D. Beck, K. Blaum, H. Brand, F. Herfurth, S. Schwarz, A new control system for ISOLTRAP, Nucl. Instrum. Methods Phys. Res. A 527 (3) (2004) 567–579, http://dx.doi.org/10.1016/j.nima.2004.02.043.
[34] S. Knauer, P. Fischer, G. Marx, B. Schabinger, L. Schweikhard, R.N. Wolf, Multi-reflection time-of-flight mass spectrometry with combined in-trap lift

capture and mirror-switch ejection, Int. J. Mass Spectrom. 423 (2017) 46–53, http://dx.doi.org/10.1016/j.ijms.2017.10.007.
[35] P. Fischer, S. Knauer, G. Marx, L. Schweikhard, In-depth study of in-trap high-resolution mass separation by transversal ion ejection from a multi-reflection time-of-flight device, Rev. Sci. Instrum. 89 (1) (2018), 015114, http://dx.doi.org/10.1063/1.5009167.
[36] D. Strasser, T. Geyer, H.B. Pedersen, O. Heber, S. Goldberg, B. Amarant, A. Diner, Y. Rudich, I. Sagi, M. Rappaport, D.J. Tannor, D. Zajfman, Negative mass instability for interacting particles in a 1D Box: theory and application, Phys. Rev. Lett. 89 (28) (2002), 283204.
[37] M. Rosenbusch, S. Kemnitz, R. Schneider, L. Schweikhard, R. Tschiersch, R.N. Wolf, Towards systematic investigations of space-charge phenomena in multi-reflection ion traps, AIP Conf. Proc. 1521 (1) (2013) 53–62, http://dx.doi.org/10.1063/1.4796061.
[39] M. Berglund, M. Wieser, Isotopic compositions of the elements 2009 (IUPAC Technical Report), Pure Appl. Chem. 83 (2) (2011) 397–410, http://dx.doi.org/10.1351/PAC-REP-10-06-02.
[40] M. Wang, G. Audi, F.G. Kondev, W.J. Huang, S. Naimi, X. Xu, The AME2016 atomic mass evaluation (II). Tables, graphs and references, Chinese Phys. C 41 (3) (2017), 030003 http://stacks.iop.org/1674-1137/41/i=3/a=030003.

7.4 Multiple-ion-ejection multi-reflection time-of-flight mass spectrometry for single-reference wide-band mass measurements

Multiple-ion-ejection multi-reflection time-of-flight mass spectrometry for single-reference mass measurements with lapping ion species

Paul Fischer[a)] and Lutz Schweikhard
Institut für Physik, Universität Greifswald, 17487 Greifswald, Germany

(Dated: 14 October 2019)

Repeated switching of electric potentials within a single experimental cycle is introduced for a multi-reflection time-of-flight mass spectrometer (also known as electrostatic ion beam trap) in order to eject different ion species after different storage times. The method is demonstrated with two cluster ions with considerably different mass-to-charge ratios (the $A = 624$ and 832 isotopologes of Pb_3^+ and Pb_4^+, respectively) for the specific case where the sequential ejections result in an identical number of revolution periods. Thus, the ions' flight lengths are identical, and the resulting time-of-flight values allow single-reference mass determination. The requirements for the switching time window are studied in detail. For the present system and ion pair, the relative mass uncertainty is found to be $3 \cdot 10^{-7}$ for short measurements (≈ 10 minutes) and $6 \cdot 10^{-8}$ for longer ones (≈ 2 hours).

PACS numbers: 07.75.+h, 29.30.-h, 37.10.Ty

I. INTRODUCTION

Since the introduction of the multi-reflection concept by Wollnik[1] in 1990 and its independent implementation by Zajfman[2] and Benner[3] in 1997, multi-reflection time-of-flight (MR-ToF) mass spectrometers have carved their way into several branches of physics and chemistry. Offering a method of purely electrostatical ion trapping, these devices—also referred to as electrostatic ion beam traps (EIBTs)—have found widespread appreciation for their unique combination of properties. Ions are retained between two electrostatic mirrors in analogy to an optical resonator[2,4], allowing their storage for hundreds of milliseconds for room-temperature[5] to several minutes for cryogenic setups[6].

For studies on gas-phase clusters and molecules, the virtually unrestricted mass range and open geometry of MR-ToF devices enable studies of molecular properties[7–11]. Capacitive pickup detection (Fourier-transform MR-ToF) has been employed to further increase versatility[12–14] and even investigate large, highly-charged molecules[15,16]. In nuclear physics, multi-reflection is employed in fast mass spectrometers with mass resolving powers $R \geq 100\,000$[17–20]. Applications include direct precision mass measurements[21–25], isobar separation[26–28], and—recently introduced—in-trap collinear laser spectroscopy (CLS)[29,30].

The principal feature of ions being reflected back and forth, however, can also lead to one of the traps' most restricting properties: Species of different mass-to-charge ratio m/q will eventually start lapping one another. This is most prominent in wide-band investigations, where ion signals in ToF spectra quickly lose their continuous relationship between m/q and flight time. For the field of precision mass measurements, this increases the complexity of a calibration based on known reference species[31]. On the other hand, it may be favorable or even necessary to use reference ions with large mass differences due to low production rates or the lack of proper isobaric candidates.

Here, we report a measurement scheme relying on multiple selective ejections of individual ion species from an MR-ToF analyzer. While all species are captured simultaneously, their release is timed according to their m/q such that each one completes the same number of revolutions. Thus, ToF mass spectrometry with fixed flight lengths is restored which allows single-reference mass determination.

II. EXPERIMENTAL SETUP

The present system (Fig. 1) combines a high-vacuum laser-ablation source for the production of metal-cluster ions similar to those reported by other groups[32–35] with an MR-ToF analyzer. A detailed description has been given recently[20]. In short, ions are produced by irradiation of metal targets with a Nd:YAG laser ($\lambda = 532$ nm, ≤ 15 mJ pulse energy, 10 Hz repetition rate), accelerated to 2 kV, and guided onto the analyzer's axis with a quadrupole deflector. The analyzer consists of two stacks of six mirror electrodes each, the outer four of which are used to form the axial reflecting potential walls and the inner two ion lenses for transversal refocusing. An in-trap lift electrode[36] is used to lower the ions' total energy between the mirrors for capture by switching its potential from ≈ 800 V to ground. A delay with respect to the laser pulse ("capture time") accounts for the travel time of the species of interest from the source. For the present study, ion ejection towards a post-trap detector is realized by lowing the potentials of the outermost two electrodes of the exit-side mirror to ground with fast low-noise high-

a)paul.fischer@uni-greifswald.de

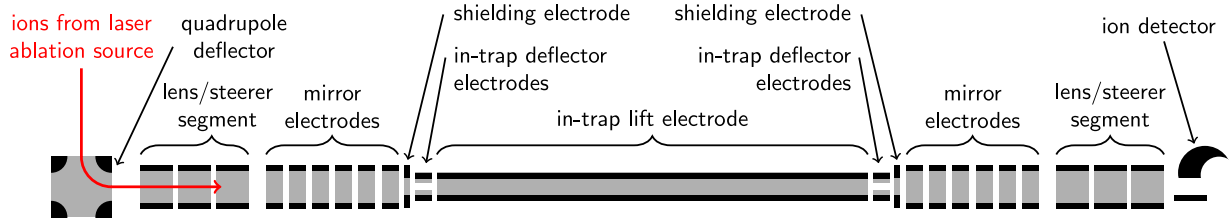

FIG. 1. Overview of the experimental setup. The ion path is indicated by a red arrow.

voltage switches (Stahl Electronics, HS-2000). This combination of in-trap lift capture and mirror-switch release retains the advantages of the lift electrode with respect to an easily-adjustable ion energy while ensuring that a large percentage of all stored species can be observed in a given spectrum[37].

Ion detection is performed with an off-axis channeltron detector, a fast preamplifier (ORTEC, VT120a), and a fast multiscaler/TDC (Fast ComTec, MCS6A). The control of the experimental timing pattern and switching operations is performed with a LabVIEW-based control software[38] and a Field-Programmable-Gate-Array card (National Instruments, PCI-7811R).

Ion selection/isolation within the analyzer is achieved with sets of segmented ring electrodes between the lift and mirror electrodes ("in-trap deflector electrodes" in Fig. 1). The potentials applied to opposing parts of a ring are switched between ground and $\pm 10\,\mathrm{V}$ to form a radially-deflecting electric field. When the switching frequency and phase are synchronized to a species of interest, it will never pass the ring during a deflecting potential configuration while ions with different m/q ratios eventually will. This technique of transversal ejection is well suited to select ions with defined mass numbers[39] and can also be used to perform simultaneous selection for species of disparate m/q values[40].

III. MASS SELECTION AND MEASUREMENT PRINCIPLE

A common challenge in wide-band MR-ToF investigations, especially for applications on the molecular level, is the presence of a large number of molecular isotopes ("isotopologues") from only a few initially-captured molecular species. This is illustrated in Fig. 2 by "N-versus-ToF" plots[41] showing flight time (x-axis) as a function of an incremental number N of revolution periods for an ion species (here $^{208}Pb_3^+$) in the trap. In the lower plots, each horizontal slice represents the storage time being increased by a value matching a single period. This is changed to 10 periods in the upper plots. Consequently, the $^{208}Pb_3^+$ signal forms a straight vertical line in the plots while the signals of other species move at various angles. The bottom plots show ion separation on the molecular level over the first few revolutions, the top ones the separation of individual isotopologues. The signals on the left of the first spectrum of the bottom plots result from heavier, non-trapped ions reaching the detector after their single-path flight.

The left-hand plots are recorded without the application of any selection mechanism, resulting in all captured species remaining in the trap. While only three distinct signals from three cluster sizes are observed initially ($n = 3$ through 5), the number of natural lead isotopes yields an abundance of ion species with different m/q values that quickly separate over some tens of revolutions. Once the resolving power reaches several tens of thousands in the upper left-hand plot, matching individual signals to their respective species becomes virtually impossible without scanning over multiple laps[37] or employing some form of in-trap ion selection[39,42–46].

For the right-hand plots of Fig. 2, the method of transversal ejection is employed for a simultaneous selection of two isotopologues with disparate m/q values[40], namely $^{208}Pb_3^+$ and $^{208}Pb_4^+$. After $N \approx 250$ ($^{208}Pb_3^+$) periods, only two signals are observed in the spectra (top right-hand plot), namely those of the two selected species. These have been specifically chosen for the present investigations because their mass numbers, $A = 624$ and 832, can only be formed by a single combination of natural lead isotopes each. Other mass numbers may be formed by multiple combinations, leading to ion species requiring mass resolving powers on the order of 10^6, which is beyond the present capabilities of MR-ToF devices[18,19].

Single-reference mass measurements in an MR-ToF device are, in principle, identical to those performed with any kind of time-of-flight mass spectrometer, that is, the mass of an unknown species m with flight time t is determined as

$$m = m_{\mathrm{ref}} \left(\frac{t - t_0}{t_{\mathrm{ref}} - t_0} \right)^2 \qquad (1)$$

from a species with known mass m_{ref} and flight time t_{ref}. The common offset t_0 incorporates any delay between the start of the data acquisition and the actual start of the ions from the source. This method is known to reach some 10^{-7} of accuracy[31,47], however, it requires identical

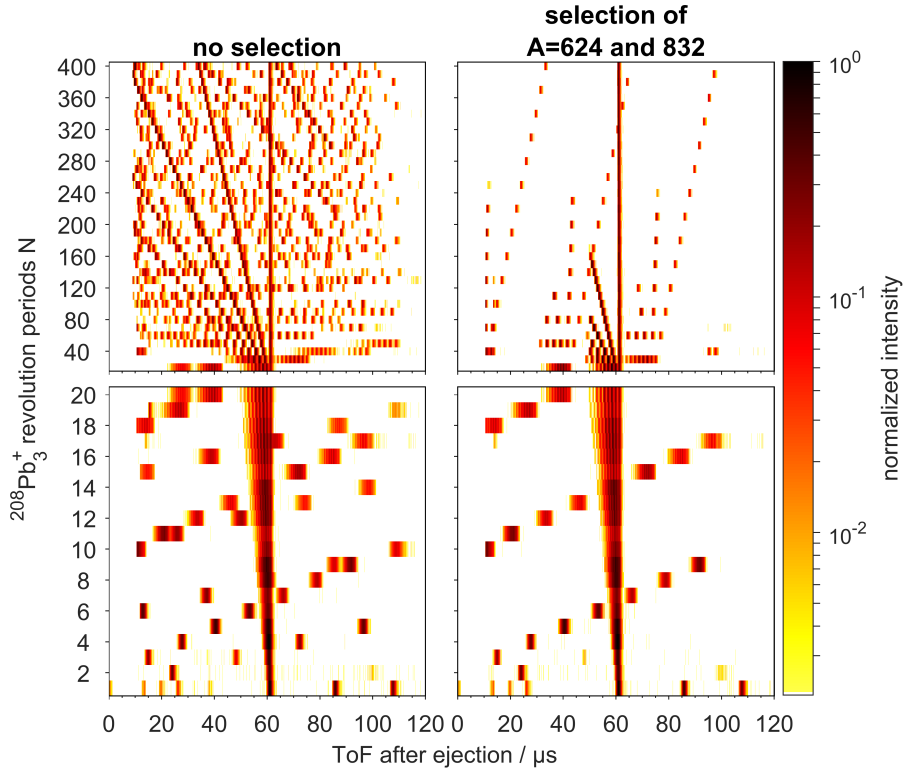

FIG. 2. "N-versus-ToF" plots without (left) and with (right) transversal ejection for selection of $^{208}Pb_3^+$ and $^{208}Pb_4^+$, with bottom plots for revolutions 1 through 20 and top ones for 20 through 400 in steps of 10.

flight lengths for both ions. It is thus only applicable for species that have not yet lapped one another, meaning—for measurements involving at least some hundreds of revolutions to reach reasonable levels of accuracy and mass resolving power—it is typically restricted to pairs of isobars.

For measurements employing reference species with large mass differences and taking into account lapping effects, the determination of the unknown mass becomes more complicated. It generally requires the use of multiple measurements at different revolution periods[41] and/or several reference species[21]. To circumvent this, the present study employs a scheme of two subsequent ejections from the analyzer to maintain identical flight lengths for both ions. This is illustrated in Fig. 3 by a time-of-flight spectrum that has been recorded with a single experimental sequence repeatedly applied for about ten minutes.

The start of the data acquisition is synchronized to the source-laser pulse and the ion capture and selection shown in Fig. 2 is performed to restrict the retention of ion species to $^{208}Pb_3^+$ and $^{208}Pb_4^+$ only. After a storage time amounting to 959 $^{208}Pb_3^+$ periods, roughly 80.25 ms, the exit-side mirror is opened to release this species and record its flight time. The mirror potential is re-raised immediately after the ejection to retain the $^{208}Pb_4^+$ ions, which are trapped for another 12.41 ms to also complete

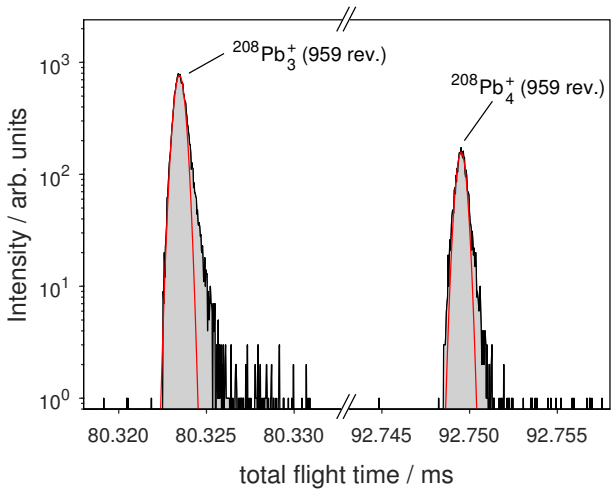

FIG. 3. Time-of-flight spectrum for $^{208}Pb_3^+$ and $^{208}Pb_4^+$ at the same number of revolutions in the same experimental cycle.

959 laps. The mirror is opened for a second time to record the heavier species' signal in the same spectrum. Using Gaussian fits (red curves in Fig. 3) restricted to the upper parts of the ToF signals, the ions' flight times t are determined.

Care has been taken to find the common offset t_0, as

forming the partial derivative of (1) and its limit for long flight times $t_0 \ll t,\, t_{\mathrm{ref}}$,

$$\frac{\partial_m}{\partial_{t_0}} = 2m_{\mathrm{ref}} \frac{(t-t_{\mathrm{ref}})(t-t_0)}{(t_{\mathrm{ref}}-t_0)^3} \tag{2}$$

$$\lim_{t_0\to 0} \frac{\partial_m}{\partial_{t_0}} = 2m_{\mathrm{ref}} \frac{t(t-t_{\mathrm{ref}})}{t_{\mathrm{ref}}^3}\,, \tag{3}$$

reveals that the sensitivity to a t_0 uncertainty increases with larger flight-time differences between the ions. While some tens of nanoseconds due to, e.g., cable lengths are generally less critical for the determination of an isobaric species' mass, it becomes more important for cases such as the present. Therefore, t_0 has been determined by measuring the delay times of all relevant cables and that of the source-laser pulse with respect to the sync trigger starting the data acquisition. The values have been added and subtracted accordingly, yielding a grand total of $t_0 = 116(5)\,\mathrm{ns}$. To reduce its uncertainty for cases with even larger mass differences, t_0 can be affirmed occasionally by additional reference measurements as demonstrated, e.g., by Rosenbusch et al.[25].

The mass of the $^{208}\mathrm{Pb}_4^+$ ion can now be calculated directly from that of $^{208}\mathrm{Pb}_3^+$ using (1) and the well-known mass of the ^{208}Pb atom[48]. For the present measurement, the resulting value of 831.90729(25) u exhibits a relative discrepancy $\Delta m/m = 1.6 \cdot 10^{-7}$ to the literature value with an uncertainty of $\delta m/m = 3.0 \cdot 10^{-7}$, the expected level of accuracy. The multiple-ejection scheme allows the mass determination to be performed with a single measurement cycle without additional reference species. This directly correlates to improved statistics per unit of measurement time.

Apart from trivial timings such as the one for the switching of the in-trap lift, only the revolution period T_{ref} of the reference species has to be roughly known/determined prior to the measurement. The period of the ion to be measured scales with T_{ref} and the square root of the ions' mass ratio, allowing its calculation to set up the switching timings. Due to the actual periods being non-critical for the mass evaluation, even a rough estimate from the ions' mass numbers is sufficient. The required level of precision only needs to ensure the ions' ejection at the correct revolution numbers and their selection via transversal ejection. As long as the timing requirements are respected (see next section), the experimental cycle can be set up with some leeway with respect to the switching operations. A similar measurement procedure based on interweaved cycles for reference and analyte ions has been demonstrated recently[49]. However, this approach still requires the use of several measurement sequences in addition to several RF-traps for the MR-ToF mass spectrometer's loading scheme.

IV. TIMING REQUIREMENTS

It is obvious that switching operations for releasing the correct ion species after the right number of revolutions

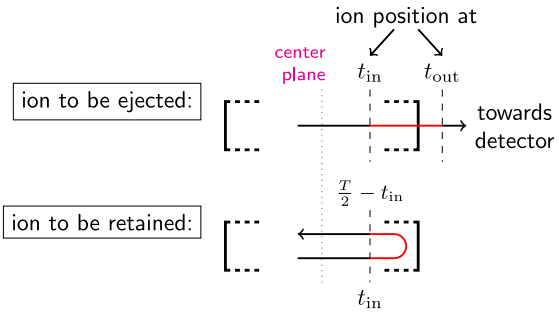

FIG. 4. Illustration of the timing requirements for ion ejection (top) and retention (bottom). For both cases, no switching can be performed while the species in question is in a location indicated by red lines. The mirror potentials must be switched to the correct potentials during the remaining time. Vertical lines show the trap's center plane and the planes associated with the respective timing limits.

are a prerequisite of the present measurements. However, the actual criterion for a successful mass determination is more demanding: voltages have to be lowered and raised while all ions are sufficiently far away from the corresponding electrodes to not sample changing electric fields. While they may still be released, aberrant ion flight times resulting from improper ejection timings will lead to systematic errors.

The timing restrictions can be visualized by specific ion positions in the trap. Once an ion has passed such a position while moving towards the mirror, it will be influenced by a change in its potential. Similarly, when moving away from the mirror, the ion will be far enough to again allow switching operations. For simplicity and generality, these points are expressed in terms of an ion's revolution period T, where 0 denotes its crossing of the trap's center plane with direction towards the exit side and $0.5\,T$ the crossing in the opposite direction. Consequently, $0.25\,T$ and $0.75\,T$ describe the turn-around points in the exit- and entry-side mirrors, respectively. There are two timing limits (Fig. 4):

- t_{in}, which denotes the time from which on an ion moving toward the exit-side mirror is disturbed by the potential switching. Consequently, the mirror must be fully lowered before the ion reaches the corresponding position. Due to the symmetry of the device, t_{in} also describes the time past which an ion will no longer be disturbed after its reflection. Thus, for any species to be *retained*, the mirror must not be in the low state and may not be switched between t_{in} and $0.5\,T - t_{\mathrm{in}}$ (red line in the lower part of Fig. 4).

- t_{out}, the time at which an ejected species has moved far enough from the trap after passing the lowered mirror potential for it not to be disturbed by the switching back. Thus, the mirror must be in the

low state and may not be switched between t_{in} and t_{out} for proper ejection (red line in the upper part of Fig. 4).

To determine the values for the timing limits of the present system, ToF spectra such as that of Fig. 3 are recorded for various switching times of the first ejection (of the $^{208}\mathrm{Pb}_3^+$ species). Figure 5 shows the relative deviation of the resulting mass for $^{208}\mathrm{Pb}_4^+$, i.e. the species to be initially retained during the release of $^{208}\mathrm{Pb}_3^+$, from its literature value. Note that the abscissa shows the relative time of the ions' revolution period with respect to their crossing of the center plane, as explained above. For both the opening of the potential (left data points) and the closing after the ejection (right data points), the timing for which the mass calculation fails is readily apparent. The determined critical values are $t_{\mathrm{in}} = 0.16\,T$ and $t_{\mathrm{out}} = 0.28\,T$, respectively.

Since the relative position of different ion species in the analyzer is governed by their respective revolution periods and, thus, their m/q ratios, sequential ejection is not possible for arbitrary revolution numbers. This is illustrated in Fig. 6: After the ions have traveled from the source to the trap (gray bars), they start revolving between the mirrors (colored bars). The times viable for ejection of the light and retention of the heavy species shift against one another due to the difference in revolution periods. For the lighter species with a revolution period T_{L} to be released, the mirror potential has to be switched down no later than $t_{\mathrm{in,L}} = 0.16\,T_{\mathrm{L}}$ and be re-raised no sooner than $t_{\mathrm{out,L}} = 0.28\,T_{\mathrm{L}}$, which is indicated by the green segments on the upper bar. While this is, in principle, possible on every revolution, the heavier species with revolution period T_{H} needs to be retained during this first opening. It is unaffected by any switching of the exit-side mirror potential for most of its period (green segments of the lower bar), however, the voltages need to be up for the time from $t_{\mathrm{in,H}} = 0.16\,T_{\mathrm{H}}$ to $0.5\,T_{\mathrm{H}} - t_{\mathrm{in,H}} = 0.34\,T_{\mathrm{H}}$, as indicated by the red segments.

Therefore, both bars in Fig. 6 being green at the same time means that the ejection of the lighter ion species is possible, that is, the trap can be opened for its release while the heavier species is in a portion of its period where it is unaffected by the switching. To determine what portion of revolution numbers is viable on average, the probability of the green bar of the lighter species coinciding with the red bar of the heavier one is considered. No overlap, even by a small amount, is allowed, as the mirror potential would have to be simultaneously low and high to suit the ejected and retained species, respectively. The duration of the "window" t_{w} of such an overlap is

$$\begin{aligned} t_{\mathrm{w}} &= t_{\mathrm{out,L}} - t_{\mathrm{in,L}} + (0.5\,T_{\mathrm{H}} - t_{\mathrm{in,H}}) - t_{\mathrm{in,H}} \\ &= (0.28 - 0.16)\,T_{\mathrm{L}} + (0.5 - 0.32)\,T_{\mathrm{H}}\,, \end{aligned} \tag{4}$$

that is, the length of a red bar in T_{H} plus the length of a green bar in T_{L}. Since the ratio of revolution periods is given by the mass ratio of the two species, $T_{\mathrm{L}} = \sqrt{m_{\mathrm{L}}/m_{\mathrm{H}}}\,T_{\mathrm{H}}$, (4) can be normalized to T_{H} to give the relative portion for the present setup,

$$\frac{t_{\mathrm{w}}}{T_{\mathrm{H}}} = 0.12\sqrt{\frac{m_{\mathrm{L}}}{m_{\mathrm{H}}}} + 0.18\,. \tag{5}$$

For the present ion pair, with $m_{\mathrm{L}} = 624\,\mathrm{u}$ and $m_{\mathrm{H}} = 832\,\mathrm{u}$, this amounts to roughly 0.28, i.e. about one out of four ($^{208}\mathrm{Pb}_4^+$) revolutions is, on average, not viable.

For large mass differences $m_{\mathrm{H}} \gg m_{\mathrm{L}}$, where the revolution period of the lighter species is much shorter than that of the heavier one, (5) simplifies to

$$\lim_{\frac{m_{\mathrm{L}}}{m_{\mathrm{H}}}\to 0} \frac{t_{\mathrm{w}}}{T_{\mathrm{H}}} = 0.18\,. \tag{6}$$

The portion of revolution periods nonviable for ejection takes its minimum value—roughly one in five for the present setup—which is now solely defined by the longer period. In contrast, for ions with nearly identical mass, (5) becomes

$$\lim_{\frac{m_{\mathrm{L}}}{m_{\mathrm{H}}}\to 1} \frac{t_{\mathrm{w}}}{T_{\mathrm{H}}} = 0.30\,, \tag{7}$$

which is its maximum possible value. These results are accommodating, as the multiple-ejection technique aims to provide measurements with reference species far away in mass: As is evident from the two limiting cases, the timing prerequisites become less restrictive for larger mass differences.

Note that only the first ion ejection has been considered above due to it being the critical of the two. Once a species has left the trap while the other one has

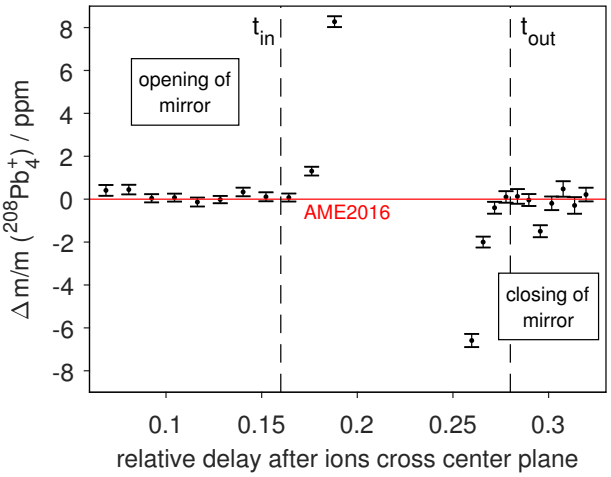

FIG. 5. Deviation of calculated ion mass from its literature value for different switching timings for the lowering (left) and raising (right) of the mirror potential. The left and right data points result from individual measurements. The dashed vertical lines show the timing limits t_{in} and t_{out} as defined in the text.

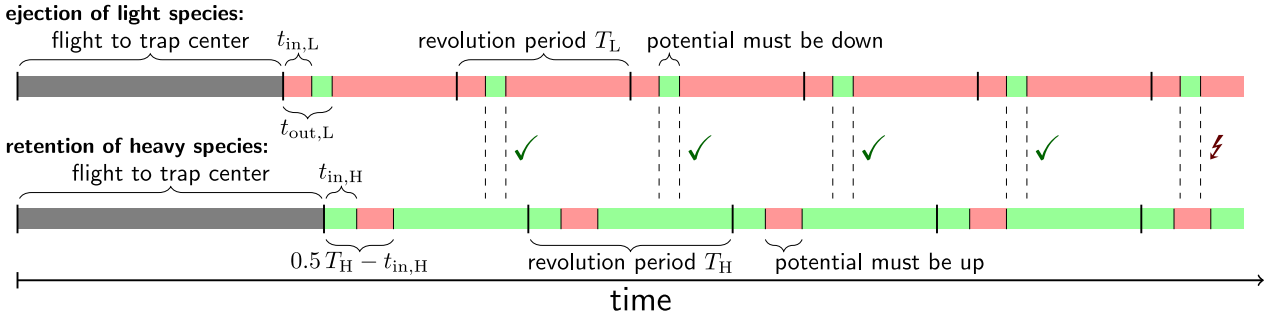

FIG. 6. Illustration of the portions of ion species' revolution periods affected by switching operations of exit-side mirror potentials, with ratio of the revolution periods chosen for the present study ($^{208}Pb_3^+$ and $^{208}Pb_4^+$). The checkmarks indicate whether ejection of the lighter species is possible without disturbance of the heavier one. For more information, see text.

been successfully retained, the second ejection is reduced to a "normal" potential switching without additional constraints. The multiple-ejection scheme is, however, not restricted to releasing ions after identical revolution numbers. Heeding the above timing considerations, ion species can be individually ejected at different times to, e.g., selectively pass them to downstream measurement setups in an order disconnected from their m/q ratios. A similar approach has been demonstrated recently using a specifically-timed in-trap lift ejection[50].

Lastly, multiple-ejection measurements could, in theory, also be performed by solely utilizing the in-trap lift for all ejections. Timings can be found for which ions can be retained in the mirror potentials or the lift electrode during the opening of the trap, as has been recently reported for multiple-capture schemes[40]. However, due to the more selective nature of the in-trap lift, such measurements would be somewhat more demanding in terms of timing allowances.

V. LONG-TERM ACCURACY AND EFFECT OF MIRROR STABILIZATION

We have recently shown that long-term ToF drifts of ions with disparate m/q values scale with the total flight time in an MR-ToF analyzer, regardless of the amount of lapping that has taken place[47]. It follows that, for ions that are ejected simultaneously, these drifts can be corrected during data evaluation by means of any correction-ion species with a sufficient count rate. This is routinely done for precision mass measurements[18,25,47,51]. For the multiple-ejection scheme, this ability is lost, at least to some extent, due to investigations being performed at fixed flight paths instead of times. Thus, a stable trap configuration becomes significantly more important.

The four reflecting mirror potentials of the present setup are therefore actively stabilized by means of a software-implemented PID controller following Wienholtz et al.[52]. For each of these potentials, the voltage from a low-noise power supply (iseg Spezialelektronik, EHS 8240) is filtered by a high-voltage low-pass setup ($40\,\mu$F, $1\,\mathrm{M}\Omega$). Their outputs are supplied to the mirror electrodes and precision high-voltage dividers simultaneously (Ohm-Labs, KV-30A or Caddock, HVD5-A50M-050-05). The reduced voltages are measured with precision multimeters (Keithley, Model 2002 or DMM7510) and used to re-adjust the initial output voltages through

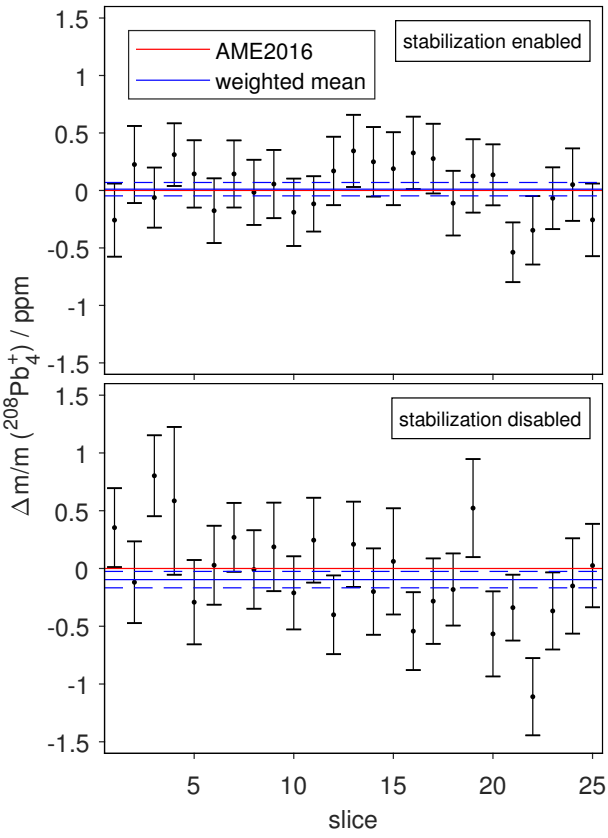

FIG. 7. Relative deviation of $^{208}Pb_4^+$ mass values from repeated measurements like the one shown in Fig. 3 for a setup with (top) and without (bottom) stabilization of the mirror voltages by means of the PID controller.

the PC-based PID regulation at a cycle rate of 10 Hz. This type of stabilzation has been shown to significantly reduce drifts in ion flight times, as their sensitivity to the mirror potentials far outweighs that to, e.g., ambient temperature[52]. Additionally, the low-pass filters help to dampen ringing and ensure small recovery times after the switching to open and close the exit-side mirror.

To characterize the multiple-ejection performance for long-time measurements, the mass of $^{208}Pb_4^+$ is determined repeatedly. Each slice in Fig. 7 represents 250 s of measurement time with a cycle rate of 10 Hz, yielding a total of around 1.75 h. The average count rate is 3.7 and 0.7 counts per cycle for the $n = 3$ and 4 species, respectively. The measurements shown in the top and bottom have been performed with the mirror-voltage stabilization enabled and disabled, respectively. The mean uncertainty of the individual measurements (black error bars) is comparable between both configurations, namely $2.9 \cdot 10^{-7}$ and $3.7 \cdot 10^{-7}$ for the top and bottom run. However, the ions' ToF drift increases significantly when the voltage stabilization is disabled. Due to the individual measurements taking some minutes to reach sufficient statistics and both species not exhibiting strictly identical drifts as explained above, the results become more erratic.

An in-depth investigation of the voltage stabilization on all four mirror electrodes (as an extension of recent investigations[52]) is subject of ongoing work. However, for the present measurements, its positive effect is clearly evident. The weighted mean of the $^{208}Pb_4^+$ mass shows a discrepancy of $\Delta m/m = 9.6 \cdot 10^{-8}$ to the literature value in the the run without the PID controller (solid blue line in Fig. 7). The uncertainty of the weighted mean is $\delta m/m = 7.1 \cdot 10^{-8}$ (dashed blue lines), there is thus a systematic deviation in the overall result. For the measurement with the enabled PID controller, the discrepancy reduces significantly to $\Delta m/m = 1.1 \cdot 10^{-8}$ with an uncertainty $\delta m/m = 5.8 \cdot 10^{-8}$.

VI. SUMMARY

The present study illustrates the use of an MR-ToF-based measurement scheme for single-reference mass determinations using ion species with large mass differences. Multiple mirror-switching operations are performed to selectively release ions different ejections times. This allows two species to complete the same number of revolutions despite their difference in revolution period and multiple lappings of one another over the storage duration. The mass of one species can be directly calculated using the other as reference, akin to regular, single-path ToF mass spectrometry. The resulting mass uncertainty in the present study is $3 \cdot 10^{-7}$ for a ten-minute measurement and $6 \cdot 10^{-8}$ for a measurement spanning about two hours.

These values are comparable to those obtained from similar investigations with isobaric references. Thus, they open the door for uncomplicated precision MR-ToF mass measurements in cases where close-by reference species are not readily available. The need for measurement cycles with different references or storage times is eliminated, which directly improves the experimental duty cycle and stability against long-term drifts.

ACKNOWLEDGMENTS

The authors thank F. Wienholtz for helping to set up the voltage stabilization for the mirror potentials.

[1] H. Wollnik and M. Przewloka. Time-of-flight mass spectrometers with multiply reflected ion trajectories. *Int. J. Mass Spectrom.*, 96(3):267–274, 1990, doi:https://doi.org/10.1016/0168-1176(90)85127-N.

[2] D. Zajfman, O. Heber, L. Vejby-Christensen, I. Ben-Itzhak, M. Rappaport, R. Fishman, and M. Dahan. Electrostatic bottle for long-time storage of fast ion beams. *Phys. Rev. A*, 55:R1577–R1580, 1997, doi:https://doi.org/10.1103/PhysRevA.55.R1577.

[3] W. H. Benner. A Gated Electrostatic Ion Trap To Repetitiously Measure the Charge and m/z of Large Electrospray Ions. *Anal. Chem.*, 69(20):4162–4168, 1997, doi:https://doi.org/10.1021/ac970163e.

[4] M. Dahan, R. Fishman, O. Heber, M. Rappaport, N. Altstein, D. Zajfman, and W. J. van der Zande. A new type of electrostatic ion trap for storage of fast ion beams. *Rev. Sci. Instrum.*, 69(1):76–83, 1998, doi:https://doi.org/10.1063/1.1148481.

[5] O. Heber, P. D. Witte, A. Diner, K. G. Bhushan, D. Strasser, Y. Toker, M. L. Rappaport, I. Ben-Itzhak, N. Altstein, D. Schwalm, A. Wolf, and D. Zajfman. Electrostatic ion beam trap for electron collision studies. *Rev. Sci. Instrum.*, 76(1):013104, 2005, doi:https://doi.org/10.1063/1.1832192.

[6] C. Breitenfeldt, M. W. Froese, K. Blaum, S. George, M. Grieser, M. Lange, S. Menk, R. Repnow, D. Schwalm, L. Schweikhard, R. von Hahn, and A. Wolf. Spreading times of ion-bunches in the Cryogenic Trap for Fast ion beams. *Int. J. Mass Spectrom.*, 396:1–4, 2016, doi:http://dx.doi.org/10.1016/j.ijms.2015.11.011.

[7] O. Aviv, B. Kafle, V. Chandrasekaran, O. Heber, M. L. Rappaport, H. Rubinstein, D. Schwalm, D. Strasser, Y. Toker, and D. Zajfman. Absolute photo-destruction and photo-fragmentation cross section measurements using an electrostatic ion beam trap. *Rev. Sci. Instrum.*, 84(5):053106, 2013, doi:https://doi.org/10.1063/1.4804646.

[8] B. Kafle, O. Aviv, V. Chandrasekaran, O. Heber, M. L. Rappaport, H. Rubinstein, D. Schwalm, D. Strasser, and D. Zajfman. Electron detachment and fragmentation of laser-excited rotationally hot Al_4^-. *Phys. Rev. A*, 92:052503, 2015, doi:https://doi.org/10.1103/PhysRevA.92.052503.

[9] C. Breitenfeldt, K. Blaum, S. George, J. Göck, G. Guzmán-Ramírez, J. Karthein, T. Kolling, M. Lange, S. Menk, C. Meyer, J. Mohrbach, G. Niedner-Schatteburg, D. Schwalm, L. Schweikhard, and A. Wolf. Long-Term Monitoring of the Internal Energy Distribution of Isolated Cluster Systems. *Phys. Rev. Lett.*, 120:253001, 2018, doi:http://dx.doi.org/10.1103/PhysRevLett.120.253001.

[10] P. Fischer and L. Schweikhard. Photofragmentation of $Bi_n^{+/-}$ clusters (n = 2-19) in an electrostatic ion beam trap. *Eur. Phys. J. D*, 73(5):105, 2019, doi:https://doi.org/10.1140/epjd/e2019-100027-0.

[11] P. Fischer and L. Schweikhard. Isotope-resolved photodissociation pathways of lead-doped bismuth clusters from tandem multi-reflection time-of-flight mass spectrometry (in press). *Phys. Rev. Res.*, 2019.

[12] D. Zajfman, Y. Rudich, I. Sagi, D. Strasser, D.W. Savin, S. Goldberg, M. Rappaport, and O. Heber. High resolution mass spectrometry using a linear electrostatic ion

beam trap. *Int. J. Mass Spectrom.*, 229(1):55–60, 2003, doi:https://doi.org/10.1016/S1387-3806(03)00255-0.

[13]R. T. Hilger, P. J. Wyss, R. E. Santini, and S. A. McLuckey. Absorption Mode Fourier Transform Electrostatic Linear Ion Trap Mass Spectrometry. *Anal. Chem.*, 85(17):8075–8079, 2013, doi:https://doi.org/10.1021/ac401935e.

[14]E. T. Dziekonski, R. E. Santini, and S. A. McLuckey. A dual detector Fourier transform electrostatic linear ion trap utilizing in-trap potential lift. *Int. J. Mass Spectrom.*, 405:1–8, 2016, doi:https://doi.org/10.1016/j.ijms.2016.05.010.

[15]R. Antoine, T. Doussineau, P. Dugourd, and F. Calvo. Multiphoton dissociation of macromolecular ions at the single-molecule level. *Phys. Rev. A*, 87:013435, 2013, doi:https://doi.org/10.1103/PhysRevA.87.013435.

[16]E. E. Pierson, D. Z. Keifer, N. C. Contino, and M. F. Jarrold. Probing higher order multimers of pyruvate kinase with charge detection mass spectrometry. *Int. J. Mass Spectrom.*, 337:50–56, 2013, doi:https://doi.org/10.1016/j.ijms.2013.01.002.

[17]P. Schury, M. Wada, Y. Ito, S. Naimi, T. Sonoda, H. Mita, A. Takamine, K. Okada, H. Wollnik, S. Chon, H. Haba, D. Kaji, H. Koura, H. Miyatake, K. Morimoto, K. Morita, and A. Ozawa. A multi-reflection time-of-flight mass spectrograph for short-lived and super-heavy nuclei. *Nucl. Instrum. Meth. B*, 317:537–543, 2013, doi:https://doi.org/10.1016/j.nimb.2013.06.025.

[18]T. Dickel, W.R. Plaß, A. Becker, U. Czok, H. Geissel, E. Haettner, C. Jesch, W. Kinsel, M. Petrick, C. Scheidenberger, A. Simon, and M.I. Yavor. A high-performance multiple-reflection time-of-flight mass spectrometer and isobar separator for the research with exotic nuclei. *Nucl. Instrum. Meth. A*, 777:172–188, 2015, doi:https://doi.org/10.1016/j.nima.2014.12.094.

[19]F. Wienholtz, D. Atanasov, S. Kreim, V. Manea, M. Rosenbusch, L. Schweikhard, A. Welker, and R. N. Wolf. Towards ultrahigh-resolution multi-reflection time-of-flight mass spectrometry at ISOLTRAP. *Phys. Scripta*, T166:014068, 2015, doi:https://doi.org/10.1088/0031-8949/2015/t166/014068.

[20]S. Knauer, P. Fischer, G. Marx, M. Müller, M. Rosenbusch, B. Schabinger, L. Schweikhard, and R. N. Wolf. A multi-reflection time-of-flight setup for the improvement and development of new methods and the study of atomic clusters. *Int. J. Mass Spectrom.*, 446:116189, 2019, doi:https://doi.org/10.1016/j.ijms.2019.116189.

[21]F. Wienholtz, D. Beck, K. Blaum, Ch Borgmann, M. Breitenfeldt, R. B. Cakirli, S. George, F. Herfurth, J. D. Holt, M. Kowalska, S. Kreim, D. Lunney, V. Manea, J. Menendez, D. Neidherr, M. Rosenbusch, L. Schweikhard, A. Schwenk, J. Simonis, J. Stanja, R. N. Wolf, and K. Zuber. Masses of exotic calcium isotopes pin down nuclear forces. *Nature*, 498(7454):346–349, 2013, doi:http://dx.doi.org/10.1038/nature12226. Letter.

[22]D. Atanasov, P. Ascher, K. Blaum, R. B. Cakirli, T. E. Cocolios, S. George, S. Goriely, F. Herfurth, H.-T. Janka, O. Just, M. Kowalska, S. Kreim, D. Kisler, Yu. A. Litvinov, D. Lunney, V. Manea, D. Neidherr, M. Rosenbusch, L. Schweikhard, A. Welker, F. Wienholtz, R. N. Wolf, and K. Zuber. Precision Mass Measurements of $^{129\text{-}131}$Cd and Their Impact on Stellar Nucleosynthesis via the Rapid Neutron Capture Process. *Phys. Rev. Lett.*, 115:232501, 2015, doi:https://doi.org/10.1103/PhysRevLett.115.232501.

[23]Y. Ito, P. Schury, M. Wada, F. Arai, H. Haba, Y. Hirayama, S. Ishizawa, D. Kaji, S. Kimura, H. Koura, M. MacCormick, H. Miyatake, J. Y. Moon, K. Morimoto, K. Morita, M. Mukai, I. Murray, T. Niwase, K. Okada, A. Ozawa, M. Rosenbusch, A. Takamine, T. Tanaka, Y. X. Watanabe, H. Wollnik, and S. Yamaki. First Direct Mass Measurements of Nuclides around Z=100 with a Multireflection Time-of-Flight Mass Spectrograph. *Phys. Rev. Lett.*, 120:152501, 2018, doi:https://doi.org/10.1103/PhysRevLett.120.152501.

[24]M. Mougeot, D. Atanasov, K. Blaum, K. Chrysalidis, T. Day Goodacre, D. Fedorov, V. Fedosseev, S. George, F. Herfurth, J. D. Holt, D. Lunney, V. Manea, B. Marsh, D. Neidherr, M. Rosenbusch, S. Rothe, L. Schweikhard, A. Schwenk, C. Seiffert, J. Simonis, S. R. Stroberg, A. Welker, F. Wienholtz, R. N. Wolf, and K. Zuber. Precision mass measurements of $^{58-63}$Cr: Nuclear collectivity towards the $n = 40$ island of inversion. *Phys. Rev. Lett.*, 120:232501, 2018, doi:https://doi.org/10.1103/PhysRevLett.120.232501.

[25]M. Rosenbusch, Y. Ito, P. Schury, M. Wada, D. Kaji, K. Morimoto, H. Haba, S. Kimura, H. Koura, M. MacCormick, H. Miyatake, J. Y. Moon, K. Morita, I. Murray, T. Niwase, A. Ozawa, M. Reponen, A. Takamine, T. Tanaka, and H. Wollnik. New mass anchor points for neutron-deficient heavy nuclei from direct mass measurements of radium and actinium isotopes. *Phys. Rev. C*, 97:064306, 2018, doi:https://doi.org/10.1103/PhysRevC.97.064306.

[26]W. R. Plaß, T. Dickel, U. Czok, H. Geissel, M. Petrick, K. Reinheimer, C. Scheidenberger, and M. I. Yavor. Isobar separation by time-of-flight mass spectrometry for low-energy radioactive ion beam facilities. *Nucl. Instrum. Meth. B*, 266(19):4560–4564, 2008, doi:http://dx.doi.org/10.1016/j.nimb.2008.05.079.

[27]R. N. Wolf, D. Beck, K. Blaum, Ch. Böhm, Ch. Borgmann, M. Breitenfeldt, F. Herfurth, A. Herlert, M. Kowalska, S. Kreim, D. Lunney, S. Naimi, D. Neidherr, M. Rosenbusch, L. Schweikhard, J. Stanja, F. Wienholtz, and K. Zuber. Online separation of short-lived nuclei by a multi-reflection time-of-flight device. *Nucl. Instrum. Meth. A*, 686:82–90, 2012, doi:http://dx.doi.org/10.1016/j.nima.2012.05.067.

[28]T. Y. Hirsh, N. Paul, M. Burkey, A. Aprahamian, F. Buchinger, S. Caldwell, J. A. Clark, A. F. Levand, L. L. Ying, S. T. Marley, G. E. Morgan, A. Nystrom, R. Orford, A. P. Galván, J. Rohrer, G. Savard, K. S. Sharma, and K. Siegl. First operation and mass separation with the CARIBU MR-TOF. *Nucl. Instrum. Meth. B*, 376:229–232, 2016, doi:https://doi.org/10.1016/j.nimb.2015.12.037.

[29]F. M. Maier, P. Fischer, H. Heylen, V. Lagaki, S. Lechner, P. Plattner, S. Sels, F. Wienholtz, W. Nörtershäuser, L. Schweikhard, and S. Malbrunot-Ettenauer. Simulations of a proof-of-principle experiment for collinear laser spectroscopy within a multi-reflection time-of-flight device. *Hyperfine Interact.*, 240(1):54, 2019, doi:https://doi.org/10.1007/s10751-019-1575-x.

[30]S. Sels, P. Fischer, H. Heylen, V. Lagaki, S. Lechner, F.M. Maier, P. Plattner, M. Rosenbusch, F. Wienholtz, R. N. Wolf, W. Nörtershäuser, L. Schweikhard, and S. Malbrunot-Ettenauer. First steps in the development of the Multi Ion Reflection Apparatus for Collinear Laser Spectroscopy. *Nucl. Instrum. Meth. B*, 2019, doi:https://doi.org/10.1016/j.nimb.2019.04.076.

[31]Y. Ito, P. Schury, M. Wada, S. Naimi, T. Sonoda, H. Mita, F. Arai, A. Takamine, K. Okada, A. Ozawa, and H. Wollnik. Single-reference high-precision mass measurement with a multireflection time-of-flight mass spectrograph. *Phys. Rev. C*, 88:011306, 2013, doi:https://doi.org/10.1103/PhysRevC.88.011306.

[32]R. L. Hettich. Structural investigations of aluminum cluster ions, Al_n^- (n=3-50). *J. Am. Chem. Soc.*, 111(23):8582–8588, 1989, doi:https://doi.org/10.1021/ja00205a004.

[33]A. Drescher, J. Kitching, J. E. Crawford, J. K. P. Lee, and G. Thekkadath. Studies of Sb and Bi cluster produced by laser desorption. *Z. Phys. D*, 19(4):203–206, 1991, doi:https://doi.org/10.1007/BF01448292.

[34]H. S. Kim, T. D. Wood, A. G. Marshall, and J. Lee. Production of gold cluster ions by laser desorption/ionization Fourier-transform ion cyclotron resonance mass spectrometry. *Chem. Phys. Lett.*, 224(5):589–594, 1994, doi:https://doi.org/10.1016/0009-2614(94)00584-2.

[35]C. Stoermer, J. Friedrich, and M. M. Kappes. Observation of multiply charged cluster anions upon pulsed UV laser ablation of metal surfaces under high vacuum. *Int. J. Mass Spectrom.*, 206(1):63–78, 2001, doi:https://doi.org/10.1016/S1387-3806(00)00390-0.

[36]R. N. Wolf, G. Marx, M. Rosenbusch, and L. Schweikhard. Static-mirror ion capture and time focusing for electrostatic ion-

beam traps and multi-reflection time-of-flight mass analyzers by use of an in-trap potential lift. *Int. J. Mass Spectrom.*, 313:8–14, 2012, doi:http://dx.doi.org/10.1016/j.ijms.2011.12.006.

[37] S. Knauer, P. Fischer, G. Marx, B. Schabinger, L. Schweikhard, and R. N. Wolf. Multi-reflection time-of-flight mass spectrometry with combined in-trap lift capture and mirror-switch ejection. *Int. J. Mass Spectrom.*, 423:46–53, 2017, doi:https://doi.org/10.1016/j.ijms.2017.10.007.

[38] D. Beck, K. Blaum, H. Brand, F. Herfurth, and S. Schwarz. A new control system for ISOLTRAP. *Nucl. Instrum. Meth. A*, 527(3):567–579, 2004, doi:https://doi.org/10.1016/j.nima.2004.02.043.

[39] P. Fischer, S. Knauer, G. Marx, and L. Schweikhard. In-depth study of in-trap high-resolution mass separation by transversal ion ejection from a multi-reflection time-of-flight device. *Rev. Sci. Instrum.*, 89(1):015114, 2018, doi:https://doi.org/10.1063/1.5009167.

[40] P. Fischer, G. Marx, and L. Schweikhard. Multiple ion capture and separation in an electrostatic storage device. *Int. J. Mass Spectrom.*, 435:305–314, 2019, doi:https://doi.org/10.1016/j.ijms.2018.11.010.

[41] P. Schury, Y. Ito, M. Wada, and H. Wollnik. Wide-band mass measurements with a multi-reflection time-of-flight mass spectrograph. *Int. J. Mass Spectrom.*, 359:19–25, 2014, doi:http://dx.doi.org/10.1016/j.ijms.2013.11.005.

[42] Y. Toker, N. Altstein, O. Aviv, M. L. Rappaport, O. Heber, D. Schwalm, D. Strasser, and D. Zajfman. The kick-out mass selection technique for ions stored in an Electrostatic Ion Beam Trap. *J. Instrum.*, 4(09):P09001, 2009.

[43] R. T. Hilger, R. Santini, and S. A. Mcluckey. Square Wave Modulation of a Mirror Lens for Ion Isolation in a Fourier Transform Electrostatic Linear Ion Trap Mass Spectrometer. *Int. J. Mass Spectrom.*, 362:1–8, 2014, doi:https://doi.org/10.1016/j.ijms.2014.02.003.

[44] T. Dickel, W. R. Plaß, W. Lippert, J. Lang, M. I. Yavor, H. Geissel, and C. Scheidenberger. Isobar Separation in a Multiple-Reflection Time-of-Flight Mass Spectrometer by Mass-Selective Re-Trapping. *J. Am. Soc. Mass Spectrom.*, 28(6):1079–1090, 2017, doi:https://doi.org/10.1007/s13361-017-1617-z.

[45] J. T. Johnson, I. J. Carrick, G. S. Eakins, and S. A. McLuckey. Mirror Switching for High-Resolution Ion Isolation in an Electrostatic Linear Ion Trap. *Anal. Chem.*, 91(14):8789–8794, 2019, doi:https://doi.org/10.1021/acs.analchem.9b00874.

[46] J. T. Johnson, I. J. Carrick, G. S. Eakins, and S. A. McLuckey. Simultaneous Isolation of Nonadjacent m/z Ions Using Mirror Switching in an Electrostatic Linear Ion Trap. *Anal. Chem.*, 91(19):12574–12580, 2019, doi:https://doi.org/10.1021/acs.analchem.9b03560.

[47] P. Fischer, S. Knauer, G. Marx, and L. Schweikhard. Non-isobaric time-of-flight correction for isobar resolving in MR-ToF mass spectrometry. *Int. J. Mass Spectrom.*, 432:44–51, 2018, doi:https://doi.org/10.1016/j.ijms.2018.07.004.

[48] M. Wang, G. Audi, F. Kondev, W. Huang, S. Naimi, and X. Xu. The AME2016 atomic mass evaluation (II). Tables, graphs and references. *Chinese Phys. C*, 41:030003, 2017, doi:https://doi.org/10.1088/1674-1137/41/3/030003.

[49] P. Schury, Y. Ito, M. Rosenbusch, H. Miyatake, M. Wada, and H. Wollnik. Improving wide-band mass measurements in a multi-reflection time-of-flight mass spectrograph by usage of a concomitant measurement scheme. *Int. J. Mass Spectrom.*, 433:40–46, 2018, doi:https://doi.org/10.1016/j.ijms.2018.08.007.

[50] F. Wienholtz, S. Kreim, M. Rosenbusch, L. Schweikhard, and R. N. Wolf. Mass-selective ion ejection from multi-reflection time-of-flight devices via a pulsed in-trap lift. *Int. J. Mass Spectrom.*, 2017, doi:http://dx.doi.org/10.1016/j.ijms.2017.07.016.

[51] R. N. Wolf, D. Beck, K. Blaum, Ch. Böhm, Ch. Borgmann, M. Breitenfeldt, N. Chamel, S. Goriely, F. Herfurth, M. Kowalska, S. Kreim, D. Lunney, V. Manea, E. Minaya Ramirez, S. Naimi, D. Neidherr, M. Rosenbusch, L. Schweikhard, J. Stanja, F. Wienholtz, and K. Zuber. Plumbing Neutron Stars to New Depths with the Binding Energy of the Exotic Nuclide ^{82}Zn. *Phys. Rev. Lett.*, 110:041101, 2013, doi:https://doi.org/10.1103/PhysRevLett.110.041101.

[52] F. Wienholtz, K. Blaum, J. Karthein, D. Lunney, S. Malbrunot-Ettenauer, V. Manea, M. Mougeot, L. Schweikhard, T. Steinsberger, and R. N. Wolf. Improved stability of multi-reflection time-of-flight mass spectrometers through passive and active voltage stabilization. *Nucl. Instrum. Meth. B*, 2019, doi:https://doi.org/10.1016/j.nimb.2019.04.061.

7.5 Photofragmentation of $Bi_n^{+/-}$ clusters (n = 2–19) in an electrostatic ion beam trap

Eur. Phys. J. D (2019) 73: 105
https://doi.org/10.1140/epjd/e2019-100027-0

THE EUROPEAN PHYSICAL JOURNAL D

Regular Article

Photofragmentation of $Bi_n^{+/-}$ clusters ($n = 2-19$) in an electrostatic ion beam trap

Paul Fischer[a] and Lutz Schweikhard

Institut für Physik, Universität Greifswald, 17487 Greifswald, Germany

Received 16 January 2019 / Received in final form 26 February 2019
Published online 21 May 2019

Abstract. Photofragmentation spectra for small bismuth-cluster cat- and anions are recorded for the investigation of their fragmentation pathways as a function of cluster size. To this end, the ions of interest are stored and size-selected in an electrostatic ion beam trap/a multi-reflection time-of-flight mass spectrometer with high resolving power. The subsequent photoexcitation is timed to their turn-around point in the trap's mirror potential. In this novel approach, charged fragment clusters exhibit the same energy as the precursor ions and, thus, can be further stored and investigated with identical trap configurations. The results suggest a high stability of the neutral bismuth tetramer in accordance with previous reports, which is attributed to bismuth clusters exhibiting semimetal properties. Additionally, there is evidence for the loss of larger neutral fragments.

1 Introduction and motivation

The properties of the Group 15 elements are known to vary widely: starting off with the nonmetals nitrogen and phosphorus, the group incorporates arsenic and antimony, which are classified as semimetals, and eventually leads to bismuth and its classification as a post-transition metal like lead and tin [1]. Applications are similarly diverse across the individual members, with bismuth specifically proving to be candidate of interest for alloys useful for (near-)infrared optoelectronics [2] or spintronics [3].

Gas-phase bismuth clusters produced by laser vaporization have been studied since the 1980s [4–6]. The fragmentation channels of the cations Bi_n^+ have been probed by collision-induced dissociation (CID) for $n = 3$–14 [6,7], surface-induced dissociation (SID) for $n = 3$–8 [8], and photoexcitation at $\lambda = 248$ nm for $n = 2$–8 [5]. All studies find that small clusters with $n < 8$ show a preference for the loss of neutral monomers, dimers, and trimers, with $n = 8$ marking the switch to dominant loss of neutral tetramers Bi_4. The experiments suggest increased stability of the neutral dimer and tetramer species, which has also been found in theoretical work based on density-functional calculations [9–12].

The experimental information of anionic clusters Bi_n^- is comparatively less extensive. Photoelectron-spectroscopy (PES) measurements have been performed [13–15]; however, the anions' fragmentation behavior has – to our knowledge – not yet been probed experimentally. The neutral clusters have been investigated for their magnetic moments utilizing Stern–Gerlach deflection [16], where paramagnetic behavior is observed for odd sizes.

In the present study, photoexcitation at $\lambda = 532$ nm is employed to investigate the fragmentation pathways of bismuth-cluster cat- and anions with $n = 2$–19. To this end, an electrostatic ion beam trap (EIBT) [17–19] is used to store the cluster ions between two electrostatic ion mirrors. These highly versatile ion-trap devices, also referred to as multi-reflection time-of-flight (MR-ToF) mass spectrometers, exhibit high mass resolving powers ($R \geq 10^5$) and have proven to be valuable tools for ion separation prior to nuclear precision experiments [20–27] next to their application for direct mass measurements [21,25–30]. For the study of cluster and molecular properties, the electrostatic nature of EIBTs permits investigations over virtually unrestricted mass ranges and their open geometry and absence of magnetic fields allows overlapping of electron [31] or laser beams [32–36] with the stored ions.

EIBT-based photofragmentation studies of small metal clusters have been performed by Aviv et al. [32,34,35,37] by operating the trap in "non-bunching" mode, where stored ions quickly fill the entirety of the axial space. Additional in-trap deflectors are then utilized to extract fragment ions and perform time-of-flight evaluations. In contrast, ion bunches are retained in the present study instead, and the trap is used to select an ion species of interest. The system's high mass resolving power and sensitivity can, thus, be used to suppress contaminant ions without the need for additional devices or preparation steps. The laser pulse is timed to excite the ions at their turn-around point in a mirror potential, i.e. when they have a kinetic energy of (close to) zero but

[a] e-mail: paul.fischer@uni-greifswald.de

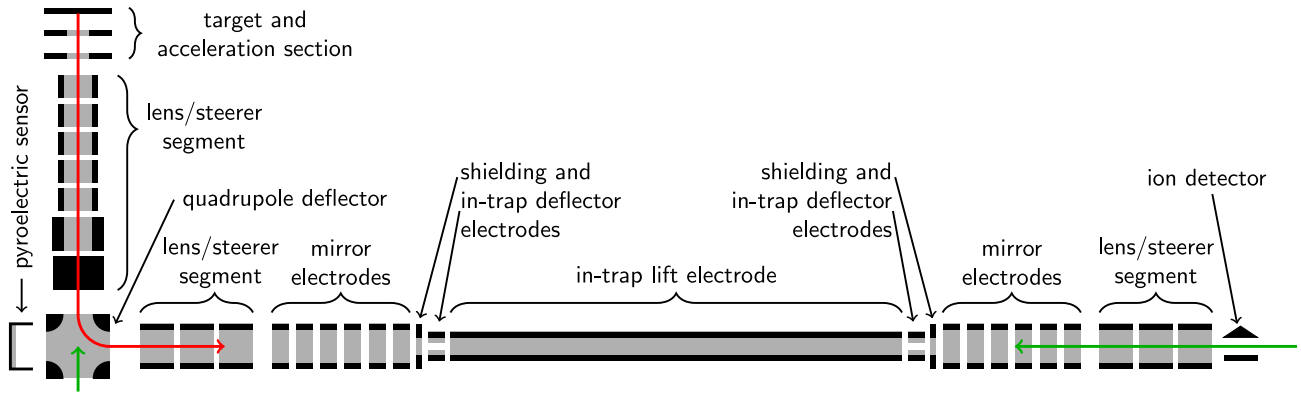

Fig. 1. Schematic of the experimental setup. From top left to bottom right: target plate and dual-stage acceleration section, ion-optical lenses and steerers, quadrupole deflector, entry-side lens/steerer, MR-ToF analyzer with in-trap lift electrode, transversal deflector electrodes, and stacks of six mirror electrodes on each side, exit-side lens/steerer, channeltron ion detector with conversion dynode. The ion path is indicated as red, the source and photoexcitation laser beams as green arrows.

retain their full potential energy. This feature has already been employed in reflectron mass spectrometers by several groups [38–44]. Prompt fragmentation, i.e. before substantial re-acceleration, thus results in the fragment ions leaving the mirror potential as individual bunches with the same total energy as the precursor, allowing a direct mass analysis by use of the same post-trap detection equipment.

2 Experimental setup

The present setup (Fig. 1) has already been partially described in [45–48]. A laser-ablation source similar to those of [49–52] is utilized to produce small metal-cluster ions via laser irradiation of target plates in vacuum (Continuum: MiniLite laser, $\leq$15 mJ pulse energy at $\lambda = 532$ nm, 6 ns pulse length, 10 Hz repetition rate). The ions are accelerated to 2010 eV with a two-stage extraction section [53] and guided into the EIBT via a quadrupole deflector and several ion-optical elements. The potentials of the trap's electrostatic mirrors are given in [46]: of the six electrodes of each mirror, the outermost four are used to form the reflecting potential wall while the innermost two refocus stored ions during each revolution, thus ensuring radial confinement.

The experiment sequence after the ions' arrival at the trap is depicted in Figure 2. An in-trap lift electrode [54–57] is used to lower the ions' total energy between the mirrors by switching the tube's potential from a preset voltage to ground (Figs. 2a and 2b). In the present study, this lift voltage is chosen as $+/-811$ V for the trapping of cat- and anions, respectively. The delay between the source-laser pulse and the switching of the lift electrode is denoted as the m/q-dependent capture time t_{cap} [48]. When no switching is employed at all ("single-path operation"), all ions reach the detector at increasing flight times according to their m/q value and the system resembles a conventional linear ToF mass spectrometer with two acceleration stages [53].

For MR-ToF operation, a mass range of interest can be preselected via the capture time. The ions are trapped for

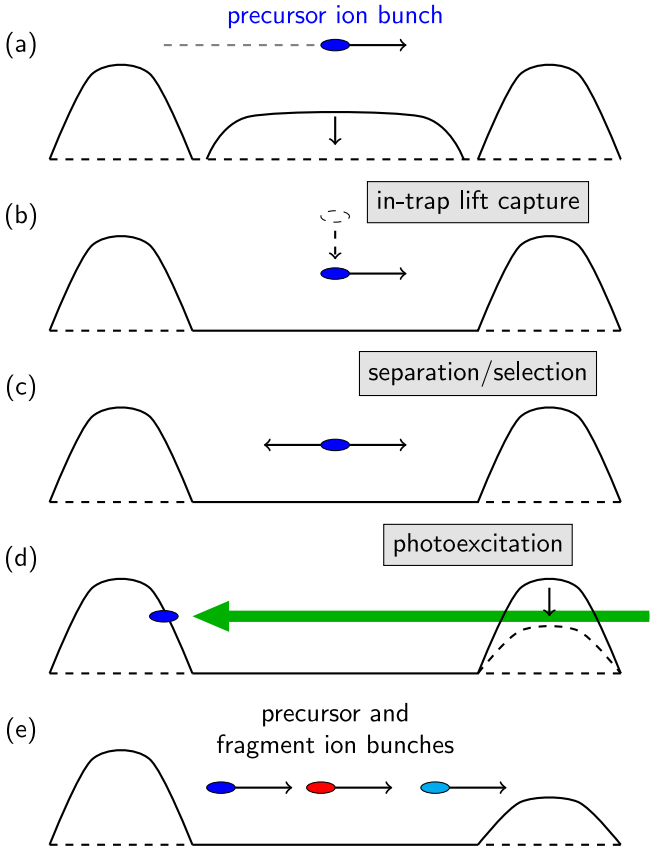

Fig. 2. Schematic illustration of the experimental cycle for photoexcitation of a selected ion species. For details, see text.

the length of a storage time t_s (Fig. 2c), which is chosen to correlate to 400 of their revolution periods for the present study. Depending on the ions' mass-to-charge ratio, this amounts to several tens of milliseconds. During storage, different ion species will separate in time due to their difference in velocity, allowing their selection by transversal ejection of unwanted species ([46] and references therein): A sliced in-trap deflector electrode (see Fig. 1) is

periodically switched between ground and some deflector voltage, allowing undisturbed passage for ions with an m/q value selected by the switching frequency, phase, and duty cycle.

Photoexcitation is subsequently performed on a selected ion species using a second Nd:YAG laser (identical model as source laser) at $\lambda = 532\,\text{nm}$ Figure 2d. The excitation-laser beam is guided through the trap axially (see Fig. 1), the pulse timing is set by adjusting its delay to the source-laser pulse via a frequency generator (Keysight Technologies, 33522A). Specifically, the delay is chosen such that it amounts to the sum of the capture time, which is in turn adjusted to capture the ion species of interest when it is in the center of the in-trap lift, and its revolution period $T(n)$ times 400.75. Since one period is defined as the time needed for the ions to reach the middle of the lift tube again (with a direction of motion towards the exit-side), the additional three quarters of a period ensure their location at their turn-around point in the entry-side mirror.

The excitation-laser pulse energy is monitored on a shot-to-shot basis with a pyroelectric sensor (left of the quadrupole bender in Fig. 1) and tuned for an output of 1 mJ for the present measurements. This produces reasonable fragment-ion intensities without significantly changing relative abundances compared to lower pulse energies (dependence on pulse energy will be discussed further at Fig. 10). Photofragmentation spectra are recorded together with reference cycles in which the excitation-laser pulse is blocked in an alternating fashion to correct long-term source-intensity drifts.

The t_{cap} values for central capture were determined carefully, as mismatches thereof would lead to the excitation-laser pulse not being synchronized to the theoretical turn-around point. Both the capture times and revolution periods of ions follow square-root functions according to their mass-to-charge ratios [48].

For cluster-fragment analysis, the exit-side mirror potential is lowered simultaneously to the timing of the excitation-laser pulse Figure 2d. More specifically, the outermost two mirror electrodes are switched from their respective voltages to ground, which lowers the maximum of the potential wall below the ions' storage energy of 1200 eV. This combined approach of in-trap lift capture and mirror-switch ejection leads to a larger "ToF ejection window" while retaining the advantage of adjusting the ion energy via the lift potential [45]. The mirror-switch ejection eliminates the need to scan an additional timing or voltage to observe different fragment ions. All fragments and the remainder of the precursor ions will reach the detector Figure 2e and – since fragment-ion flight times after the photoexcitation follow a square-root function according to their m/q value – the cluster sizes are easily identified. For significantly larger clusters or more complex fragmentation behaviors resulting from, e.g., different cluster isotopologues, the ion ejection can also be delayed to perform multi-reflection operation and utilize the full mass resolving power of the MR-ToF device on the fragments [58].

Ion detection is performed with a channeltron detector including a 5 kV conversion dynode. The detector signals are amplified (ORTEC, VT120a, 46 dB) and recorded with a fast multiscaler (FAST ComTec GmbH, MCS6A). Its start is synchronized to the source-laser pulse, i.e. the time of the ions' start in the source. The control of the experimental timing pattern is performed with a LabVIEW-based control software [59] and a Field-Programmable-Gate-Array card (National Instruments, PCI-7811R).

3 Results and discussion

3.1 Cluster production

With laser-pulse energies of 0.5−1 mJ, the present laser-ablation source produces a high abundance of small-sized clusters, the distribution of which can be investigated in the single-path operation scheme (Fig. 3). For both polarities, the cluster sizes $n \leq 5$ are readily produced while larger clusters are less abundant.

The intensity distribution of bismuth cations shows local maxima at $n = 3$, 7, 10, 16, and 21. The $n = 5$ cation is the largest cluster produced in high abundance before a significant drop in relative intensity occurs for the following sizes. This is in general agreement with previous observations on bismuth spectra produced by laser vaporization [6,8,60] and sputtering [6]. Particularly the $n = 3$, 5, and 7 cations are expected to exhibit increased stability according to simple electron counting rules of polyhedral structures ("Wade's rules" [61]). The bismuth atom's s^2p^3 configuration leads to a total of 8, 14, and 20 valence p electrons, respectively, which corresponds to the stable numbers of $2n + 2$, $2n + 4$, and $2n + 6$.

It has been reported that neutral clusters with sizes larger than 5 have not been observed when probed with photoionization in the presence of larger charged species [60]. This may indicate that the formation of larger clusters relies on aggregation processes supported by collisional cooling. It was also suggested that cationic cluster growth is primarily limited to ion-neutral condensation, as ionization presumably only occurs during and shortly after the laser pulse when high energies are present.

Anionic clusters, in contrast, could grow via neutral condensation and pick up an electron later, depending on electron affinities, electron attachment cross sections, and stable electron configurations [60]. This may explain the overall smoother distribution of anionic cluster-size abundances observed in Figure 3. Following the rules of electron counting, stable structures should occur for $n = 1$, 3, and 5 ($2n + 2$, $2n + 4$, $2n + 6$ p electrons). However, although Bi_1^- and Bi_3^- are observed in high abundance, Bi_2^- is even more prominent, which is in agreement with previous results [13,50,60]. Other (minor) local maxima can be observed for $n = 10$, 13, 16, and 19.

The cluster intensity drops somewhat at $n \geq 21$ and $n \geq 19$ for cat- and anions, respectively. Note that the source-laser pulse energy has been purposely set to a low value ($\approx$0.5 mJ) for the measurements shown in Figure 3 to prevent detector saturation on the signals of small cluster sizes. While the individual intensities allow a relative comparison of production/ionization rates, the pulse

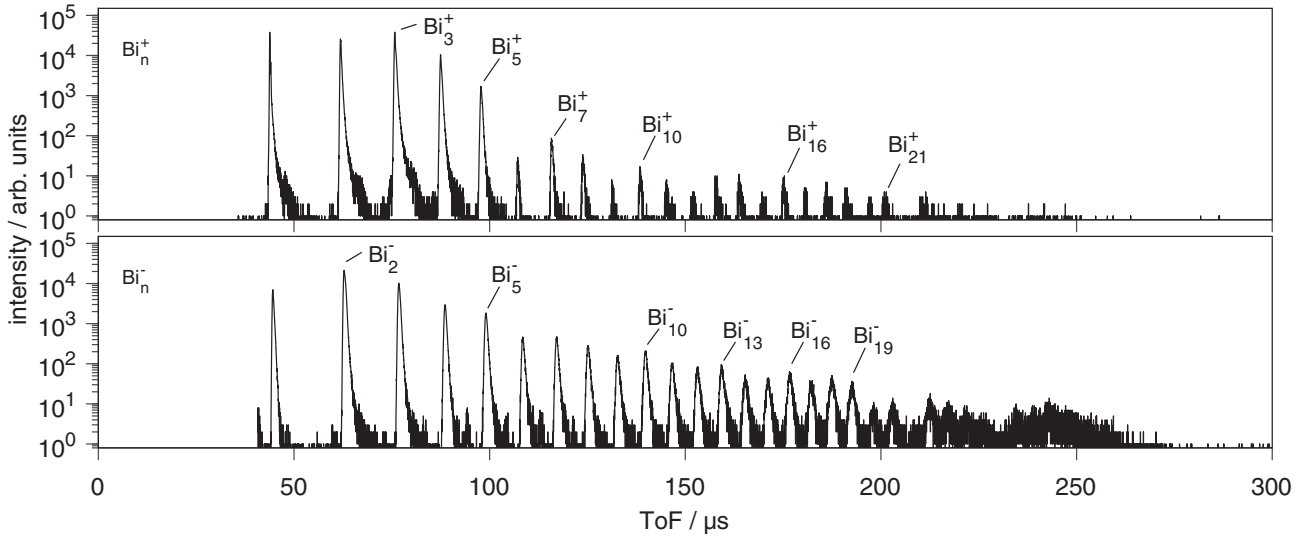

Fig. 3. Single-path spectrum of $Bi_n^{+/-}$ clusters produced with the present laser ablation source. Selected signals are marked.

energy can be tuned such that comparable, sufficiently-high count rates are achieved in multi-reflection operation for specific species of interest.

3.2 In-trap photoexcitation

According to the measurement cycle outlined in Section 2, an individual cluster size is captured by lowering its total energy with the in-trap lift and stored for 400 revolutions to select it for photoexcitation. The steps of the cycle are visualized in Figure 4 for the case of the bismuth heptamer anion, Bi_7^-.

Without transversal ejection (Fig. 4a), signals of a number of "contaminant" ion species are present in the ToF spectrum due to other, simultaneously-stored cluster sizes lapping the ion of interest. For bismuth clusters specifically, low-abundance Bi–Pb compound clusters resulting from target impurities have also been observed (see Fig. 10 in [48]). For larger clusters, several hundred revolution periods are needed to separate them from the species of interest and eject them transversally (a selection resolving power of around 4000 is needed for the largest invesitaged species Bi_{19}). Accordingly, a duty cycle setting of 65° (see [46] for definition) has been chosen for all measurements performed in the present study and the deflector pulses of the ejection are applied for the first 395 revolution periods.

With the transversal ejection enabled, all ion species but the selected precursor cluster size are removed from the trap (Fig. 4b). Thus, upon photoexcitation the spectra only show the precursor and the new ion signals originating from its fragmentation (Fig. 4c). The time-of-flight axis in all three spectra is chosen such that zero coincides with the timing of the excitation-laser pulse and the simultaneous switching of the exit-side mirror potential. For the example of Bi_7^- (Fig. 4) the capture time $t_{\mathrm{cap}}(7) = 78.5\,\mu\mathrm{s}$ and revolution period $T(7) = 128.1324\,\mu\mathrm{s}$ lead to a total excitation-laser delay of $t_{\mathrm{cap}}(7) + 400.75\,T(7) = 51427.6\,\mu\mathrm{s}$.

A variation of the excitation-laser pulse delay has been performed for Bi_5^- to demonstrate the influence of the timing (Fig. 5). For a delay of 0, the pulse coincides with the theoretical turn-around point at 400.75 revolution periods. Since $T(5) = 108.3\,\mu\mathrm{s}$ and $t_{\mathrm{cap}}(5) = 66.3\,\mu\mathrm{s}$, the delay steps of 1 μs amount to mismatches of roughly 0.9% with respect to the revolution period or 1.5% with respect to the capture time.

As is readily apparent from the ToF spectra (top of Fig. 5), delay mismatches lead to asymmetrical results around the expected turn-around timing. For

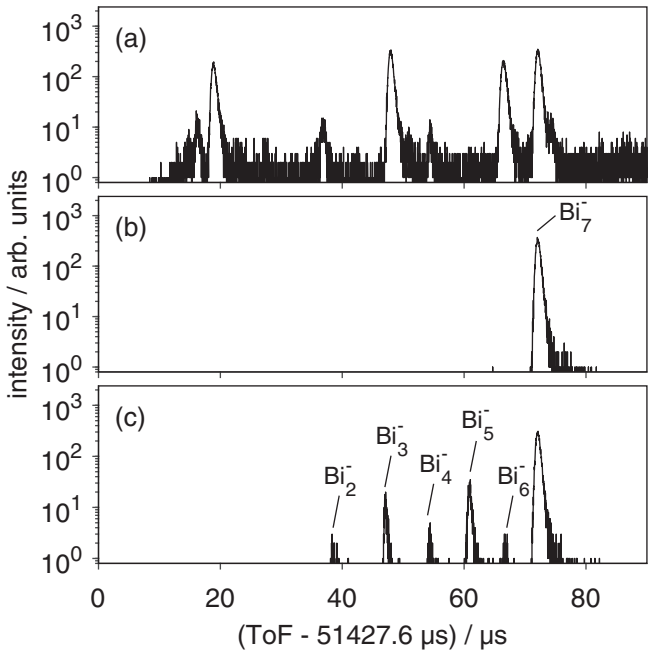

Fig. 4. ToF spectra after 400 Bi_7^- revolution periods. (a) No transversal ejection and no photoexcitation is employed. (b) Transversal ejection is enabled for the first 395 revolution periods and synchronized to retain Bi_7^-. (c) In addition, the excitation-laser pulse is enabled to interact with Bi_7^- in the entry-side mirror after 400 periods.

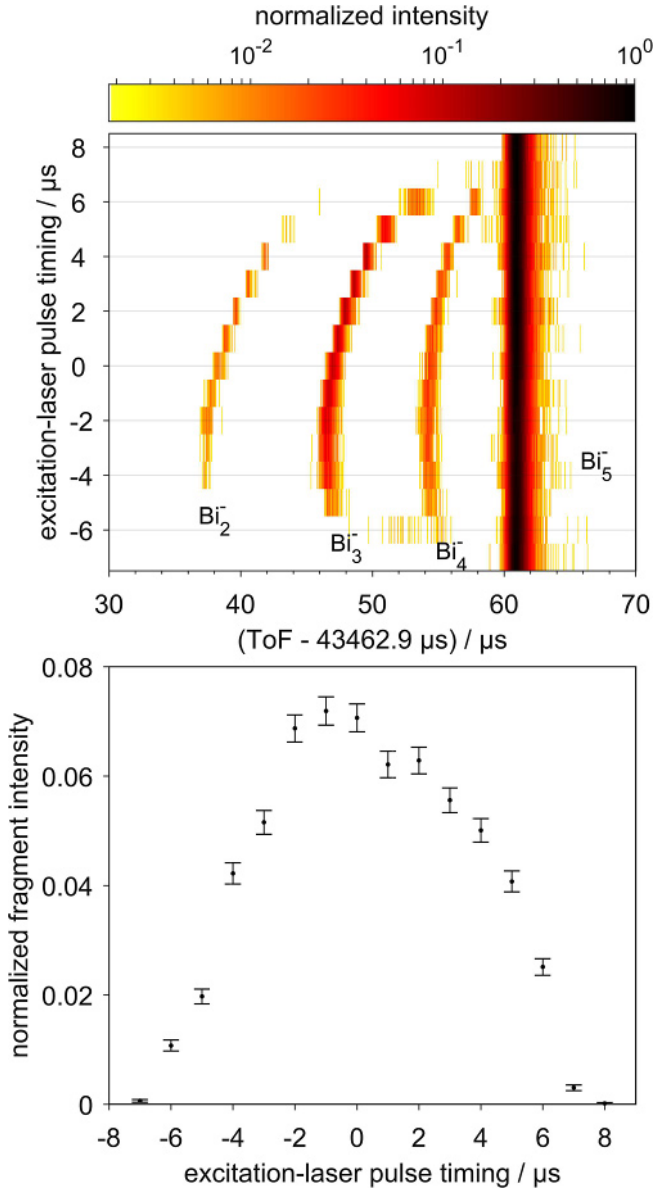

Fig. 5. Top: 2D plot of ToF spectra after photoexcitation of selected Bi_5^- ions (rightmost signal) with Bi_2^-, Bi_3^-, and Bi_4^- fragment signals for different excitation-laser pulse timings. Bottom: total fragment intensities as function of pulse timing.

singly-charged ions, the kinetic energy of the fragment,

$$E_f = \frac{m_f}{m_p} E_p, \tag{1}$$

is the portion of the kinetic energy of the precursor E_p given by the mass ratio of both ions. Accordingly, post-turn-around fragmentation leads to fragment ions exhibiting less kinetic energy after their full acceleration from the mirror potential with increasing delays, as E_p continuously increases. This leads to ion signals shifting to longer flight times for positive timing delays. For pre-turn-around fragmentation, the lowered energy of the fragments results in an additional shift of the actual turn-around point towards lower potentials and thus shortens the traveled flight path.

Although the angle of incidence of ions entering the mirror potential is expected to be small due to phase-space selection occurring over the first 400 revolutions of storage, stable trajectories could still exhibit nonzero values. For photoexcitation studies performed at the turn-around point of a reflectron, where incidence angles have to be larger, early and late fragmentations are known to lead to different changes in post-reflection ion trajectories [39].

Both angle and energy deviations of fragment ions lead to intensity losses in the present setup, as the electrostatic deflectors between the trap and ion detector (see Fig. 1) will not properly focus/steer aberrant ions. However, we expect the "loss" of kinetic energy to be the primary reason for the decreasing intensity with both positive and negative pulse-timing values.

The fact that the shortest fragment-ion flight times are not observed at "0" could be explained by the compensating effect of earlier turn-around points stated above. The present measurements have been performed with the pulse timing set to "0" to ensure maximum fragment intensity. Time-of-flight shifts during the measurement due to fluctuations in the trap's potential or geometric configuration have recently been shown to scale with the number of revolution periods [47]. For the chosen experimental conditions and storage times, fluctuations in the ions' revolution period are insignificant in the context of pulse-timing strictness. The results of the scan shown in Figure 5 are qualitatively identical for different precursor cluster sizes, the allowed window of pulse timings scales with the revolution period.

We note in passing that there is some timing-dependent ToF focusing of the fragment signals (see top of Fig. 5). This is related to the conditions of the ions' re-acceleration by the mirror and of no consequence for the present measurements. We also note that fragmentation processes with time constants significantly longer than the turn-around time will not lead to ion signals as presented here. However, the reader is also referred to the explanations for the additional signal observed in the $n = 16$ anion photoexcitation spectrum in Figure 11. An in-depth investigation of these effects is beyond the scope of the present study but will be subject of future work.

3.3 Photofragmentation

A 2D color-intensity plot of all fragmentation spectra recorded in this study (Fig. 6) reveals fragmentation patterns beyond the sequential evaporation of neutral atoms typically associated with metal clusters. While small clusters ($n \leq 8$ for both ion polarities) do lose single neutral atoms, the pathway is quickly superseded by the loss of neutral (presumably) dimers Bi_2 and tetramers Bi_4. This behavior is akin to that previously observed for clusters of non-metallic materials such as carbon, for which neutral C_3 loss is a dominant channel [62], or silicon, which prefers the formation of Si_6^+ [63]. In fact, gas-phase bismuth clusters have been characterized to exhibit semimetal properties based on their geometrical structure and

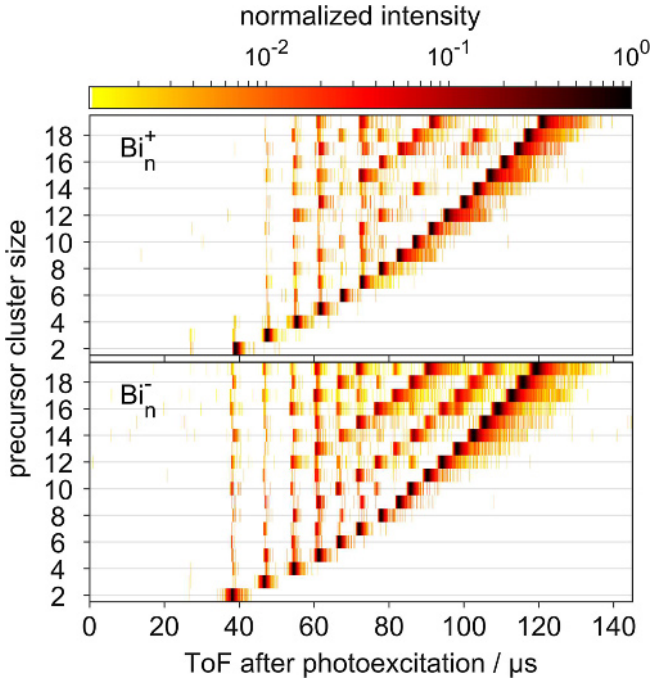

Fig. 6. Overview of the performed photoexcitation measurements for $Bi_n^{+/-}$, $n = 2$–19. Spectra have been normalized to their respective maximum.

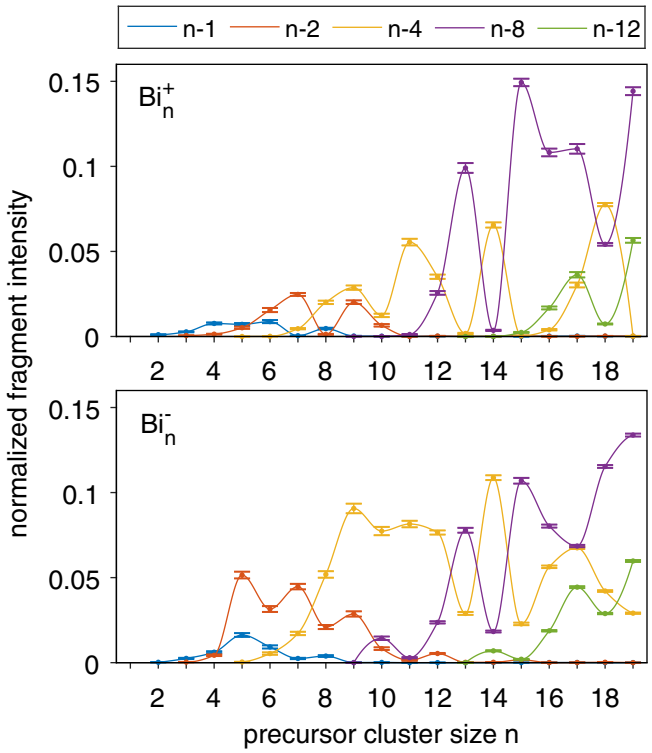

Fig. 7. Relative intensities of high-abundance fragments for precursor cluster sizes $n = 2$–19. Curves resulting from piecewise interpolation are drawn to guide the eye.

fragmentation behavior in a variety of studies [5,7,9]. Mitch et al. also found a phase transition from nanocrystalline to amorphous structures with decreasing thickness of ultrathin Bi films, which indicates a change from semimetallic to semiconducting character as well [64].

When the relative fragment intensity is plotted for given sizes of the neutral fragment lost from the cluster in analogy to neutral-loss scans in MS/MS experiments [65] (Fig. 7), certain trends become apparent. For all cluster sizes $n \leq 7$, the primary fragmentation pathway is the evaporation of monomers or dimers for both ion polarities (Fig. 8), after which the loss of larger fragments predominates.

3.3.1 Cations

For Bi_n^+ clusters, the charged fragment resulting from the loss of a neutral atom is most abundant up to a precursor size $n = 5$, after which the "$n - 2$ fragment" prevails. For $n = 6$ and 7, additional fragments correlating to the loss of a neutral trimer or tetramer can also be observed. As mentioned in the introduction, the fragmentation behavior of small bismuth cations up to $n = 14$ has been studied previously by CID, SID, and photoexcitation [5–8]. The results vary slightly in terms of which fragment ion is most readily observed for a specific precursor, however, the prevalent finding for $n \leq 5$ is monomer and dimer loss.

The Bi_8^+ ion marks a switch of the dominant fragmentation pathway towards the loss of a neutral tetramer, Bi_4 (Fig. 9), which has been observed in all previous fragmentation studies [5–8]. Both the neutral dimer and tetramer are expected to exhibit increased stability from their number of valence p electrons ($2n + 2$ and $2n + 4$, respectively), and both species are indeed observed in neutral cluster-ensembles produced by laser vaporization [4,60] and vapors from oven sources [66]. In fact, the neutral dimer and tetramer of antimony, the closest group 15 neighbor to bismuth, are also found similarly [4,60,67–69], and the dominant channel in unimolecular dissociation for Sb_n^+ clusters with $n \geq 8$ is neutral tetramer breakoff [69].

Density-functional calculations have found the geometric structure of Bi_4 as a tetrahedron with T_d symmetry [9–12]. Its binding and fragmentation energies are large, furthering the assumption of the neutral tetramer being of significant importance for the bismuth fragmentation behavior. In fact, Kelting et al. found the "$n - 4$ Fragment" in highest abundance for all cations in the range from $n = 8$ to 14 [7] and unimolecular dissociation studies performed by Ross et al. yield the same result with the notable exception of Bi_{10}^+ [6]. Fragmentation pathways predicted by Yuan et al. suggest the loss of neutral tetramers to be preferred for all cations from $n = 8$ up to 22 [9]. Fragmentation energies calculated for Bi_{10}^+ are comparatively close for the loss of a neutral dimer, trimer, and tetramer [7], which is in agreement with its photofragmentation spectrum showing a larger number of high-abundance fragment signals.

In the present study, the fragmentation via the Bi_4 channel is prevalent up to $n = 14$, with the exception of the Bi_{13}^+ precursor, where a high amount of Bi_5^+ $(n-8)$ fragments is observed instead (Fig. 9). This, together with

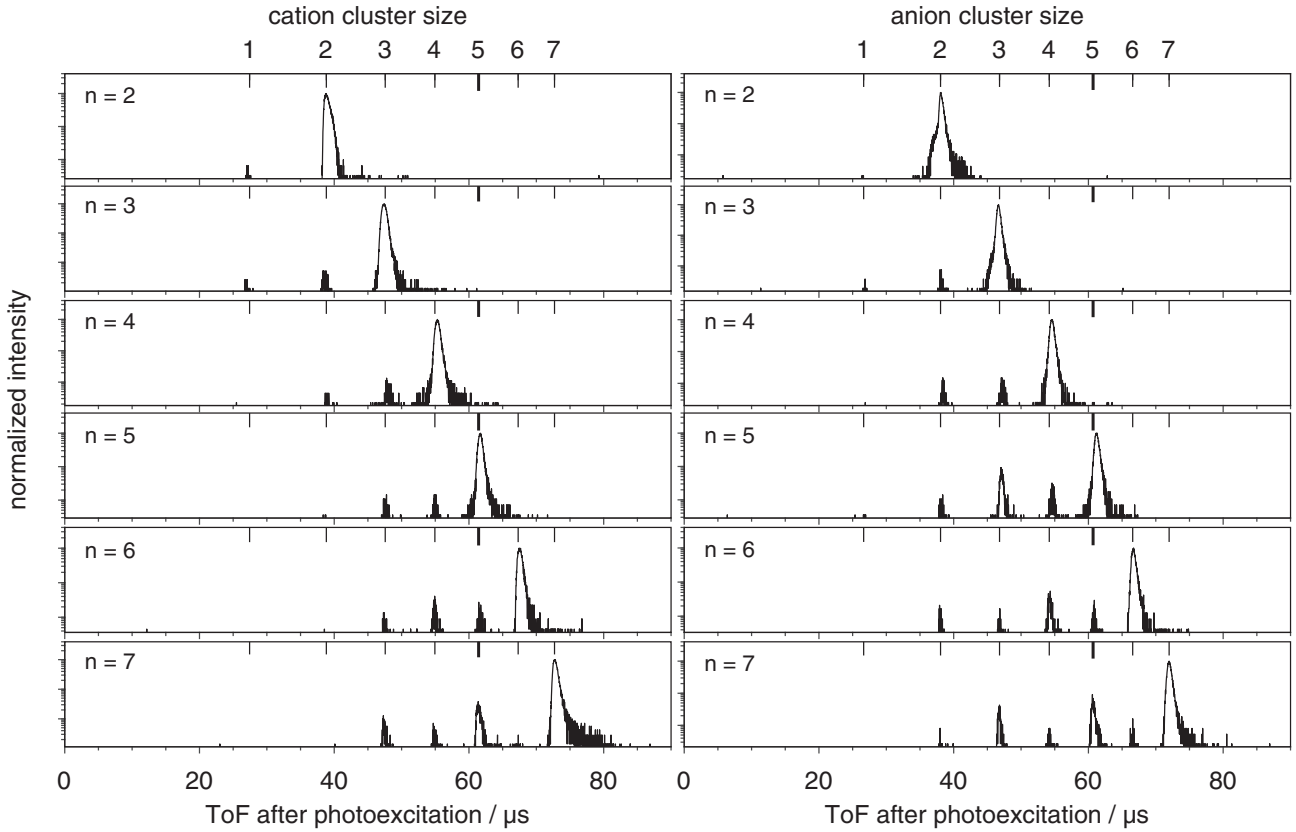

Fig. 8. Photofragmentation spectra (normalized to their maxima) obtained from precursor clusters $Bi_n^{+/-}$, $n = 2$–7.

the observation that Bi_{14}^+ produces a "fragmentation footprint" very similar to that of Bi_{10}^+, suggests the presence of sequential fragmentation processes. Precursors could lose a neutral tetramer and lead to excited $n-4$ fragment ions with vibrational energies still high enough for further dissociation. For the example of the $n = 13$ precursor, this results in the loss of an additional neutral di- or tetramer according to the fragmentation channels observed for direct excitation of the smaller clusters. A variation of the excitation-laser pulse energy E_{pulse} for photoexcitation of Bi_{13}^+ is therefore performed to reveal the behavior of individual fragment intensities I with changing photon densities (Fig. 10). As is readily apparent, all fragment species follow the same trend, in fact, the ratio between the fragments is constant within the measurement's uncertainty. The curves fitted to the data follow an exponential function

$$I\left(E_{\mathrm{pulse}}\right) = R\left(1 - e^{-kE_{\mathrm{pulse}}}\right), \qquad (2)$$

where R describes a fragment ion's branching ratio and k the fitting constant of a characteristic pulse energy $\varepsilon = k^{-1}$. For low pulse energies, the curves can be approximated by linear functions.

The results of the pulse-energy variation suggest the fragment ions to be products of competing, single-photon fragmentation pathways, which is implying the direct loss of a neutral octamer Bi_8 in contrast to sequential tetramer decay. Investigations for different precursor clusters yield comparable results, with most high-abundance fragments maintaining a fixed ratio and only some minor species growing disproportionally abundant for high pulse energies. This discrepancy could be partially explained by calculated fragmentation energies [7]: the $Bi_{13}^+ \longrightarrow Bi_9^+ + Bi_4$ fragmentation is reported to consume 0.85 eV by Kelting et al., another subsequent $Bi_9^+ \longrightarrow Bi_5^+ + Bi_4$ tetramer loss consumes an additional 0.92 eV. With the present photon energy of 2.33 eV, the full sequence could be expected to conclude with a single absorbed photon. However, considering that Bi_5^+ is exceptionally dominant in the $n = 13$ spectrum regardless of pulse energy and that increased decay times beyond a few microseconds will lead to signals not being observed, this explanation seems less likely. Note that Yuan et al. calculate fragmentation energies of 1.53 eV and 1.24 eV for the sequential neutral tetramer loss of Bi_{13}^+, which would put it out of range for a single-photon process.

A conclusive result on whether neutral octamer or sequential tetramer loss is the dominant pathway in the present study cannot be derived from the current data set. It seems likely that both channels contribute to the observed signals; a more definite answer asks for an investigation incorporating the variation of the laser-photon energy and/or time-resolved measurements as have been performed with a Penning-trap setup for different cluster species [70–73].

The fragmentation of Bi_n^+ with $n > 14$ has, to our knowledge, not yet been probed experimentally. In the

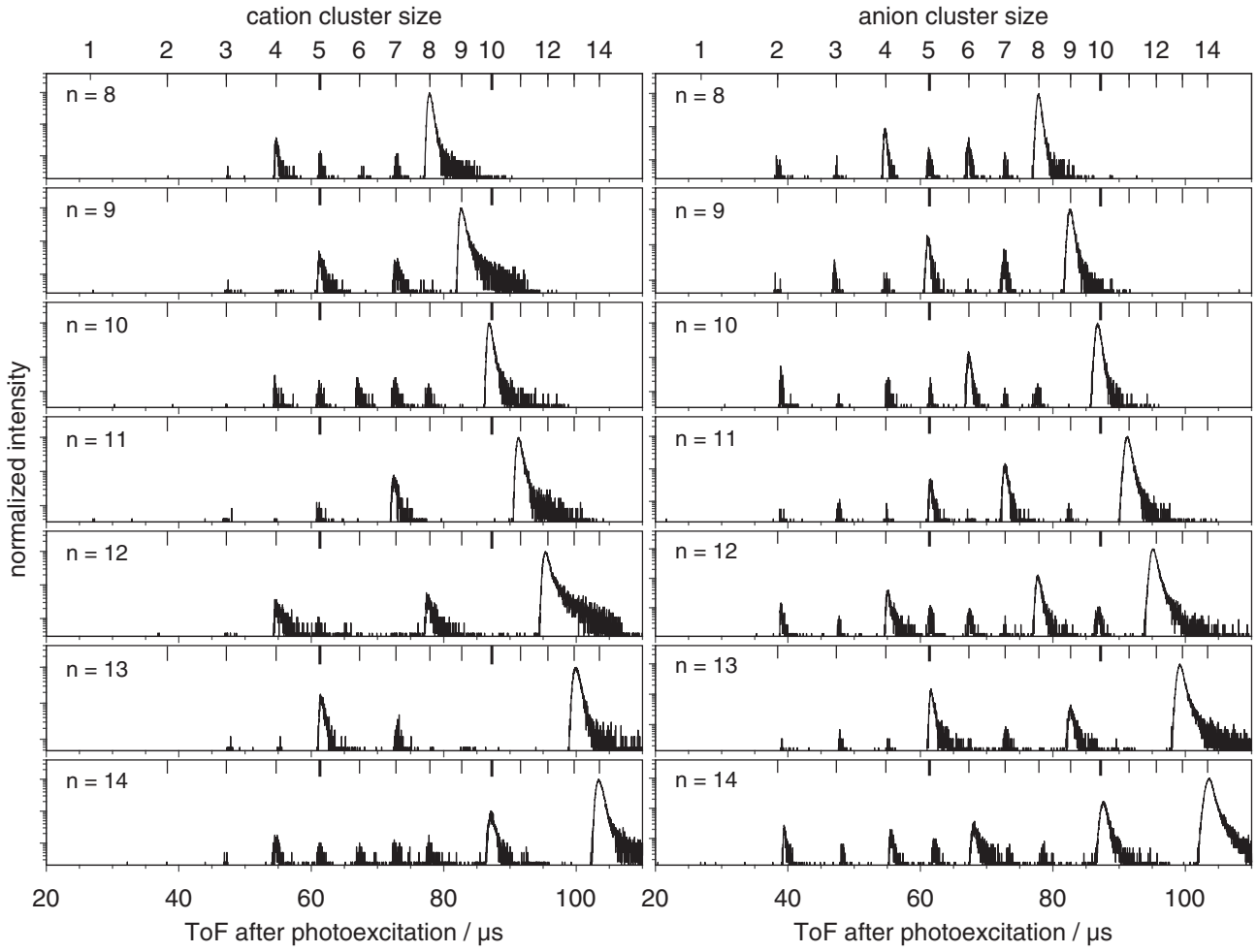

Fig. 9. Photofragmentation spectra (normalized to their maxima) obtained from precursor clusters $Bi_n^{+/-}$, $n = 8$–14.

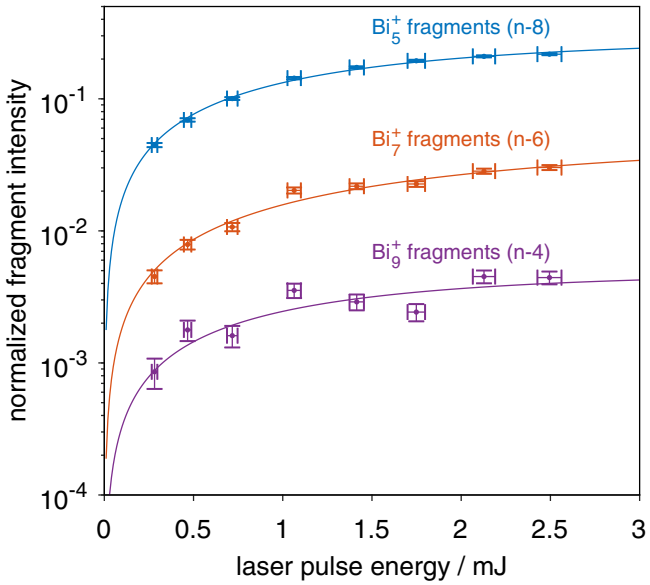

Fig. 10. Relative intensities of dominant fragment ions from photoexcitation of Bi_{13}^+ as a function of excitation-laser pulse energy.

present study, the precursors $n = 15$–19 show a behavior somewhat resuming that observed for the smaller clusters (Fig. 11). ToF spectra are dominated by $(n-8)$-fragment ions while those with $n-4$ and $n-12$ are also observed. Interestingly, the abundance of the species associated with the loss of a single neutral tetramer seems to perform an oscillation with a $4n$ period, increasing from close to no signal intensity for the Bi_{15}^+ precursor to most abundant fragment for Bi_{18}^+. At $n = 19$, the result again resembles that of $n = 15$. Bi_{18}^+ marks the continuation of the possible sequential behavior of Bi_{10}^+ and Bi_{14}^+, again suggested by the "fragmentation footprint" of Bi_{10}^+. However, Bi_{17}^+ shows no clear correlation to its tetramer-predecessor Bi_{13}^+ as, in fact, the Bi_9^+ ion now exhibits the highest intensity of all fragments.

3.3.2 Anions

Contrary to their cationic counterparts, Bi_n^- clusters have not yet been probed experimentally with respect to their fragmentation. Figures 8, 9, and 11 also show the photofragmentation spectra for the respective anion

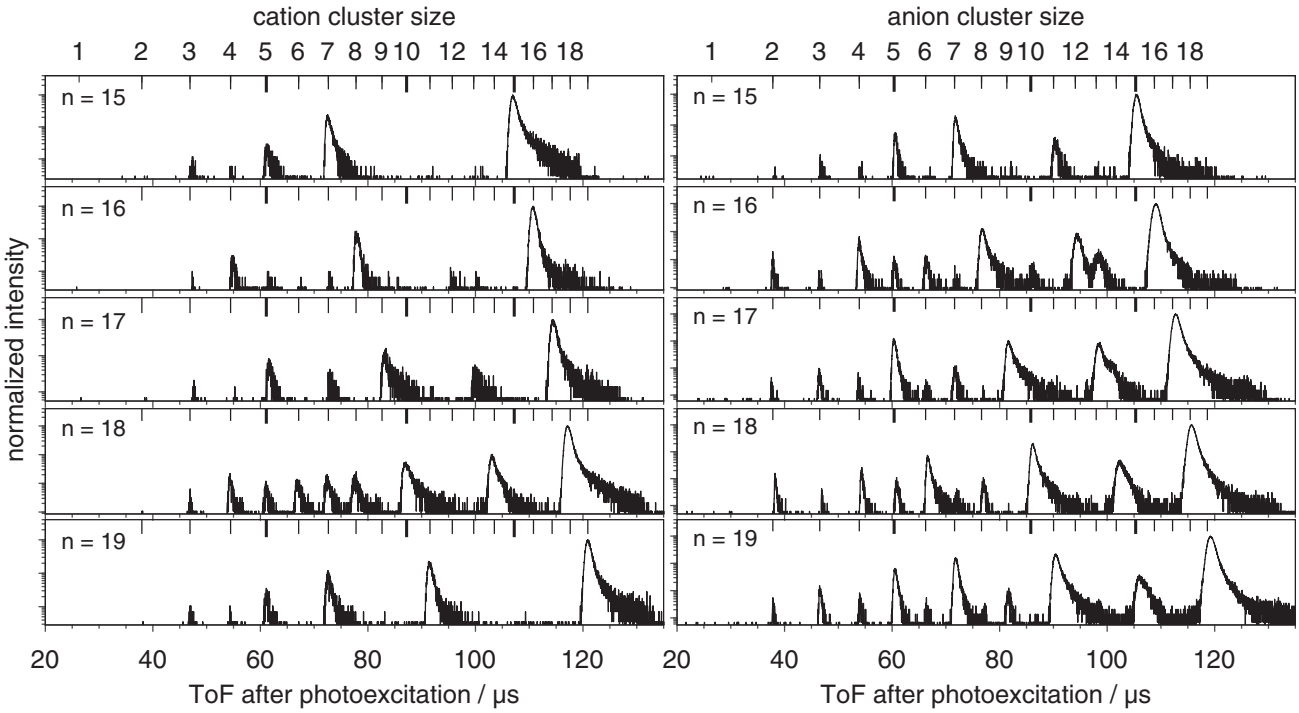

Fig. 11. Photofragmentation spectra (normalized to their maxima) obtained from precursor clusters $Bi_n^{+/-}$, $n = 15$–19.

cluster sizes $n = 2$–7, 8–14, and 15–19 recorded under identical conditions as the cations.

Similarly to the small cations, the $n \leq 7$ anions' pathways are mainly restricted to the loss of monomers and dimers, with $n = 8$ marking the switch to tetramer loss as predominant fragmentation channel. This furthers the assumption that bismuth fragmentation is characterized by the increased stability of the Bi_4 neutral more than it is by the configuragtion of the charged fragment. Additionally, a strong odd-even fluctuation can be observed in the $n - 2$ curve for $n = 4$–10 in the bottom part of Figure 7, indicating that odd-sized Bi_n^- exhibit a stronger preference for dimer loss than their even-sized neighbors. While the calculated stability of bismuth anions evaluated from the clusters' binding energies does show odd-even fluctuations [10,12], the odd-sized anions are, in fact, more stable (like the cations). This agrees with the bismuth atom having five valence electrons, resulting in closed shells at odd numbers for singly-charged species.

An explanation for the observed odd-even fluctuations can be given when the normalized numbers of total detected ions in the photoexcitation spectra are taken into account: the blue data points in Figure 12 show the ratio of detected signal (including unreacted precursor ions) with respect to the reference spectra recorded without photoexcitation. Consequently, any value below 1 indicates a loss of ions between the measurement cycles, presumably by electron evaporation. Neutralized particles cannot be observed with the present setup due to the off-axis geometry of the ion detector (see Fig. 1), which in turn is necessary to clear the trap's longitudinal axis for the excitation laser beam. However, since the reference and excitation cycles are recorded in an alternating fashion,

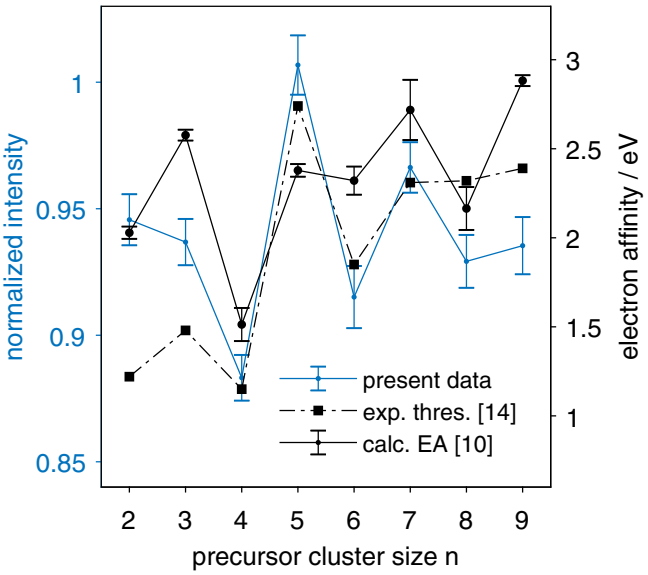

Fig. 12. Normalized total signal intensity (including all fragments and remaining precursor) of the photoexcitation spectra of Bi_n^- with respect to reference spectra (blue). Black data sets represent experimental threshold energies from PES measurements taken from [14] and calculated electron affinities taken from [10]. The error bars on the calculated EA values represent the spread between vertical and adiabatic EAs.

the discrepancy in detected ion rates (which is negligible for the recorded cation spectra) can be accredited to ion neutralization. We note for completeness that, in general, the direct observation of neutrals in EIBT studies is possible if, e.g., the excitation laser is guided into the trap

transversally [36] or the trap itself is of nonlinear geometry [32].

The calculated electron affinity (EA) of neutral bismuth clusters, i.e. the energy difference between the neutral and anionic species, also shows odd-even fluctuations [10–12], with the odd-sized clusters again exhibiting larger values (solid black line in Fig. 12). Thus, these cluster sizes show increased stability against electron evaporation, as confirmed by photoelectron-spectroscopy (PES) measurements on Bi_n^- [14]. Specifically, the experimental threshold energies (dash-dotted black line in Fig. 12) for the cluster sizes $n = 4$–7 are given as 1.15, 2.74, 1.85, and 2.31 eV, marking the largest fluctuations over the investigated size range (Bi_4^- exhibits the lowest observed value, again indicating the high stability of the neutral). The values for larger clusters still show oscillations, although on a much smaller scale.

Both results are in good agreement with the present study, as the clusters with low electron affinities ($n = 4$, 6, 8) show lower relative ion count rates, i.e. higher rates for electron evaporation. The photon energy is expected to thermalize to the system's vibrational degrees of freedom, from which it is accessible for fragmentation processes [37]. It follows that the ratio of cluster fragmentation as cooling channel increases with increasing electron affinity, as direct electron detachment becomes less likely. The exact interplay between both processes depends on a number of factors such as fragmentation energy, EA, and the coupling between electronic and ro-vibrational degrees of freedom and is, thus, beyond the scope of the present study. However, the agreement of the curves in Figure 12 is consistent with the explanation of the oscillations observed in Figure 7 as a result of the EA fluctuations rather than those of the clusters' atomic binding energies.

Similarly to the cations, the anionic clusters from $n = 8$ to 14 show tetramer breakoff as dominant fragmentation pathway (Fig. 9), again with the exception of Bi_{13}^-, where the $n - 8$ fragment is most abundant. A difference to the $n = 13$ cation spectrum is the strong presence of Bi_9^-, whereas Bi_9^+ is virtually absent. For the other cluster sizes of this range, the relative intensity of the $n-4$ fragments is also increased compared to the cationic clusters (see Fig. 7, yellow lines). The overall number of charged fragment species in the anion spectra is increased as well, to the point where most fragment sizes with $n \geq 2$ are present in every spectrum. Again, these results mostly hold under variation of the excitation-laser pulse energy. The results could hint at cation fragmentation being affected by the stability of the charged fragments to a larger extend, whereas anion fragmentation – with the additional cooling channel of electron evaporation – is less sensitive.

Comparing the anion photofragmentation spectra for $n = 15$–19 to those of the cations, the most noticeable difference is the less pronounced change of the $n - 4$ fragment's intensity as a function of precursor cluster size. While the spectra are again largely dominated by the $n-8$ fragments, the abundance of the individual fragment clusters changes more smoothly. Only for $n = 17$ are the pathways of neutral tetramer and octamer (and/or sequential tetramer) breakoff almost balanced. This marks a significant difference to the cations, where tetramer loss is most pronounced at $n = 18$ instead.

Note that the anion spectrum of the $n = 16$ precursor shows an anomaly in the form of an additional signal trailing the Bi_{12}^- $(n-4)$ one. Although it may at first sight seem like an unexpected neutral trimer breakoff, it can be shown that this is not the case. Investigations including the continued storage of the fragment clusters for several laps after the photoexcitation have revealed that this signal's revolution period is not compliant with that of any bismuth cluster size at the storage energy of 1200 eV. However, the period is found for Bi_8^- at 800 eV. This is consistent with a delayed fragmentation $Bi_{12}^- \rightarrow Bi_8^- + Bi_4$ in the field-free drift section of the in-trap lift after a prompt reaction $Bi_{16}^- \rightarrow Bi_{12}^- + Bi_4$ at the turn-around point. The exact point of where delayed fragmentation occurs during the passage through the lift is inconsequential, as fragment and precursor ions exhibit identical velocities under field-free conditions. However, due to disproportional acceleration/deceleration in the potentials of the remaining mirror and post-ejection lens electrodes, the accumulated "aberrant" Bi_8^- fragments reach the detector slightly later than the remaining Bi_{12}^- ions. The signal's position on the ToF axis is, thus, somewhat coincidental. The observation of this delayed reaction indicates the presence of sequential fragmentation processes.

While the fragments result from decay-pathway competition in most cases (see Fig. 10 and discussion), other delayed decay processes cannot be fully excluded. For example, note that a similar low-abundance signal might be partially overlapping with the Bi_{13}^- signal in the $n = 17$ spectrum. In the present study, no further instances of pronounced delayed fragmentation have been identified.

4 Summary and outlook

The present study introduces a novel approach to EIBT-based photoexcitation studies, where a stored ion bunch is irradiated with a pulsed laser beam guided axially through the trap. The pulse is timed to excite the ions at their turn-around point, leading to fragment ions exhibiting kinetic energies identical to those of the precursors after their re-acceleration. The system's excellent capabilities as an ion separator can thus be used to both preselect ions of interest and investigate the resulting fragments.

Photofragmentation spectra of bismuth clusters are recorded to both further the experimental study of their fragmentation pathways and asses the MR-ToF technique's capabilities for the investigation of molecular decays. For the cationic species, the results found in previous studies are reproduced and expanded to larger cluster sizes. Fragmentation of bismuth-cluster anions is probed for the first time experimentally. In both cases, the prevalence of neutral tetramer breakoff as a dominant decay channel found in previous experimental and theoretical work is confirmed. This decay behavior is accredited to bismuth clusters exhibiting semimetal character well into the investigated size range. The high stability of the Bi_4 neutral plays an important role in the observed

fragmentations, although discrepancies between cat- and anion results suggest the stability of the charged fragment to be an additional factor. For larger clusters, evidence for neutral octamer breakoff is found, however, a conclusive disentanglement from channels of sequential tetramer loss requires further investigation. In the course of the present study, time-resolved measurements of delayed decay processes have been triggered, which are subject of ongoing work.

Author contribution statement

LS and PF conceived the experiment. PF performed the measurements and data evaluation. PF and LS performed the interpretation of the experimental results and prepared the manuscript.

References

1. N.N. Greenwood, A. Earnshaw, *Chemistry of the Elements*, 2nd edn. (Elsevier, Amsterdam, 1997)
2. M. Ferhat, A. Zaoui, Phys. Rev. B **73**, 115107, (2006)
3. B. Fluegel, S. Francoeur, A. Mascarenhas, S. Tixier, E.C. Young, T. Tiedje, Phys. Rev. Lett. **97**, 067205 (2006)
4. R.G. Wheeler, K. Laihing, W.L. Wilson, M.A. Duncan, Chem. Phys. Lett. **131**, 8 (1986)
5. M.E. Geusic, R.R. Freeman, M.A. Duncan, J. Chem. Phys. **88**, 163 (1988)
6. M.M. Ross, S.W. McElvany, J. Chem. Phys. **89**, 4821 (1988)
7. R. Kelting, A. Baldes, U. Schwarz, T. Rapps, D. Schooss, P. Weis, C. Neiss, F. Weigend, M.M. Kappes, J. Chem. Phys. **136**, 154309 (2012)
8. T.M. Bernhardt, B. Kaiser, K. Rademann, Z. Phys. D **40**, 327 (1997)
9. H.K. Yuan, H. Chen, A.L. Kuang, Y. Miao, Z.H. Xiong, J. Chem. Phys. **128**, 094305 (2008)
10. L. Gao, P. Li, H. Lu, S.F. Li, Z.X. Guo, J. Chem. Phys. **128**, 194304 (2008)
11. J.M. Jia, G.B. Chen, D.N. Shi, B.L. Wang, Eur. Phys. J. D **47**, 359 (2008)
12. D. Liang, W. Shen, C. Zhang, P. Lu, S. Wang, Mod. Phys. Lett. B **31**, 1750260 (2017)
13. M.L. Polak, J. Ho, G. Gerber, W.C. Lineberger, J. Chem. Phys. **95**, 3053 (1991)
14. M. Gausa, R. Kaschner, G. Seifert, J.H. Faehrmann, H.O. Lutz, K.-H. Meiwes-Broer, J. Chem. Phys. **104**, 9719 (1996)
15. M.-H. Mikkelä, M. Tchaplyguine, S. Urpelainen, K. Jänkälä, O. Björneholm, M. Huttula, J. Appl. Phys. **112**, 084326 (2012)
16. S. Yin, X. Xu, R. Moro, W.A. de Heer, Phys. Rev. B **72**, 174410 (2005)
17. H. Wollnik, M. Przewloka, Int. J. Mass Spectrom. **96**, 267 (1990)
18. D. Zajfman, O. Heber, L. Vejby-Christensen, I. Ben-Itzhak, M. Rappaport, R. Fishman, M. Dahan, Phys. Rev. A **55**, R1577 (1997)
19. M. Dahan, R. Fishman, O. Heber, M. Rappaport, N. Altstein, D. Zajfman, W.J. van der Zande, Rev. Sci. Instrum. **69**, 76 (1998)
20. R.N. Wolf, D. Beck, K. Blaum, C. Böhm, C. Borgmann, M. Breitenfeldt, N. Chamel, S. Goriely, F. Herfurth, M. Kowalska, S. Kreim, D. Lunney, V. Manea, E. Minaya Ramirez, S. Naimi, D. Neidherr, M. Rosenbusch, L. Schweikhard, J. Stanja, F. Wienholtz, K. Zuber, Phys. Rev. Lett. **110**, 041101 (2013)
21. D. Atanasov, P. Ascher, K. Blaum, R.B. Cakirli, T.E. Cocolios, S. George, S. Goriely, F. Herfurth, H.-T. Janka, O. Just, M. Kowalska, S. Kreim, D. Kisler, Y.A. Litvinov, D. Lunney, V. Manea, D. Neidherr, M. Rosenbusch, L. Schweikhard, A. Welker, F. Wienholtz, R.N. Wolf, K. Zuber, Phys. Rev. Lett. **115**, 232501 (2015)
22. N.A. Althubiti, D. Atanasov, K. Blaum, T.E. Cocolios, T. Day Goodacre, G.J. Farooq-Smith, D.V. Fedorov, V.N. Fedosseev, S. George, F. Herfurth, K. Heyde, S. Kreim, D. Lunney, K.M. Lynch, V. Manea, B.A. Marsh, D. Neidherr, M. Rosenbusch, R.E. Rossel, S. Rothe, L. Schweikhard, M.D. Seliverstov, A. Welker, F. Wienholtz, R.N. Wolf, K. Zuber, Phys. Rev. C **96**, 044325 (2017)
23. D. Atanasov, D. Beck, K. Blaum, C. Borgmann, R.B. Cakirli, T. Eronen, S. George, F. Herfurth, A. Herlert, M. Kowalska, S. Kreim, Y.A. Litvinov, D. Lunney, V. Manea, D. Neidherr, M. Rosenbusch, L. Schweikhard, F. Wienholtz, R.N. Wolf, K. Zuber, J. Phys. G **44**, 044004 (2017)
24. V. Manea, P. Ascher, D. Atanasov, A.E. Barzakh, D. Beck, K. Blaum, C. Borgmann, M. Breitenfeldt, R.B. Cakirli, T.E. Cocolios, T. Day Goodacre, D.V. Fedorov, V.N. Fedosseev, S. George, F. Herfurth, M. Kowalska, S. Kreim, Y.A. Litvinov, D. Lunney, B. Marsh, D. Neidherr, M. Rosenbusch, R.E. Rossel, S. Rothe, L. Schweikhard, F. Wienholtz, R.N. Wolf, K. Zuber, Phys. Rev. C **95**, 054322 (2017)
25. A. de Roubin, D. Atanasov, K. Blaum, S. George, F. Herfurth, D. Kisler, M. Kowalska, S. Kreim, D. Lunney, V. Manea, E. Minaya Ramirez, M. Mougeot, D. Neidherr, M. Rosenbusch, L. Schweikhard, A. Welker, F. Wienholtz, R.N. Wolf, K. Zuber, Phys. Rev. C **96**, 014310 (2017)
26. A. Welker, N.A.S. Althubiti, D. Atanasov, K. Blaum, T.E. Cocolios, F. Herfurth, S. Kreim, D. Lunney, V. Manea, M. Mougeot, D. Neidherr, F. Nowacki, A. Poves, M. Rosenbusch, L. Schweikhard, F. Wienholtz, R.N. Wolf, K. Zuber, Phys. Rev. Lett. **119**, 192502 (2017)
27. M. Mougeot, D. Atanasov, K. Blaum, K. Chrysalidis, T. Day Goodacre, D. Fedorov, V. Fedosseev, S. George, F. Herfurth, J.D. Holt, D. Lunney, V. Manea, B. Marsh, D. Neidherr, M. Rosenbusch, S. Rothe, L. Schweikhard, A. Schwenk, C. Seiffert, J. Simonis, S.R. Stroberg, A. Welker, F. Wienholtz, R.N. Wolf, K. Zuber, Phys. Rev. Lett. **120**, 232501 (2018)
28. F. Wienholtz, D. Beck, K. Blaum, C. Borgmann, M. Breitenfeldt, R.B. Cakirli, S. George, F. Herfurth, J.D. Holt, M. Kowalska, S. Kreim, D. Lunney, V. Manea, J. Menendez, D. Neidherr, M. Rosenbusch, L. Schweikhard, A. Schwenk, J. Simonis, J. Stanja, R.N. Wolf, K. Zuber, Nature **498**, 346 (2013)
29. M. Rosenbusch, P. Ascher, D. Atanasov, C. Barbieri, D. Beck, K. Blaum, C. Borgmann, M. Breitenfeldt, R.B. Cakirli, A. Cipollone, S. George, F. Herfurth, M. Kowalska, S. Kreim, D. Lunney, V. Manea, P. Navrátil, D. Neidherr, L. Schweikhard, V. Somà, J. Stanja, F. Wienholtz, R.N. Wolf, K. Zuber, Phys. Rev. Lett. **114**, 202501 (2015)

30. Y. Ito, P. Schury, M. Wada, F. Arai, H. Haba, Y. Hirayama, S. Ishizawa, D. Kaji, S. Kimura, H. Koura, M. MacCormick, H. Miyatake, J.Y. Moon, K. Morimoto, K. Morita, M. Mukai, I. Murray, T. Niwase, K. Okada, A. Ozawa, M. Rosenbusch, A. Takamine, T. Tanaka, Y.X. Watanabe, H. Wollnik, S. Yamaki, Phys. Rev. Lett. **120**, 152501 (2018)
31. O. Heber, P.D. Witte, A. Diner, K.G. Bhushan, D. Strasser, Y. Toker, M.L. Rappaport, I. Ben-Itzhak, N. Altstein, D. Schwalm, A. Wolf, D. Zajfman, Rev. Sci. Instrum. **76**, 013104 (2005)
32. O. Aviv, Y. Toker, M. Errit, K.G. Bhushan, H.B. Pedersen, M.L. Rappaport, O. Heber, D. Schwalm, D. Zajfman, Rev. Sci. Instrum. **79**, 083110 (2008)
33. T. Doussineau, C. Yu Bao, C. Clavier, X. Dagany, M. Kerleroux, R. Antoine, P. Dugourd, Rev. Sci. Instrum. **82**, 084104 (2011)
34. O. Aviv, B. Kafle, V. Chandrasekaran, O. Heber, M.L. Rappaport, H. Rubinstein, D. Schwalm, D. Strasser, Y. Toker, D. Zajfman, Rev. Sci. Instrum. **84**, 053106 (2013)
35. B. Kafle, O. Aviv, V. Chandrasekaran, O. Heber, M.L. Rappaport, H. Rubinstein, D. Schwalm, D. Strasser, D. Zajfman, Phys. Rev. A **92**, 052503 (2015)
36. C. Breitenfeldt, K. Blaum, S. George, J. Göck, G. Guzmán-Ramírez, J. Karthein, T. Kolling, M. Lange, S. Menk, C. Meyer, J. Mohrbach, G. Niedner-Schatteburg, D. Schwalm, L. Schweikhard, A. Wolf, Phys. Rev. Lett. **120**, 253001 (2018)
37. O. Aviv, Y. Toker, D. Strasser, M.L. Rappaport, O. Heber, D. Schwalm, D. Zajfman, Phys. Rev. A **83**, 023201 (2011)
38. P.Y. Cheng, K.F. Willey, J.E. Salcido, M.A. Duncan, Int. J. Mass Spectrom. **102**, 67 (1990)
39. D.S. Cornett, M. Peschke, K. LaiHing, P.Y. Cheng, K.F. Willey, M.A. Duncan, Rev. Sci. Instrum. **63**, 2177 (1992)
40. L.N. Ding, P.D. Kleiber, Y.C. Cheng, M.A. Young, S.V. O'Neil, W.C. Stwalley, J. Chem. Phys. **102**, 5235 (1995)
41. W.J. Jia, K.W.D. Ledingham, C.T.J. Scott, C. Kosmidis, R.P. Singhal, Rapid Commun. Mass Spectrom. **9**, 761 (1995)
42. J. Husband, F. Aguirre, P. Ferguson, R.B. Metz, J. Chem. Phys. **111**, 1433 (1999)
43. X. Yang, Q. Wu, Y. Hu, S. Yang, Int. J. Mass Spectrom. **202**, 55 (2000)
44. B.K.A. Jaeger, M. Savoca, O. Dopfer, N.X. Truong, Int. J. Mass Spectrom. **402**, 49 (2016)
45. S. Knauer, P. Fischer, G. Marx, B. Schabinger, L. Schweikhard, R.N. Wolf, Int. J. Mass Spectrom. **423**, 46 (2017)
46. P. Fischer, S. Knauer, G. Marx, L. Schweikhard, Rev. Sci. Instrum. **89**, 015114 (2018)
47. P. Fischer, S. Knauer, G. Marx, L. Schweikhard, Int. J. Mass Spectrom. **432**, 44 (2018)
48. P. Fischer, G. Marx, L. Schweikhard, Int. J. Mass Spectrom. **435**, 305 (2019)
49. R.L. Hettich, J. Am. Chem. Soc. **111**, 8582 (1989)
50. A. Drescher, J. Kitching, J.E. Crawford, J.K.P. Lee, G. Thekkadath, Z. Phys. D **19**, 203 (1991)
51. H.S. Kim, T.D. Wood, A.G. Marshall, J. Lee, Chem. Phys. Lett. **224**, 589 (1994)
52. C. Stoermer, J. Friedrich, M.M. Kappes, Int. J. Mass Spectrom. **206**, 63 (2001)
53. W.C. Wiley, I.H. McLaren, Rev. Sci. Instrum. **26**, 1150 (1955)
54. R.N. Wolf, G. Marx, M. Rosenbusch, L. Schweikhard, Int. J. Mass Spectrom. **313**, 8 (2012)
55. M. Rosenbusch, S. Kemnitz, R. Schneider, L. Schweikhard, R. Tschiersch, R.N. Wolf, AIP Conf. Proc. **1521**, 53 (2013)
56. P. Chauveau, P. Delahaye, G. De France, S. El Abir, J. Lory, Y. Merrer, M. Rosenbusch, L. Schweikhard, R.N. Wolf, Nucl. Instrum. Meth. B **376**, 211 (2016)
57. T.Y. Hirsh, N. Paul, M. Burkey, A. Aprahamian, F. Buchinger, S. Caldwell, J.A. Clark, A.F. Levand, L.L. Ying, S.T. Marley, G.E. Morgan, A. Nystrom, R. Orford, A.P. Galván, J. Rohrer, G. Savard, K.S. Sharma, K. Siegl, Nucl. Instrum. Meth. B **376**, 229 (2016)
58. S. Knauer, P. Fischer, G. Marx, M. Müller, M. Rosenbusch, B. Schabinger, L. Schweikhard, R.N. Wolf, A multi-reflection time-of-flight setup for methodical developments and the study of atomic clusters (under review)
59. D. Beck, K. Blaum, H. Brand, F. Herfurth, S. Schwarz, Nucl. Instrum. Meth. A **527**, 567 (2004)
60. M.E. Geusic, R.R. Freeman, M.A. Duncan, J. Chem. Phys. **89**, 223 (1988)
61. K. Wade, Adv. Inorg. Chem. Radiochem. **18**, 1 (1976)
62. M.E. Geusic, M.F. Jarrold, T.J. McIlrath, R.R. Freeman, W.L. Brown, J. Chem. Phys. **86**, 3862 (1987)
63. L.A. Bloomfield, R.R. Freeman, W.L. Brown, Phys. Rev. Lett. **54**, 2246 (1985)
64. M.G. Mitch, S.J. Chase, J. Fortner, R.Q. Yu, J.S. Lannin, Phys. Rev. Lett. **67**, 875 (1991)
65. K.L. Busch, G.L. Glish, S.A. Mcluckey, *Mass Spectrometry/mass Spectrometry: Techniques and Applications of Tandem Mass Spectrometry*, 1st edn. (Wiley-VCH, 1988)
66. F.J. Kohl, K.D. Carlson, J. Am. Chem. Soc. **90**, 4814 (1968)
67. G. DeMaria, J. Drowart, M.G. Inghram, J. Chem. Phys. **31**, 1076 (1959)
68. J. Kordis, K.A. Gingerich, J. Chem. Phys. **58**, 5141 (1973)
69. C. Bréchignac, P. Cahuzac, F. Carlier, M. de Frutos, J. Leygnier, J.P. Roux, J. Chem. Phys. **102**, 763 (1995)
70. C. Walther, G. Dietrich, M. Lindinger, K. Lützenkirchen, L. Schweikhard, J. Ziegler, Chem. Phys. Lett. **256**, 77 (1996)
71. C. Walther, G. Dietrich, M. Lindinger, K. Lützenkirchen, L. Schweikhard, J. Ziegler, Chem. Phys. Lett. **262**, 668 (1996)
72. M. Vogel, K. Hansen, A. Herlert, L. Schweikhard, Phys. Rev. Lett. **87**, 013401 (2001)
73. M. Wolfram, S. König, S. Bandelow, P. Fischer, A. Jankowski, G. Marx, L. Schweikhard, J. Phys. B **51**, 044005 (2018)

7.6 Isotope-resolved photodissociation pathways of lead-doped bismuth clusters from tandem multi-reflection time-of-flight mass spectrometry

Isotope-resolved photodissociation pathways of lead-doped bismuth clusters from tandem multi-reflection time-of-flight mass spectrometry

Paul Fischer* and Lutz Schweikhard
Institut für Physik, Universität Greifswald, 17487 Greifswald, Germany

(Received 29 May 2019; published 28 October 2019)

The photofragmentation behavior of the lead-doped bismuth cluster $^{209}Bi_7{}^{208}Pb^+$ is investigated by use of multi-reflection time-of-flight mass spectrometry (MR-ToF MS), which serves both as precursor selector on a scale of single atomic mass units as well as high-resolution fragment analyzer. This is an implementation of a tandem MR-ToF study, where two instances of high-resolution mass spectrometry are used, namely for pre-selection and post-excitation analysis, in quick succession within a single device to determine complex dissociation patterns. The full information of the fragmentation pathways is obtained, including branching ratios describing the retention of the charge on the pure or compound cluster. The results are compared to the behavior of the analogous pure bismuth cluster $^{209}Bi_8^+$ and interpreted within the framework of well-established cluster stability rules.

DOI: 10.1103/PhysRevResearch.1.033050

I. INTRODUCTION

The properties of atomic clusters [1,2], systems located between the single atom and bulk matter, vary with their number of atoms and valence electrons. For monoatomic species, these values are inherently coupled unless different charge states are addressed. Binary systems, i.e., with atoms of two different elements, offer more freedom, as the number of atoms of the second species becomes an additional tuning parameter. Alkali-metal clusters doped with other alkali [3,4] or metal species [3,5–7] were already studied in the 1980s and 1990s. Since then, research of bimetallic clusters has been expanded significantly [8–11], with topics of interest being as diverse as, e.g., the fine-tuning of catalytic processes [12–15] and even biomedical markers [16].

Many interaction-based studies call for two instances of mass-spectrometric analysis, commonly referred to as tandem mass spectrometry, MS/MS or MS^2 [17]: once prior to the interaction to select the precursor and again afterward to resolve and analyze the reaction products. Bimetallic systems are experimentally particularly challenging, as the mass resolving power needed for compound-cluster investigations often surpasses that required for single-element species by orders of magnitude. To increase the resolving power of time-of-flight (ToF) devices [18], the principle of multi-reflection (MR) has been introduced [19] akin to the concept of electrostatic ion beam traps (EIBTs) consisting of two opposing ion mirrors [20,21]. In nuclear physics, MR-ToF devices have recently been applied for fast mass separation or ion selection [22,23] as well as precision mass measurements [24]. On the molecular level, they are appreciated for their capability as ion traps with a virtually unrestricted mass range, operated either in "non-bunching mode," where injected ion beams fill the entire trap volume [25,26], or with capacitive pickup detection (Fourier transform MR-ToF) for high-resolution mass spectrometry [27–30].

Here, we introduce the dual use of high-resolution multi-reflection time-of-flight mass separation and spectrometry in the same measurement cycle of a single device. This method constitutes a substantial extension of a recently reported approach to MR-ToF- or EIBT-based photofragmentation studies [31], which is briefly reviewed as the present method is based upon it.

II. EXPERIMENTAL SETUP

Metal clusters are produced via laser ablation [32–35], accelerated to 2 keV, and captured between two electrostatic ion mirrors with an in-trap lift electrode [36] (see Fig. 1 for experimental setup). In previous work [31], precursor bismuth cluster ions are selected on a scale of single atomic mass units employing the MR-ToF device's high resolving power. This is necessary in order to remove all other "contaminants," in particular those where a bismuth atom (mass number $A = 209$) is replaced by a lead atom ($A = 204, 206, 207, 208$) due to impurities of the ablation target (see Fig. 10 in [37]). After 400 revolution periods (some tens of milliseconds depending on cluster size), the isobar-selected precursor is irradiated by a laser pulse. The pulse timing is synchronized such that the ion bunch is located at its turnaround point in the trap's entry-side mirror potential, implying a kinetic energy of (close to) zero at the time of laser interaction. Fragment ions thus have the same energy as the precursor regardless of mass and can be studied with the same post-trap detector configuration.

The investigations reported in Ref. [31] are limited to clusters consisting only of ^{209}Bi atoms, as bismuth has just

*Corresponding author: paul.fischer@uni-greifswald.de

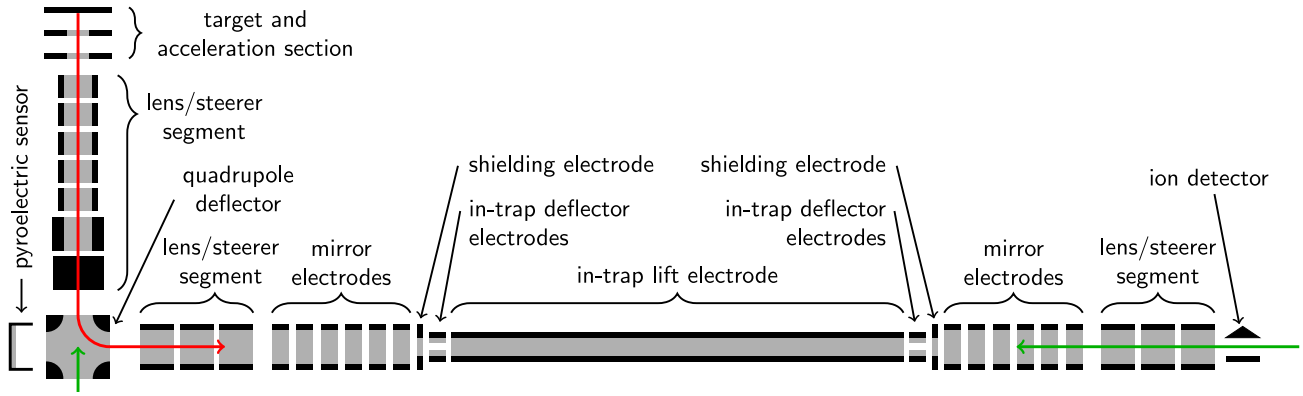

FIG. 1. Overview of the experimental setup, with ion path indicated in red, source and interaction laser beams in green.

this one naturally occurring isotope. Thus, the challenge of the fragment analysis never rises beyond that of cluster sizes Bi_n, where n denotes the number of atoms in the molecule. For small clusters, the required mass resolving power of the second MS stage is consequently only on the order of $R = m/\Delta m \lesssim 20$, which is easily accessible with linear ToF MS [18]: The ions were released by switching off the exit-side mirror potential simultaneously to the excitation-laser pulse to record their "single-path" flight times to the detector. The overall experimental cycle can be described as MR-ToF MS/ToF MS. The high resolving power of the MR-ToF operation is needed in the first stage to suppress contaminant ions in the form of low-abundance compound clusters $Bi_{n-m}Pb_m$ ($m < n$) or, in the general case, molecular isotopes ("isotopologues") [38] and ensure unambiguous results. For the second step of product ion analysis, the low resolving power of linear ToF MS is fully sufficient.

For the present study of lead-doped bismuth clusters, the laser-ablation target is purposely changed to an alloy containing 25 at% Pb and 75 at% Bi to enhance their production rate and select them for photoexcitation. Fragmentation of a compound cluster is inherently more complex and can be understood as the loss of a neutral (compound) cluster from the selected n-atomic precursor, i.e.,

$$Bi_{n-m}Pb_m^+ \rightarrow Bi_{n-m-x}Pb_{m-y}^+ + Bi_xPb_y, \qquad (1)$$

where $x, y \in \{0, 1, 2, \dots\}$ and $x \leqslant n - m, y \leqslant m$. Note that it is impossible to investigate such behaviors in the previous MR-ToF MS/ToF MS–style measurement [31], as the mass resolving power needed to distinguish the charged product species quickly rises to $R > 1000$ with increasing n.

While there are other approaches of tandem mass spectrometry, they offer no viable alternative for cases like the present. Quadrupole mass filters (QMFs), in particular "triple quad" setups [39], have been used to investigate metal clusters [40,41]. In addition, they have also been employed for precursor selection prior to, e.g., (reflectron-)ToF MS [42,43]. However, limitations imposed by QMF devices include a low mass resolving power on the order of a few hundred and a typical maximum m/q ratio below 10 000 u/e. Fourier-transform ion-cyclotron resonance (FT-ICR) mass spectrometers are another option for (among others) cluster studies [44–46], as they offer excellent resolving powers reaching up to several millions [47,48]. However, ICR measurements are based on high magnetic fields provided by superconducting magnets, which can complicate optical access to the interaction region. In addition, the magnetic fields lead to m/q restrictions [47,49], typically on the order of a few thousand atomic mass units over elementary charges, and a limited sensitivity. Several tens or hundreds of ions are needed per experimental cycle unless the ions have exceedingly high charge states or the detection is restricted to only very narrow bandwidths.

MR-ToF devices, in contrast, perform single-ion counting with negligible background, allowing measurements even for species with very low count rates (in the present study, only one Bi_5^+ event is observed in about 3000 cycles; see Fig. 4 below) that are inaccessible to ICR spectrometers. At the same time, MR-ToF resolving powers can be pushed to several 100 000 [50].

Here, we report the introduction of an advanced measurement scheme: After the high-resolution MR-ToF precursor selection and subsequent cluster-laser interaction, the ions are stored further for high-resolution mass analysis. For a demonstration of the (MR-ToF MS)^2 scheme, $^{209}Bi_7{}^{208}Pb^+$ with mass number $A = 1671$ is selected as precursor to characterize the change in its fragmentation behavior with respect to the pure octamer, $^{209}Bi_8^+$ with $A = 1672$. The first MS stage accordingly calls for a separation resolving power $R \gtrsim 2000$, which is easily surpassed with the present value of $R \approx 10\,000$ at 400 revolution periods [38].

III. RESULTS AND DISCUSSION

Figure 2 shows fragmentation spectra for both species of interest measured without additional post-excitation storage. While the pure cluster (a) has already been discussed in detail [31], the resolving power is not sufficient for the compound (b): Namely, the unresolved fragment species with mass difference $\Delta m = 1$ u, marked in violet, yellow, and orange, prevent comprehensive evaluation of the dissociation pathways. While the relative change in fragment abundances between the precursor species is obvious (see also values listed in Table I),

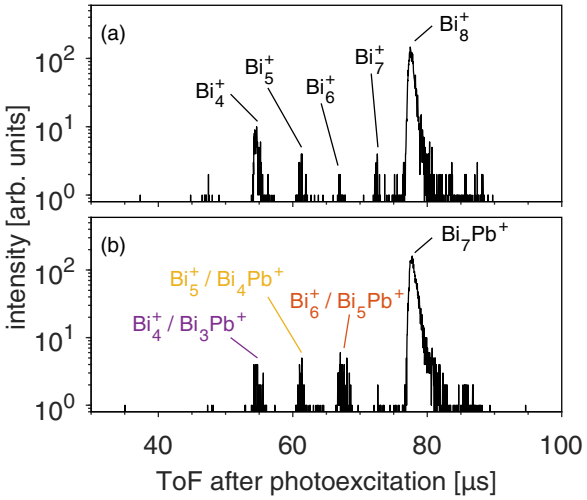

FIG. 2. Single-path time-of-flight spectra of Bi_8^+ (a) and Bi_7Pb^+ (b) after photoexcitation at $\lambda = 532$ nm as introduced in Ref. [31]. Note that the resolving power is not sufficient to distinguish the Bi cluster fragments from the Bi-Pb compounds in the bottom spectrum (marked violet, yellow, and orange).

the branching ratios

$$B = \frac{I_{\mathrm{BiPb}}}{I_{\mathrm{BiPb}} + I_{\mathrm{Bi}}} \tag{2}$$

for lead-containing fragments, where I_{BiPb} and I_{Bi} are the intensities of the compound and pure cluster ion species, respectively, are not accessible from the single-path spectrum.

In order to determine these ratios, the experimental cycle is changed to the (MR-ToF MS)^2 mode by delaying the ions' ejection after the photoexcitation for several tens to hundreds of additional revolution periods. All fragments are retained and lap each other according to their mass-to-charge ratio. The pure and compound species for the same fragment sizes separate at sufficiently high (post-excitation) revolution numbers, as illustrated in Fig. 3 for the $n = 5$ species.

A single measurement has been performed with an additional post-excitation storage time corresponding to 162, 145, and 132 revolutions of the $n = 4$, 5, and 6 fragment species, respectively (Fig. 4). This storage time has been chosen such that all species of interest that appear in the spectrum are sufficiently resolved and do not overlap. The present mass resolving power in this second MS stage is $R \approx 10\,000$ and thus sufficient to distinguish all fragment species. This allows the determination of the branching ratios B defined in Eq. (2). A separate measurement was performed for the low-

TABLE I. Relative fragment abundances in Fig. 2. The value for fragment cluster sizes n includes the compound clusters $Bi_{n-1}Pb^+$ in the case of the Bi_7Pb^+ precursor. The abundances of $n \leqslant 3$ fragment ions are negligible.

	$n = 4$	$n = 5$	$n = 6$	$n = 7$
Bi_8^+	0.63(3)	0.16(2)	0.06(1)	0.12(2)
Bi_7Pb^+	0.31(3)	0.23(3)	0.42(3)	0.04(1)

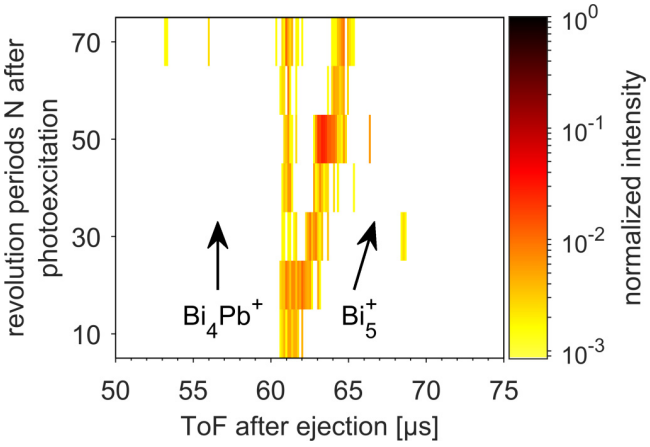

FIG. 3. Color-intensity N-versus-ToF plot [51,52] showing the separation of cluster species for $n = 5$ fragments over several tens of post-excitation revolution periods.

abundance $n = 7$ fragment at 84 post-excitation revolution periods. All values are listed in Table II and illustrated in Fig. 5.

For a purely statistical fragmentation process, i.e., with identical probabilities for all possible pathways, simple atom counting yields a branching ratio

$$B_{\mathrm{stat}} = \frac{n_{\mathrm{frag}}}{n_{\mathrm{frag}} + (n_{\mathrm{prec}} - n_{\mathrm{frag}})} = \frac{n_{\mathrm{frag}}}{n_{\mathrm{prec}}} \tag{3}$$

for lead-containing ions, where n_{frag} and n_{prec} are the sizes of the fragment and precursor cluster ions, respectively. Since $I_{\mathrm{BiPb}} \sim n_{\mathrm{frag}}$ and $I_{\mathrm{Bi}} \sim (n_{\mathrm{prec}} - n_{\mathrm{frag}})$, the above equation follows directly from (2). Comparing the experimental results (Table II) to B_{stat}, it is readily apparent that both the $n = 4$ and $n = 6$ fragment species exhibit a ratio skewed toward higher values, that is, toward more compound clusters than naively expected. Analogously, the $n = 5$ and 7 species show lower

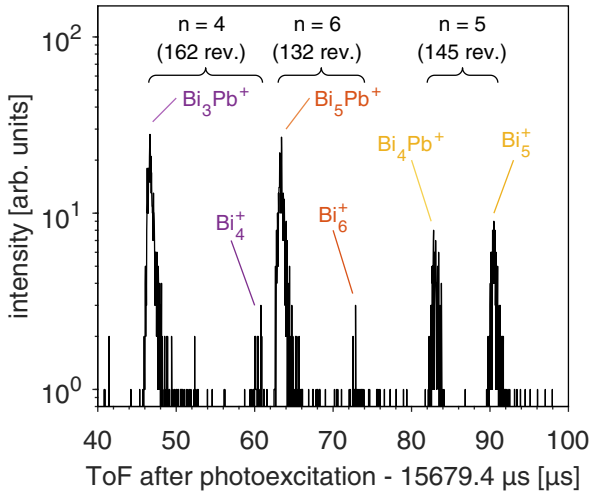

FIG. 4. Multi-reflection time-of-flight spectrum with 15 679.4 μs of additional storage time after the photoexcitation of Bi_7Pb^+. Signals with identical label colors are resolved species of the respective mixtures in Fig. 2.

TABLE II. Measured branching ratios B for fragment clusters resulting from the photoexcitation of Bi_7Pb^+ and expected ratios B_{stat} for a purely statistical dissociation behavior.

	$n = 4$	$n = 5$	$n = 6$	$n = 7$
B	0.94(1)	0.44(3)	0.95(1)	0.46(6)
B_{stat}	0.500	0.625	0.750	0.875

values, correlating to a preference of the pure cluster retaining the charge.

Closed geometrical structures [53] or electronic shells [54] are known to yield clusters associated with "magic numbers," most prominently found by Knight *et al.* in sodium-cluster abundance spectra [55]. More importantly for the present case, a set of electron counting rules ("Wade's rules" [56]) is known to lead to increased stability if the number of a cluster's valence p electrons equals $2n + 2$ (*closo*-), $2n + 4$ (*nido*-), or $2n + 6$ (*arachno*-species). Bi and Pb supply 3 and 2 of these "skeletal electrons" per atom due to their s^2p^2 and s^2p^3 configuration, respectively. Recently, density functional calculations have found that stable Bi-Pb compound clusters are expected to follow these rules to a very high degree [57].

The deviation of the measured branching ratios B from their element-abundance-based values B_{stat} can be understood qualitatively in the framework of these studies. For the example of the $n = 4$ fragments, the possible pathways with respect to the retention of the charge result in $Bi_3Pb^+ + Bi_4$ or $Bi_3Pb + Bi_4^+$. Note that the charged compound cluster Bi_3Pb^+ has 10 valence p electrons ($2n + 2$) and the neutral bismuth tetramer 14 ($2n + 4$). Both fragments are expected to show increased stability within the context of Wade's rules. In fact, neutral Bi_4 (and Bi_2 to a lesser extend) is known to be exceptionally stable from previous fragmentation studies [31,58–61], neutral-cluster vapors [62–64], and density functional calculations [65–68]. In contrast, the alternative pathway leads to two fragments with odd electron numbers, which are expected to be less stable. Thus, the high abundance of the charged compound cluster arises from favorable product configurations.

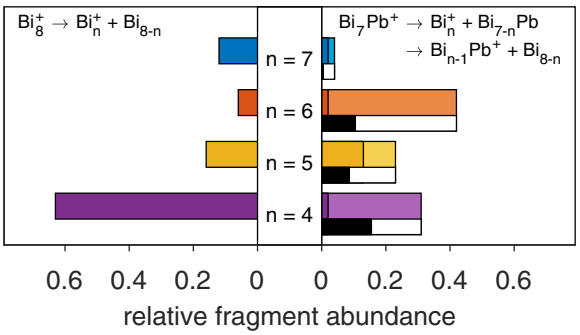

FIG. 5. Fragment abundances from photoexcitation of the pure (left) and compound (right) precursor species. For each fragment size n, i.e., total number of atoms in the fragment cluster, the pure species' abundance is given in darker, the compound's in lighter color. The black-and-white bars on the right indicate the purely statistical ratios according to B_{stat} (see text).

Since the difference in the number of valence electrons between Bi and Pb is one, the above trend holds for all cluster sizes n: One cluster species (pure or compound) will exhibit an even number of electrons while the other shows an odd number. The stable species alternates with n. Thus, the $n = 6$ fragment branching ratio behaves analogously to that of $n = 4$ while the pathway with the charge being retained on the pure cluster is favored for $n = 5$ and 7. In the latter cases, this leads to lower branching ratios than calculated from pure statistics, in agreement with Table II.

Thus, the B values are fully explained by the fragmentation behavior resulting from the substituted lead atom (Figs. 2 and 5). For the pure bismuth cluster, it is largely defined by the high stability of the neutral tetramer: $Bi_8^+ \rightarrow Bi_4^+ + Bi_4$ has 63(3)% fragment abundance. Following this pathway, the decays leading to stable configurations of the charged fragments $n = 5$ [16(2)%] and $n = 7$ [12(2)%] are preferred. The dissociation leading to the charged $n = 6$ fragment with its odd number of valence electrons is least frequent [6(1)%].

In contrast, due to the loss of a valence electron from the substitution, the compound cluster's most abundant pathways are the break-off of a neutral bismuth dimer and tetramer,

$$\begin{aligned}
\mathbf{Bi_7Pb^+} &\rightarrow \mathbf{Bi_7^+} + \mathrm{Pb}\ 2(1)\% \\
&\rightarrow \mathrm{Bi_6Pb^+} + \mathrm{Bi}\ 2(1)\% \\
&\rightarrow \mathrm{Bi_6^+} + \mathrm{BiPb}\ 2(1)\% \\
&\rightarrow \mathbf{Bi_5Pb^+} + \mathbf{Bi_2}\ 40(3)\% \\
&\rightarrow \mathbf{Bi_5^+} + \mathbf{Bi_2Pb}\ 13(2)\% \\
&\rightarrow \mathrm{Bi_4Pb^+} + \mathrm{Bi_3}\ 10(1)\% \\
&\rightarrow \mathrm{Bi_4^+} + \mathrm{Bi_3Pb}\ 2(1)\% \\
&\rightarrow \mathbf{Bi_3Pb^+} + \mathbf{Bi_4}\ 29(3)\%, \qquad (4)
\end{aligned}$$

as either leads to stable configurations for both the neutral and charged fragment. The clusters with increased stability are indicated in bold in the reaction equation (4), where the relative abundances of the corresponding fragment ions have been included. Compared to the pure cluster (see values in Table I), the loss of Bi_4 is 34% less abundant while the loss of Bi_2 is more abundant by the same amount. This likely results from the very high stability of the Bi_5Pb^+ ion: Across the investigated (n, m) space for $Bi_{n-m}Pb_m$, Seifried *et al.* have found only two clusters with a single lead atom fulfilling all imposed stability criteria (see Fig. 6 in Ref. [57]), Bi_5Pb^+ and the present precursor Bi_7Pb^+. The present measurement thus agrees with their findings based on density functional calculations. The next dominant fragmentation pathways of the compound cluster in terms of abundance are those yielding charged $n = 5$ fragments, where both competing channels are about equally populated [10(1)% and 13(2)%]. All remaining pathways are negligible in terms of their abundances.

In particular, the abundance of the $n = 7$ products decreases significantly compared to the analog photofragmentation of the pure Bi precursor, even though the more highly abundant $Bi_8^+ \rightarrow Bi_7^+ + Bi$ pathway leads to an unfavorable odd-numbered neutral bismuth atom. However, by this neutral-atom emission Bi_8^+ turns into an even-numbered and thus more stable species. In contrast, Bi_7Pb^+ has been proposed to have a very high stability itself [57]. Thus, for this

stable compound cluster, neutral-atom break-off is found to be less favorable than the competing decay channels by the present investigations.

IV. CONCLUSIONS

In summary, the present studies have unveiled stability changes resulting from doping atomic bismuth clusters with a lead atom. The measurements were possible only due to the introduction of an advanced experimental technique, namely tandem multi-reflection time-of-flight mass spectrometry (MR-ToF MS)^2, which combines high-resolution precursor selection and high-resolution fragment analysis in a single device with very high sensitivity. This development opens the door to the study of reactions that have so far been inaccessible.

[1] R. Johnston, *Atomic and Molecular Clusters* (Taylor & Francis, Abingdon, United Kingdom, 2002).

[2] J. Alonso, *Structure and Properties of Atomic Nanoclusters*, 2nd ed. (Imperial College Press, London, United Kingdom, 2011).

[3] M. M. Kappes, P. Radi, M. Schär, and E. Schumacher, Probes for electronic and geometrical shell structure effects in alkali-metal clusters: Photoionization measurements on K_xLi, K_xMg, and $K_xZn(x < 25)$, Chem. Phys. Lett. **119**, 11 (1985).

[4] S. Pollack, C. R. C. Wang, T. A. Dahlseid, and M. M. Kappes, Optical absorption probes of Li_xNa_{4-x} $(x = 1, 2)$: Geometry, substitution isomers, and composition-dependent electron delocalization, J. Chem. Phys. **96**, 4918 (1992).

[5] K. Hoshino, T. Naganuma, Y. Yamada, K. Watanabe, A. Nakajima, and K. Kaya, Ionization potentials of cobalt-sodium bimetallic clusters (Co_nNa_m), J. Chem. Phys. **97**, 3803 (1992).

[6] C. Yeretzian, Electronic structure effects in bimetallic M_xN clusters (M = alkali, N = divalent metal), J. Phys. Chem. **99**, 123 (1995).

[7] U. Heiz, A. Vayloyan, E. Schumacher, C. Yeretzian, M. Stener, P. Gisdakis, and N. Rösch, Na_xAu and Cs_xAu bimetal clusters: Finite size analogs of sodium-gold and cesium-gold compounds, J. Chem. Phys. **105**, 5574 (1996).

[8] E. Janssens, H. Tanaka, S. Neukermans, R. E. Silverans, and P. Lievens, Two-dimensional magic numbers in mass abundances of photofragmented bimetallic clusters, New J. Phys. **5**, 46 (2003).

[9] R. Ferrando, J. Jellinek, and R. L. Johnston, Nanoalloys: From theory to applications of alloy clusters and nanoparticles, Chem. Rev. **108**, 845 (2008).

[10] R. Johnston, *Metal Nanoparticles and Nanoalloys*, Vol. 3 (Elsevier, Amsterdam, Netherlands, 2012).

[11] F. Calvo, *Nanoalloys: From Fundamentals to Emergent Applications* (Elsevier, Amsterdam, Netherlands, 2013).

[12] J. M. Thomas, B. F. G. Johnson, R. Raja, G. Sankar, and P. A. Midgley, High-performance nanocatalysts for single-step hydrogenations, Acc. Chem. Res. **36**, 20 (2003).

[13] J.-H. Liu, A.-Q. Wang, Y.-S. Chi, H.-P. Lin, and C.-Y. Mou, Synergistic effect in an Au-Ag alloy nanocatalyst: CO oxidation, J. Phys. Chem. B **109**, 40 (2005).

[14] D. Wang, A. Villa, F. Porta, L. Prati, and D. Su, Bimetallic gold/palladium catalysts: Correlation between nanostructure and synergistic effects, J. Phys. Chem. C **112**, 8617 (2008).

[15] H. T. Le, S. M. Lang, J. D. Haeck, P. Lievens, and E. Janssens, Carbon monoxide adsorption on neutral and cationic vanadium doped gold clusters, Phys. Chem. Chem. Phys. **14**, 9350 (2012).

[16] Y. Cao, R. Jin, and C. A. Mirkin, DNA-modified core-shell Ag/Au nanoparticles, J. Am. Chem. Soc. **123**, 7961 (2001).

[17] K. L. Busch, G. L. Glish, and S. A. Mcluckey, *Mass Spectrometry/Mass Spectrometry: Techniques and Applications of Tandem Mass Spectrometry*, 1st ed. (Wiley-VCH, Weinheim, Germany, 1988).

[18] R. Cotter, *Time-of-Flight Mass Spectrometry: Instrumentation and Applications in Biological Research* (American Chemical Society, Washington, D.C., United States, 1997).

[19] H. Wollnik and M. Przewloka, Time-of-flight mass spectrometers with multiply reflected ion trajectories, Int. J. Mass Spectrom. **96**, 267 (1990).

[20] W. H. Benner, A gated electrostatic ion trap to repetitiously measure the charge and m/z of large electrospray ions, Anal. Chem. **69**, 4162 (1997).

[21] D. Zajfman, O. Heber, L. Vejby-Christensen, I. Ben-Itzhak, M. Rappaport, R. Fishman, and M. Dahan, Electrostatic bottle for long-time storage of fast ion beams, Phys. Rev. A **55**, R1577 (1997).

[22] R. Wolf, D. Beck, K. Blaum, C. Böhm, C. Borgmann, M. Breitenfeldt, F. Herfurth, A. Herlert, M. Kowalska, S. Kreim, D. Lunney, S. Naimi, D. Neidherr, M. Rosenbusch, L. Schweikhard, J. Stanja, F. Wienholtz, and K. Zuber, On-line separation of short-lived nuclei by a multi-reflection time-of-flight device, Nucl. Instrum. Methods Phys. Res., Sect. A **686**, 82 (2012).

[23] R. N. Wolf, D. Beck, K. Blaum, C. Böhm, C. Borgmann, M. Breitenfeldt, N. Chamel, S. Goriely, F. Herfurth, M. Kowalska, S. Kreim, D. Lunney, V. Manea, E. Minaya Ramirez, S. Naimi, D. Neidherr, M. Rosenbusch, L. Schweikhard, J. Stanja, F. Wienholtz, and K. Zuber, Plumbing Neutron Stars to New Depths with the Binding Energy of the Exotic Nuclide ^{82}Zn, Phys. Rev. Lett. **110**, 041101 (2013).

[24] F. Wienholtz, D. Beck, K. Blaum, C. Borgmann, M. Breitenfeldt, R. B. Cakirli, S. George, F. Herfurth, J. D. Holt, M. Kowalska, S. Kreim, D. Lunney, V. Manea, J. Menendez, D. Neidherr, M. Rosenbusch, L. Schweikhard, A. Schwenk, J. Simonis, J. Stanja, R. N. Wolf, and K. Zuber, Masses of exotic calcium isotopes pin down nuclear forces, Nature (London) **498**, 346 (2013).

[25] O. Aviv, B. Kafle, V. Chandrasekaran, O. Heber, M. L. Rappaport, H. Rubinstein, D. Schwalm, D. Strasser, Y. Toker, and D. Zajfman, Absolute photo-destruction and photo-fragmentation cross section measurements using an electrostatic ion beam trap, Rev. Sci. Instrum. **84**, 053106 (2013).

[26] C. Breitenfeldt, K. Blaum, S. George, J. Göck, G. Guzmán-Ramírez, J. Karthein, T. Kolling, M. Lange, S. Menk, C. Meyer, J. Mohrbach, G. Niedner-Schatteburg, D. Schwalm, L. Schweikhard, and A. Wolf, Long-Term Monitoring of the

Internal Energy Distribution of Isolated Cluster Systems, Phys. Rev. Lett. **120**, 253001 (2018).

[27] S. Ring, H. B. Pedersen, O. Heber, M. L. Rappaport, P. D. Witte, K. G. Bhushan, N. Altstein, Y. Rudich, I. Sagi, and D. Zajfman, Fourier transform time-of-flight mass spectrometry in an electrostatic ion beam trap, Anal. Chem. **72**, 4041 (2000).

[28] K. G. Bhushan, S. C. Gadkari, J. V. Yakhmi, and V. C. Sahni, Electrostatic ion trap and Fourier transform measurements for high-resolution mass spectrometry, Rev. Sci. Instrum. **78**, 083302 (2007).

[29] T. Doussineau, C. Yu Bao, C. Clavier, X. Dagany, M. Kerleroux, R. Antoine, and P. Dugourd, Infrared multiphoton dissociation tandem charge detection-mass spectrometry of single megadalton electrosprayed ions, Rev. Sci. Instrum. **82**, 084104 (2011).

[30] R. T. Hilger, P. J. Wyss, R. E. Santini, and S. A. McLuckey, Absorption mode Fourier transform electrostatic linear ion trap mass spectrometry, Anal. Chem. **85**, 8075 (2013).

[31] P. Fischer and L. Schweikhard, Photofragmentation of $Bi_n^{+/-}$ clusters ($n = 2$–19) in an electrostatic ion beam trap, Eur. Phys. J. D **73**, 105 (2019).

[32] R. L. Hettich, Structural investigations of aluminum cluster ions, Al_n^- ($n = 3$–50), J. Am. Chem. Soc. **111**, 8582 (1989).

[33] A. Drescher, J. Kitching, J. E. Crawford, J. K. P. Lee, and G. Thekkadath, Studies of Sb and Bi cluster produced by laser desorption, Z. Phys. D **19**, 203 (1991).

[34] H. S. Kim, T. D. Wood, A. G. Marshall, and J. Lee, Production of gold cluster ions by laser desorption/ionization Fourier-transform ion cyclotron resonance mass spectrometry, Chem. Phys. Lett. **224**, 589 (1994).

[35] C. Stoermer, J. Friedrich, and M. M. Kappes, Observation of multiply charged cluster anions upon pulsed UV laser ablation of metal surfaces under high vacuum, Int. J. Mass Spectrom. **206**, 63 (2001).

[36] R. N. Wolf, G. Marx, M. Rosenbusch, and L. Schweikhard, Static-mirror ion capture and time focusing for electrostatic ion-beam traps and multi-reflection time-of-flight mass analyzers by use of an in-trap potential lift, Int. J. Mass Spectrom. **313**, 8 (2012).

[37] P. Fischer, G. Marx, and L. Schweikhard, Multiple ion capture and separation in an electrostatic storage device, Int. J. Mass Spectrom. **435**, 305 (2019).

[38] P. Fischer, S. Knauer, G. Marx, and L. Schweikhard, In-depth study of in-trap high-resolution mass separation by transversal ion ejection from a multi-reflection time-of-flight device, Rev. Sci. Instrum. **89**, 015114 (2018).

[39] R. A. Yost and C. G. Enke, Triple quadrupole mass spectrometry for direct mixture analysis and structure elucidation, Anal. Chem. **51**, 1251 (1979).

[40] K. P. Kerns, B. C. Guo, H. T. Deng, and A. W. Castleman, Collision induced dissociation of titanium-carbon cluster cations, J. Chem. Phys. **101**, 8529 (1994).

[41] K. R. Asmis, M. Brümmer, C. Kaposta, G. Santambrogio, G. von Helden, G. Meijer, K. Rademann, and L. Wöste, Mass-selected infrared photodissociation spectroscopy of $V_4O_{10}^+$, Phys. Chem. Chem. Phys. **4**, 1101 (2002).

[42] A. V. Loboda, A. N. Krutchinsky, M. Bromirski, W. Ens, and K. G. Standing, A tandem quadrupole/time-of-flight mass spectrometer with a matrix-assisted laser desorption/ionization source: Design and performance, Rapid Commun. Mass Spectrom. **14**, 1047 (2000).

[43] K. Hirsch, J. T. Lau, P. Klar, A. Langenberg, J. Probst, J. Rittmann, M. Vogel, V. Zamudio-Bayer, T. Möller, and B. von Issendorff, X-ray spectroscopy on size-selected clusters in an ion trap: From the molecular limit to bulk properties, J. Phys. B **42**, 154029 (2009).

[44] J. L. Elkind, F. D. Weiss, J. M. Alford, R. T. Laaksonen, and R. E. Smalley, Fourier transform ion cyclotron resonance studies of H_2 chemisorption on niobium cluster cations, J. Chem. Phys. **88**, 5215 (1988).

[45] P. A. Limbach, L. Schweikhard, K. A. Cowen, M. T. McDermott, A. G. Marshall, and J. V. Coe, Observation of the doubly charged, gas-phase fullerene anions C_{60}^{2-} and C_{70}^{2-}, J. Am. Chem. Soc. **113**, 6795 (1991).

[46] S. Peredkov, A. Savci, S. Peters, M. Neeb, W. Eberhardt, H. Kampschulte, J. Meyer, M. Tombers, B. Hofferberth, F. Menges, and G. Niedner-Schatteburg, X-ray absorption spectroscopy of mass-selected transition metal clusters using a cyclotron ion trap: An experimental setup for measuring XMCD spectra of free clusters, J. Electron Spectrosc. **184**, 113 (2011).

[47] A. G. Marshall, Fourier transform ion cyclotron resonance mass spectrometry, Acc. Chem. Res. **18**, 316 (1985).

[48] M. V. Buchanan and R. L. Hettich, Fourier transform mass spectrometry of high-mass biomolecules, Anal. Chem. **65**, 245A (1993).

[49] L. Schweikhard, J. Ziegler, H. Bopp, and K. Lützenkirchen, The trapping condition and a new instability of the ion motion in the ion cyclotron resonance trap, Int. J. Mass Spectrom. **141**, 77 (1995).

[50] F. Wienholtz, D. Atanasov, S. Kreim, V. Manea, M. Rosenbusch, L. Schweikhard, A. Welker, and R. N. Wolf, Towards ultrahigh-resolution multi-reflection time-of-flight mass spectrometry at ISOLTRAP, Phys. Scr. **T166**, 014068 (2015).

[51] P. Schury, Y. Ito, M. Wada, and H. Wollnik, Wide-band mass measurements with a multi-reflection time-of-flight mass spectrograph, Int. J. Mass Spectrom. **359**, 19 (2014).

[52] S. Knauer, P. Fischer, G. Marx, B. Schabinger, L. Schweikhard, and R. Wolf, Multi-reflection time-of-flight mass spectrometry with combined in-trap lift capture and mirror-switch ejection, Int. J. Mass Spectrom. **423**, 46 (2017).

[53] T. Martin, Shells of atoms, Phys. Rep. **273**, 199 (1996).

[54] W. A. de Heer, The physics of simple metal clusters: Experimental aspects and simple models, Rev. Mod. Phys. **65**, 611 (1993).

[55] W. D. Knight, K. Clemenger, W. A. de Heer, W. A. Saunders, M. Y. Chou, and M. L. Cohen, Electronic Shell Structure and Abundances of Sodium Clusters, Phys. Rev. Lett. **52**, 2141 (1984).

[56] K. Wade, Structural and bonding patterns in cluster chemistry, Adv. Inorg. Chem. Rad. **18**, 1 (1976).

[57] C. Seifried, L. Longo, P. Pollak, and F. Weigend, The chemical space of $Pb_{N-n}Bi_n$ and $(Pb_{N-n}Bi_n)^+$: A systematic study for $N = 3$–13, J. Chem. Phys. **146**, 034304 (2017).

[58] M. E. Geusic, R. R. Freeman, and M. A. Duncan, Photofragmentation of antimony and bismuth cluster cations at 248 nm, J. Chem. Phys. **88**, 163 (1988).

[59] M. M. Ross and S. W. McElvany, Production and fragmentation of antimony and bismuth cluster ions, J. Chem. Phys. **89**, 4821 (1988).

[60] T. Bernhardt, B. Kaiser, and K. Rademann, Fragmentation of clusters induced by collision with a solid surface: Comparison of antimony and bismuth cluster ions, Z. Phys. D **40**, 327 (1997).

[61] R. Kelting, A. Baldes, U. Schwarz, T. Rapps, D. Schooss, P. Weis, C. Neiss, F. Weigend, and M. M. Kappes, Structures of small bismuth cluster cations, J. Chem. Phys. **136**, 154309 (2012).

[62] F. J. Kohl and K. D. Carlson, Dissociation energies of bismuth-antimony molecules, J. Am. Chem. Soc. **90**, 4814 (1968).

[63] R. Wheeler, K. Laihing, W. Wilson, and M. Duncan, Semimetal clusters: Laser vaporization and photoionization of antimony and bismuth, Chem. Phys. Lett. **131**, 8 (1986).

[64] M. E. Geusic, R. R. Freeman, and M. A. Duncan, Neutral and ionic clusters of antimony and bismuth: A comparison of magic numbers, J. Chem. Phys. **89**, 223 (1988).

[65] H. K. Yuan, H. Chen, A. L. Kuang, Y. Miao, and Z. H. Xiong, Density-functional study of small neutral and cationic bismuth clusters Bi_n and Bi_n^+ ($n = 2$–24), J. Chem. Phys. **128**, 094305 (2008).

[66] L. Gao, P. Li, H. Lu, S. F. Li, and Z. X. Guo, Size- and charge-dependent geometric and electronic structures of Bi_n (Bi_n^-) clusters ($n = 2$–13) by first-principles simulations, J. Chem. Phys. **128**, 194304 (2008).

[67] J. M. Jia, G. B. Chen, D. N. Shi, and B. L. Wang, Structural and electronic properties of Bi_n ($n = 2$–14) clusters from density-functional calculations, Eur. Phys. J. D **47**, 359 (2008).

[68] D. Liang, W. Shen, C. Zhang, P. Lu, and S. Wang, Structural, electronic, vibrational and optical properties of Bi_n clusters, Mod. Phys. Lett. B **31**, 1750260 (2017).

8 Peer-reviewed publications

2019

13. **Stray-light suppression for MIRACLS's proof-of-principle experiment (submitted)**
V. Lagaki, P. Fischer, H. Heylen, F. Hummer, S. Lechner, S. Sels, F. M. Maier, P. Plattner, W. Nörtershäuser, L. Schweikhard, and S. Malbrunot-Ettenauer

12. **Multiple-ion-ejection multi-reflection time-of-flight mass spectrometry for single-reference wide-band mass measurements (submitted)**
P. Fischer and L. Schweikhard

11. **Isotope-resolved photodissociation pathways of lead-doped bismuth clusters from tandem multi-reflection time-of-flight mass spectrometry**
P. Fischer and L. Schweikhard
Phys. Rev. Research 1, 033050 (2019),
https://doi.org/10.1103/PhysRevResearch.1.033050

10. **A multi-reflection time-of-flight setup for the improvement and development of new methods and the study of atomic clusters**
S. Knauer, P. Fischer, G. Marx, M. Müller, M. Rosenbusch, B. Schabinger, L. Schweikhard, and R. N. Wolf
Int. J. Mass Spectrom. 446, 116189 (2019),
https://doi.org/10.1016/j.ijms.2019.116189

9. **Fluorescence detection as a new diagnostics tool for electrostatic ion beam traps**
S. Lechner, P. Fischer, H. Heylen, V. Lagaki, F. M. Maier, P. Plattner, M. Rosenbusch, S. Sels, F. Wienholtz, R. N. Wolf, W. Nörtershäuser, L. Schweikhard, and S. Malbrunot-Ettenauer
Hyperfine Interact. 240, 95 (2019),
https://doi.org/10.1007/s10751-019-1628-1

8. **Photofragmentation of $Bi_n^{+/-}$ clusters (n = 2–19) in an electrostatic ion beam trap**
P. Fischer and L. Schweikhard
Eur. Phys. J. D 73, 033050 (2019),
https://doi.org/10.1140/epjd/e2019-100027-0

7. **Simulations of a proof-of-principle experiment for collinear laser spectroscopy within a multi-reflection time-of-flight device**
F. M. Maier, P. Fischer, H. Heylen, V. Lagaki, S. Lechner, P. Plattner, S. Sels, F. Wienholtz, W. Nörtershäuser, L. Schweikhard, and S. Malbrunot-Ettenauer

Hyperfine Interact. 240, 54 (2019),
https://doi.org/10.1007/s10751-019-1575-x

6. **First steps in the development of the Multi Ion Reflection Apparatus for Collinear Laser Spectroscopy**
S. Sels, P. Fischer, H. Heylen, V. Lagaki, S. Lechner, F. M. Maier, P. Plattner, M. Rosenbusch, F. Wienholtz, R. N. Wolf, W. Nörtershäuser, L. Schweikhard, and S. Malbrunot-Ettenauer
Nucl. Instr. Methods B (2019), in press,
https://doi.org/10.1016/j.nimb.2019.04.076

5. **Multiple ion capture and separation in an electrostatic storage device**
P. Fischer, G. Marx, and L. Schweikhard
Int. J. Mass Spectrom. 435, 305-314 (2019),
https://doi.org/10.1016/j.ijms.2018.11.010

2018

4. **Non-isobaric time-of-flight correction for isobar resolving in MR-ToF mass spectrometry**
P. Fischer, S. Knauer, G. Marx, and L. Schweikhard
Int. J. Mass Spectrom. 432, 44-51 (2018),
https://doi.org/10.1016/j.ijms.2018.07.004

3. **In-depth study of in-trap high-resolution mass separation by transversal ion ejection from a multi-reflection time-of-flight device**
P. Fischer, S. Knauer, G. Marx, and L. Schweikhard
Rev. Sci. Instrum. 89, 015114 (2018),
https://doi.org/10.1063/1.5009167

2. **Disentangling the photodissociation pathways of small lead clusters by time-resolved monitoring of their delayed decays: The case of Pb_{31}^+**
M. Wolfram, S. König, S. Bandelow, P. Fischer, A. Jankowski, G. Marx, and L. Schweikhard
J. Phys. B 51, 044005 (2018),
https://doi.org/10.1088/1361-6455/aa9801

2017

1. **Multi-reflection time-of-flight mass spectrometry with combined in-trap lift capture and mirror-switch ejection**
S. Knauer, P. Fischer, G. Marx, B. Schabinger, L. Schweikhard, and R.N. Wolf
Int. J. Mass Spectrom. 423, 46-53 (2017),
https://doi.org/10.1016/j.ijms.2017.10.007

9 Acknowledgments

I want to express my gratitude to everyone who made this work possible, and to everyone who supported me over the course of these last three years. First and foremost, this is directed at Prof. Dr. Lutz Schweikhard, who has been guiding me since I started working on my Bachelor thesis. He is always open to discuss important and less important matters as well as the day-to-day lab events, and he still finds the time, sometimes within a single day, to quickly return my manuscripts with helpful comments and suggestions. Lutz continues to motivate me—at times with a little force—to tackle the things outside of my comfort zone that help me grow.

Furthermore, I thank my colleagues at Greifswald, Steffi Bandelow, Alexander Jankowski, Dr. Stephan König, Dr. Gerrit Marx, and Markus Wolfram, for their help and companionship in and out of the lab. This also applies to my friends and colleagues in other places, especially Dr. Marco Rosenbusch, Dr. Frank Wienholtz, and Dr. Robert Wolf: It is said that you should work hard until your idols become your rivals, so I am still doing my best to catch up to them.

I want to express my thanks to the MIRACLS team I had the pleasure of working with—Dr. Hanne Heylen, Varvara Lagaki, Simon Lechner, Dr. Stephan Malbrunot-Ettenauer, Peter Plattner, and Dr. Simon Sels—and to the entire collaboration, which I am glad to be a part of. I am very much looking forward to the experiment becoming the powerhouse we all expect it to be.

A special thanks is directed at the Greifswald workshop and at Erhard Eich in particular, without whom many of the smaller and larger tasks in and around the lab would be much more challenging. This is also true for Iris-Diana Passow, who is able to handle bulks of administrative work on a daily basis.

Thanks to my friends, who gave me the opportunity to decompress after a week in the lab. You know who you are. I am grateful for your trust and your affection.

Der größte Dank gilt wie immer meiner Familie und vor allem meiner Mutter für ihre bedingungslose Unterstützung und ihren fortwährenden Rückhalt.